LUSI LCLS Ultrafast Science Instruments

CONCEPTUAL DESIGN REPORT

SLAC-R-852
July 2007

Prepared for the Department of Energy under contract number DE-AC03-76SF00515
By Stanford Linear Accelerator Center, Stanford University, CA
Printed in the United States of America

LIST OF AUTHORS AND CONTRIBUTORS

J. Arthur, *Stanford Linear Accelerator Center, Stanford, CA, USA*

S. Boutet, *Stanford Linear Accelerator Center, Stanford, CA, USA*

J-C. Castagna, *Linear Accelerator Center, Stanford, CA, USA*

H. Chapman, *Lawrence Livermore National Laboratory, Livermore, CA, USA*

Y. Feng, *Stanford Linear Accelerator Center, Stanford, CA, USA*

W. Foyt, *Stanford Linear Accelerator Center, Stanford, CA, USA*

D. M. Fritz, *Stanford Linear Accelerator Center, Stanford, CA, USA*

K. J. Gaffney, *Stanford Synchrotron Radiation Laboratory, Stanford, CA, USA*

G. Grübel, *Deutsches Elektronen-Synchrotron, Hamburg, Germany*

J. Hajdu, *Stanford Linear Accelerator Center*, *Stanford, CA, USA*

J. B. Hastings, *Stanford Linear Accelerator Center, Stanford, CA, USA*

N. Kurita, *Stanford Linear Accelerator Center, Stanford, CA, USA*

J. Larsson, *Lund Institute of Technology, Lund, Sweden*

K. Ludwig, *Boston University, Boston, MA, USA*

M. Messerschmidt, *Deutsches Elektronen-Synchrotron, Hamburg, Germany*

J. Miao, *University of California at Los Angeles, Los Angeles, CA*

D. A. Reis, *University of Michigan,, Ann Arbor, MI, USA*

A. Robert, *Stanford Linear Accelerator Center, Stanford, CA, USA*

G. B. Stephenson, *Argonne National Laboratory, Argonne, IL, USA*

Th. Tschentscher, *Deutsches Elektronen-Synchrotron, Hamburg, Germany*

N. van Bakel, *Stanford Linear Accelerator Center, Stanford, CA, USA*

TABLE OF CONTENTS

LIST OF AUTHORS AND CONTRIBUTORS ..... **V**

TABLE OF CONTENTS ..... **VII**

LIST OF FIGURES ..... **XI**

LIST OF TABLES ..... **XIII**

LIST OF ACRONYMS ..... **XV**

1 - EXECUTIVE SUMMARY **1-1**

1.1. INTRODUCTION 1-1
1.2. INSTRUMENTS 1-1
1.3. PERFORMANCE CHARACTERISTICS 1-2
1.4. COST AND SCHEDULE 1-2
1.5. ACQUISITION STRATEGY 1-2

2 - PROJECT OVERVIEW **2-1**

2.1. INTRODUCTION 2-1
2.1.1. Background *2-1*
2.1.2. Summary Project Description *2-2*
2.1.3. Project Scope *2-2*
2.2. INSTRUMENTS 2-3
2.2.1. Design Goals *2-3*
2.3. ALTERNATIVE ANALYSIS 2-4
2.3.1. Cost *2-4*
2.3.2. Schedule *2-5*
2.3.3. Technical *2-5*
2.4. PROJECT SCHEDULE 2-5
2.5. COST ESTIMATE 2-5
2.6. FUNDING REQUIREMENTS 2-6
2.7. RISK ASSESSMENTS AND STRATEGIES 2-7
2.7.1. Technical Risks *2-7*
2.7.1.1. Performance of Optics 2-7
2.7.1.2. Performance of Detectors 2-7
2.7.2. Schedule Risks *2-8*
2.7.3. Cost Risks *2-8*
2.8. STAKEHOLDER INPUT 2-8
2.9. ACQUISITION STRATEGY 2-9
2.10. OVERALL LAYOUT 2-9
2.11. SUMMARY 2-9
2.12. REFERENCES 2-10

3 - X-RAY PUMP-PROBE **3-1**

3.1. SCIENTIFIC PROGRAMS 3-1
3.2. INSTRUMENT DESCRIPTION 3-3
3.2.1. Pump-Probe Techniques *3-3*
3.2.2. Overall Concept Layout *3-5*

3.2.3. XPP X-ray Beam Parameters *3-7*
3.2.4. Laser System *3-9*
3.2.5. Diffractometer System *3-11*
3.2.6. XPP 2D Detector System *3-13*
3.3. REFERENCES 3-15

4 - COHERENT X-RAY IMAGING 4-1

4.1. SCIENTIFIC PROGRAMS 4-1
4.2. INSTRUMENT DESCRIPTION 4-3
4.2.1. Coherent Imaging Technique *4-3*
4.2.2. Overall Concept Layout *4-5*
4.2.3. X-ray Beam Parameters *4-7*
4.2.4. Sample Environment *4-11*
4.2.4.1. Vacuum Requirements 4-11
4.2.4.2. Particle Injection 4-11
4.2.4.3. Laser Alignment of Particles 4-14
4.2.4.4. Fixed Target Samples 4-14
4.2.4.5. Cryo Goniometer 4-14
4.2.5. Detector Considerations *4-15*
4.3. REFERENCES 4-17

5 - X-RAY CORRELATION SPECTROSCOPY 5-1

5.1. SCIENTIFIC PROGRAMS 5-2
5.2. INSTRUMENT DESCRIPTION 5-3
5.2.1. XPCS Technique *5-3*
5.2.2. Overall Concept Layout *5-5*
5.2.3. X-ray Optics *5-7*
5.2.4. XCS 2D Detector System *5-11*
5.3. REFERENCES 5-12

6 - X-RAY OPTICS 6-1

6.1. OFFSET MONOCHROMATOR 6-1
6.2. X-RAY FOCUSING OPTICS 6-3
6.2.1. Refractive Lens Systems *6-3*
6.2.2. Kirkpatrick-Baez Mirror Systems *6-4*
6.3. X-RAY APERATURE SYSTEMS 6-4
6.4. ATTENUATOR SYSTEMS 6-6
6.5. REFERENCES 6-6

7 - X-RAY DIAGNOSTICS 7-1

7.1. INTRODUCTION 7-1
7.2. DIAGNOSTIC SUITE 7-2
7.2.1. X-ray Pop-In Intensity Monitor *7-3*
7.2.2. Hard X-ray In-Situ Intensity/Position Monitor *7-4*
7.2.3. Pop-In Position/Profile Monitor *7-5*
7.2.4. Wavefront Monitor *7-6*
7.2.4.1. Hartmann Wavefront Sensor 7-6
7.2.4.2. Diffractive Imager 7-7
7.2.5. Electro-Optic Timing Diagnostic *7-8*
7.2.5.1. Electro-Optic Sampling 7-8
7.2.5.2. Stabilized Fiber Optic LLRF Network 7-10
7.2.6. Interconnection with Control/Data Systems *7-11*
7.3. REFERENCES 7-11

8 - CONTROLS AND DATA SYSTEMS 8-1

8.1. SYSTEM SCOPE 8-1
8.2. SYSTEM OVERVIEW 8-2

8.2.1. System Functionalities *8-2*
8.3. CONTROLS SUBSYSTEM 8-4
8.3.1. Controls Architecture *8-4*
8.3.2. Control Networks *8-6*
8.3.3. Slow EPICS Controls *8-7*
8.3.4. Pulse-by-Pulse Measurement *8-9*
8.3.5. Fast Timing and Synchronization *8-11*
8.4. DATA SUBSYSTEM 8-12
8.4.1. General Requirements *8-12*
8.4.2. Data Acquisition Architecture *8-15*
8.4.3. Experimental Measurement Application *8-16*
8.4.4. On-Line Data Acquisition *8-18*
8.4.5. Offline Data Management and Analysis *8-20*
8.5. REFERENCES 8-21

9 - ENVIRONMENT, SAFETY & HEALTH 9-1

9.1. INTRODUCTION 9-1
9.2. IONIZING RADIATION 9-2
9.2.1. Radiation Shielding *9-2*
9.2.2. Personnel Protection System *9-2*
9.2.3. Beam Containment System *9-3*
9.2.4. Radiation Safety Training *9-3*
9.3. ELECTRICAL SAFETY 9-4
9.4. EMERGENCY PREPAREDNESS 9-4
9.5. SEISMIC SAFETY 9-4
9.6. EMERGENCY PLANNING 9-4
9.7. HAZARDOUS MATERIALS 9-5
9.8. FIRE SAFETY 9-5
9.9. ENVIRONMENTAL PROTECTION 9-6
9.10. QUALITY ASSURANCE 9-6
9.11. PROCEDURES AND POLICIES REFERENCES 9-7

10 - WBS DICTIONARY 10-1

10.1. INTRODUCTION 10-1
10.2. LEVEL 3 WORK BREAKDOWN STRUCTURE 10-1

LIST OF FIGURES

FIGURE 2-1. OVERALL LAYOUT OF LCLS/LUSI EXPERIMENTAL AREAS. 2-9
FIGURE 2-2. CONCEPTUAL LAYOUT OF THE NEAR EXPERIMENTAL HALL SHOWING THE LUSI XPP ENDSTATION AND LCLS AMO ENDSTATION. 2-10
FIGURE 2-3. CONCEPTUAL LAYOUT OF THE FAR EXPERIMENTAL HALL SHOWING THE LUSI CXI AND XCS ENDSTATIONS. 2-10
FIGURE 3-1. FEMTOSECOND ATOMIC DISPLACEMENTS GENERATED IN INSB AND BI IN RESPONSE TO ULTRAFAST PHOTOEXCITATION OF CHARGE CARRIERS. 3-2
FIGURE 3-2. EXPERIMENTALLY DETERMINED ELECTRON DENSITIES OF THE MYOGLOBIN MOLECULE BEFORE AND 100 PS AFTER PHOTOLYSIS. 3-3
FIGURE 3-3. SCHEMATIC REPRESENTATION OF A TIME-RESOLVED X-RAY SCATTERING EXPERIMENT. 3-4
FIGURE 3-4. SINGLE SHOT IMAGING TECHNIQUE USED FOR STUDYING IRREVERSIBLE DYNAMICS IN INSB AT THE SPPS. 3-4
FIGURE 3-5. X-RAY DATA ACQUIRED USING NON-SEQUENTIAL TECHNIQUES AT THE SPPS. 3-5
FIGURE 3-6. BLOCK DIAGRAM OF THE XPP INSTRUMENT. 3-6
FIGURE 3-7. CONCEPTUAL SCHEMATIC OF THE XPP INSTRUMENT. 3-7
FIGURE 3-8. FEL BEAM SIZE WITH USE OF A 4 M FOCUS BERYLLIUM COMPOUND REFRACTIVE LENS AND CORRESPONDING WAVEFRONT CURVATURE AS A FUNCTION OF DISTANCE FROM THE FOCUS. 3-8
FIGURE 3-9. LARGE-OFFSET AND FIXED-EXIT THIN-CRYSTAL MONOCHROMATOR PERFORMING AT 8 OR 24 KEV. 3-8
FIGURE 3-10. OPERATIONAL CONFIGURATIONS OF THE XPP LASER SYSTEM. 3-9
FIGURE 3-11. CONCEPTUAL IMAGE OF THE DETECTOR ARM OF THE XPP DIFFRACTOMETER SYSTEM. 3-11
FIGURE 3-12. CONCEPTUAL IMAGE OF THE KAPPA AND PLATFORM DIFRACTOMETER CONFIGURATIONS FOR THE XPP INSTRUMENT. 3-12
FIGURE 3-13. CONCEPTUAL SCHEMATIC OF THE SMALL ANGLE SCATTERING ALCOVE FOR THE XPP INSTRUMENT. 3-13
FIGURE 3-14. SCHEMATIC SETUP OF A DISPERSIVE X-RAY SPECTROMETER FOR THE XPP INSTRUMENT. 3-15
FIGURE 4-1. SCHEMATIC DIAGRAM OF THE SINGLE-PARTICLE DIFFRACTION IMAGING EXPERIMENT AT LCLS 4-4
FIGURE 4-2. BLOCK DIAGRAM OF THE CXI INSTRUMENT. 4-6
FIGURE 4-3. CONCEPTUAL SCHEMATIC OF THE CXI INSTRUMENT WITH 3 FOCUSING OPTICS. 4-7
FIGURE 4-4. SCHEMATIC OF THE CXI INSTRUMENT WITH A SINGLE FOCUSING OPTIC. 4-8
FIGURE 4-5. FEL BEAM SIZE WITH USE OF A 0.4 M FOCUS KB SYSTEM AND CORRESPONDING WAVEFRONT CURVATURE AS A FUNCTION OF DISTANCE FROM THE FOCUS. 4-8
FIGURE 4-6. MD SIMULATION OF RADIATION-INDUCED COULOMB EXPLOSION OF A SMALL PROTEIN OF LYSOZYME. 4-9
FIGURE 4-7. A LAUE PULSE COMPRESSOR BASED ON 'SLICED' MULTILAYERS. 4-10
FIGURE 4-8. SCHEMATICS OF THE PARTICLE INJECTOR FOR CONTAINER-LESS SAMPLE DELIVERY TO LCLS. 4-12
FIGURE 4-9. EXPERIMENTAL MEASUREMENT AND ANALYSIS OF COHERENT X-RAY DIFFRACTION OF INJECTED PARTICLES. 4-13
FIGURE 4-10. ENGINEERING CONCEPT OF THE CRYO-EM GONIOMETER STAGE FOR THE CXI INSTRUMENT 4-15
FIGURE 4-11. PLANAR SECTION THROUGH THE CENTER OF THE MOLECULAR TRANSFORM OF A SMALL PROTEIN MOLECULE LYSOZYME AND OF A LARGER VIRUS CAPSID AT SIMILAR MAXIMAL RESOLUTIONS. 4-17
FIGURE 5-1. SPECKLE PATTERN MEASURED AT 8 KEV OF A POROUS SILICA STATIC SAMPLE OF VYCOR. 5-1

FIGURE 5-2. FREQUENCY-WAVEVECTOR SPACE COVERED BY DIFFERENT EXPERIMENTAL TECHNIQUES FOR STUDYING DYNAMICS OF CONDENSED MATTER SYSTEMS. 5-2
FIGURE 5-3. ILLUSTRATION OF THE XPCS SEQUENTIAL TECHNIQUE. 5-4
FIGURE 5-4. ILLUSTRATION OF XPCS SPLIT-DELAY TECHNIQUE. 5-5
FIGURE 5-5. BLOCK DIAGRAM OF THE XCS INSTRUMENT. 5-6
FIGURE 5-6. LARGE-OFFSET FIXED-EXIT MONOCHROMATOR IN THE TRANSPORT TUNNEL. 5-7
FIGURE 5-7. LARGE-OFFSET AND FIXED-EXIT MONOCHROMATOR FOR SI(111) THIN CRYSTALS ... 5-8
FIGURE 5-8. SCHEMATIC DIAGRAM OF THE SPLIT-DELAY UNIT. 5-8
FIGURE 5-9. CONCEPTUAL LAYOUT OF THE XCS ENDSTATION WITH THE TWO DETECTOR STAGES 5-10
FIGURE 6-1. SCHEMATIC OF THE DOUBLE-CRYSTAL OFFSET MONOCHROMATOR. 6-1
FIGURE 6-2. SCHEMATIC OF A BRAGG CRYSTAL SHOWING THE χ AND θ ROTATION AXES. 6-2
FIGURE 6-3. TRANSMISSION AND EFFICIENCY OF A 2 μM PERFECT SI (111) BRAGG REFLECTION. 6-3
FIGURE 6-4. SCHEMATIC OF A SINGLE PARABOLIC REFRACTIVE LENS AND A COMPOUND STACK OF LENSES. 6-4
FIGURE 6-5. COMPOSITION OF THE SLIT BLADE USED FOR THE FRONT END OF THE LCLS. 6-5
FIGURE 6-6. PARASITIC SCATTERING OBSERVED FROM A SET OF 2 MM-THICK TUNGSTEN BLADES. 6-5
FIGURE 7-1. CONCEPTUAL DESIGN OF THE X-RAY POP-IN DIODE INTENSITY MONITOR. 7-3
FIGURE 7-2. CONCEPTUAL DESIGN OF THE HARD X-RAY IN-SITU INTENSITY/POSITION MONITOR. 7-4
FIGURE 7-3. CONCEPTUAL DESIGN OF THE X-RAY POSITION/PROFILE MONITOR. 7-5
FIGURE 7-4. OPERATIONAL SCHEMATIC OF A HARTMANN WAVEFRONT SENSOR. 7-6
FIGURE 7-5. SCHEMATIC OF DIFFRACTIVE IMAGING OF A FOCUSED BEAM FROM A BE LENS. 7-7
FIGURE 7-6. EOS DATA ACQUIRED AND ANALYZED AT THE SPPS. 7-9
FIGURE 7-7. CONCEPTUAL DESIGN OF THE ELECTRO-OPTIC DIAGNOSTIC VACUUM CHAMBER. 7-9
FIGURE 7-8. STABILIZED FIBER OPTIC LLRF NETWORK FOR FS TIMING. 7-10
FIGURE 8-1. SCHEMATIC DIAGRAM OF LUSI CONTROLS/DATA ACQUISITION SYSTEM. 8-1
FIGURE 8-2. COMPONENT LEVEL BLOCK DIAGRAM OF LUSI CONTROL SUBSYSTEM. 8-2
FIGURE 8-3. COMPONENT LEVEL BLOCK DIAGRAM OF LUSI DATA SUBSYSTEM. 8-3
FIGURE 8-4. ARCHITECTURE OF THE CONTROL SUBSYSTEM. 8-5
FIGURE 8-5. LAYERED MODEL FOR CONTROLS SUBSYSTEM. 8-5
FIGURE 8-6. BLOCK DIAGRAM OF THE OPTICS CONTROL COMPONENT. 8-8
FIGURE 8-7. LAYERED MODEL FOR DATA SUBSYSTEM. 8-12
FIGURE 8-8. DATA SUBSYSTEM ARCHITECTURE. 8-16
FIGURE 8-9. BLOCK DIAGRAM OF THE EXPERIMENTAL CONTROL. 8-17

LIST OF TABLES

TABLE 1-1. ESSENTIAL PARAMETERS FOR LUSI INSTRUMENTS. 1-2
TABLE 2-1. ESSENTIAL PARAMETERS FOR LUSI INSTRUMENTS. 2-4
TABLE 2-2. MAJOR PROJECT SCHEDULE MILESTONES. 2-5
TABLE 2-3. PRELIMINARY ESTIMATE BY WBS ELEMENTS FOR THE LUSI PROJECT. 2-6
TABLE 2-4. PROJECTED FUNDING PROFILE FOR THE LUSI PROJECT. 2-6
TABLE 3-1. SYSTEM SPECIFICATION FOR XPP INSTRUMENTATION. 3-6
TABLE 3-2. DESIGN PARAMETERS OF THE THREE BERYLLIUM COMPOUND REFRACTIVE LENS ASSEMBLIES TO BE CONSTRUCTED FOR THE XPP INSTRUMENT. 3-7
TABLE 3-3. DETECTOR SPECIFICATIONS FOR THE XPP INSTRUMENT. 3-14
TABLE 4-1. SYSTEM SPECIFICATION FOR CXI INSTRUMENTATION 4-6
TABLE 4-2. DESIGN PARAMETERS OF THE KB SYSTEM TO BE CONSTRUCTED FOR THE CXI INSTRUMENT. 4-7
TABLE 4-3. PARAMETERS FOR A LAUE CASE PULSE COMPRESSOR FOR THE LCLS 4-10
TABLE 5-1. SPECIFICATIONS OF XCS INSTRUMENT COMPONENTS. 5-6
TABLE 5-2. LONGITUDINAL COHERENCE LENGTH FOR TWO WAVELENGTHS OF 0.5 AND 1.5 Å FOR A SELECTION OF SILICON AND DIAMOND MONOCHROMATOR CRYSTALS. 5-7
TABLE 5-3. DETECTOR SPECIFICATIONS FOR THE XCS INSTRUMENT 5-11
TABLE 6-1. SPECIFICATIONS FOR OFFSET DOUBLE-CRYSTAL MONOCHROMATOR. 6-2
TABLE 7-1. EXPECTED PULSE-TO-PULSE FLUCTUATIONS OF THE LCLS X-RAY BEAM. 7-1
TABLE 7-2. SUMMARY SPECIFICATIONS OF THE LUSI DIAGNOSTICS SUITE. 7-2
TABLE 7-3. SPECIFICATIONS FOR A HARTMANN WAVEFRONT SENSOR. 7-7
TABLE 8-1. PROJECTED DATA RATES AND ACCUMULATION FOR CXI INSTRUMENT. 8-13
TABLE 9-1. MINIMUM TRAINING REQUIREMENTS FOR UNESCORTED ACCESS. 9-3

LIST OF ACRONYMS

ADC	Analog-to-Digital Conversion
AE	Acquisition Executive
ANL	Argonne National Laboratory
AMO	Atomic Molecular and Optical Science Instrument
APS	Advanced Photon Source
ASIC	Application Specific Integrated Circuit
BaBar	B (B meson) and B-bar (anti B meson) Experiment
BCR	Baseline Change Request
BCCB	Baseline Change Control Board
BES	Basic Energy Sciences
BNL	Brookhaven National Laboratory
CD	Critical Decision
CDR	Conceptual Design Report
CXI	Coherent X-ray Imaging Instrument
DAC	Detector Advisory Committee
DCD	Design Criteria Document
DESY	Deutsches Elektronen-Synchrotron
DOE	Department of Energy
DQE	Detector Quantum Efficiency
EAC	Estimate at Completion
EOS	Electro-Optic Sampling
EPICS	Experimental Physics and Industrial Control System
ESAAB	Energy Systems Acquisition Advisory Board
ES&H	Environment, Safety, and Health
ESRF	European Synchrotron Radiation Facility
EXAFS	Extended X-ray Absorption Fine Structure Spectroscopy
FAC	Facility Advisory Committee
FEE	Front-End Enclosure
FEL	Free Electron Laser
FLASH	Free-Electron Laser in Hamburg
FPD	Federal Project Director

FPGA	Field Programmable Gate Arrays
FWP	Field Work Proposal
FWHM	Full Width at Half Maximum
FY	Fiscal Year
HQ	Headquarters
IPT	Integrated Project Team
ISM	Integrated Safety Management
IRR	Instrument Readiness Review
KB	Kirkpatrick-Baez
LINAC	Linear Accelerator
LBNL	Lawrence Berkeley National Laboratory
LCCA	Life Cycle Cost Analysis
LCLS	Linac Coherent Light Source
LLNL	Lawrence Livermore National Laboratory
LLRF	Low-Level Radio Frequency
LOI	Letter of Intent
LSST	Large Synoptic Survey Telescope
LTU	Linac-to-Undulator
LUSI	LCLS Ultrafast Science Instruments
LVDT	Linear Variable Displacement Transducers
M&O	Management & Operation
MIE	Major Item of Equipment
MOU	Memorandum of Understanding
NEPA	National Environmental Protection Act
NIM	Nuclear Instrument Module
PARS	Project Assessment and Reporting System
PEP	Project Execution Plan
PD	Project Director
ODCM	Offset Double Crystal Monochromator
OPA	Optical Parametric Amplifier
QA	Quality Assurance
RF	Radio Frequency
RTEMS	Real-Time Executive for Multiprocessor Systems
SAC	Scientific Advisory Committee
SASE	Self Amplified Spontaneous Emission
SAXS	Small-Angle X-ray Scattering
SC	Office of Science

SLAC	Stanford Linear Accelerator Center
SNR	Signal-to-Noise Ratio
SPPS	Sub-Picosecond Pulse Source
SCRAMNet	Shared Common RAM Network
SSO	Stanford Site Office of DOE
TEC	Total Estimated Cost
TL	Team Leader
TPC	Total Project Cost
UCLA	University of California at Los Angeles
VE	Value Engineering
WBS	Work Breakdown Structure
XAMPS	X-ray Active Matrix Pixel Sensor
XFEL	X-ray Free Electron Laser
XCS	X-ray Correlation Spectroscopy Instrument
XPCS	X-ray Photon Correlation Spectroscopy
XPP	X-ray Pump-Probe Diffraction Instrument
XTOD	X-ray Transport, Optics, & Diagnostics
XUV	X-ray Ultraviolet

1 - EXECUTIVE SUMMARY

1.1. INTRODUCTION

The Stanford Linear Accelerator Center (SLAC), along with Argonne National Laboratory (ANL), Lawrence Livermore National Laboratory (LLNL), and the University of California at Los Angeles (UCLA), is constructing a Free-Electron Laser (FEL) facility, which will operate in the wavelength range 1.5 nm - 0.15 nm. This FEL, the Linac Coherent Light Source (LCLS), utilizes the SLAC linac and will produce sub-picosecond pulses of short wavelength X-rays with very high peak brightness and almost complete transverse coherence.

The final one-third of the SLAC linac will be used as the source of electrons for the LCLS. The high energy electrons will be transported across the SLAC Research Yard, into a tunnel which will house a long undulator. In passing through the undulator, the electrons will be bunched by the force of their own synchrotron radiation and produce an intense, monochromatic, spatially coherent beam of X-rays. By varying the electron energy, the FEL X-ray wavelength will be tunable from 1.5 nm to 0.15 nm. The LCLS will include two experimental halls as well as X-ray optics and infrastructure necessary to create a facility that can be developed for research in a variety of disciplines such as atomic physics, materials science, plasma physics and biosciences.

This Conceptual Design Report, the authors believe, confirms the feasibility of designing and constructing three X-ray instruments in order to exploit the unique scientific capability of this new LCLS facility.

The technical objective of the LCLS Ultrafast Science Instruments (LUSI) project is to design, build, and install at the LCLS three hard X-ray instruments that will complement the initial instrument included in the LCLS construction. As the science programs advance and new technological challenges appear, instrumentation needs to be developed and ready to conquer these new opportunities. The LCLS instrument concepts have been developed in close consultation with the scientific community through a series of workshops team meetings and focused reviews. In particular, the LUSI project instruments have been identified as meeting the most urgent needs of the scientific community based on the advice of the LCLS Scientific Advisory Committee (SAC) in response to an open call for letters of intent (LOI) from the breadth of the scientific community.

1.2. INSTRUMENTS

The LUSI project plans to build three hard X-ray instruments over a period of six fiscal years (FY2007 -- FY2012). One of the instruments will be optimized for hard X-ray studies of ultrafast dynamics at the atomic level, addressing basic problems in chemistry and materials science. The second instrument will concentrate on hard X-ray coherent imaging of nano-particles and large biomolecules. The third instrument will focus on the study of equilibrium dynamics in condensed systems using X-ray photon correlation spectroscopy. These instruments will complement the initial instrument being built at LCLS, which is

directed towards atomic physics. The instruments and beam transport and optics are described in Chapter 3 through Chapter 6, of this Conceptual Design Report (CDR).

1.3. PERFORMANCE CHARACTERISTICS

The LCLS will be an X-ray source with unprecedented brightness and peak power. It will provide pulses of X-rays of duration of about 100 fs or less, in a wavelength range from 1.5 nm to 0.15 nm. In average brightness it will match or exceed existing storage ring-based sources. In peak brightness, it will surpass existing sources by a factor of 10^{10}. The performance characteristics of the LUSI instruments, shown in Table 1-1, will be commensurate with these unique source characteristics.

Instrument	Parameter	Capable of Achieving	Actual Measurement
X-ray Pump-Probe	Energy Range	4 keV - 25 keV*	
	Energy Resolution	0.1 - 0.002%	
	Imaging Detector		1024x1024 pixels
Coherent X-ray Imaging	Energy Range	4 keV - 25 keV	
	Energy Resolution	0.1%	
	Imaging Detector		760x760 pixels†
X-ray Correlation Spectroscopy	Energy Range	4 keV - 25 keV	
	Energy Resolution	0.1 - 0.002%	
	Imaging Detector		1024x1024 pixels

Table 1-1. Essential Parameters for LUSI Instruments.

1.4. COST AND SCHEDULE

The Total Project Cost is estimated to be in the range $51.8 million - $60.0 million. A six-year construction schedule beginning in FY2007 is proposed.

1.5. ACQUISITION STRATEGY

The lead contractor for acquisition of the LUSI project will be Stanford University, which operates SLAC. SLAC will collaborate with two national laboratories, Brookhaven National Laboratory (BNL) and Lawrence Livermore National Laboratory (LLNL), in the design/construction of components for the three instruments.

---

* Using the fundamental and the third harmonic
† Provided by LCLS

2 - PROJECT OVERVIEW

2.1. INTRODUCTION

2.1.1. Background

The last thirty years have witnessed an exponential increase in the capability of X-ray sources, and X-ray physics has seen an explosion of new techniques and applications. The key to this huge change has been the development of synchrotron radiation sources based on high-energy electron storage rings. The scientific capabilities of synchrotron radiation X-ray sources are reflected in the fact that in the US four such facilities are operated by the Department of Energy (DOE) with a collective annual funding level of about $200 million (FY2001). In 2001, 6500 scientists made use of these facilities for their research programs, which range from fundamental physics to materials science to biology and medicine to environmental science [1]. Now, another type of high-energy accelerator has the capability to drive an X-ray source whose capabilities outshine those of a modern synchrotron source by nearly as much as the synchrotron does the 1960's laboratory source.

Advances in accelerator technology have been the driving force in the progress toward brighter synchrotron sources, with scientific applications developing in response to the availability of new sources. The rate of improvement in source capability has been tremendous: for thirty years X-ray source brightness has been increasing exponentially with a doubling time of about 10 months. A modern synchrotron radiation source is 11 orders of magnitude brighter than a 1960's laboratory X-ray source. Seldom, if ever, in history (perhaps only in the field of visible laser optics) has a scientific discipline seen its tools change so dramatically within the active life of a single generation of scientists. Such change makes it very difficult to predict the future. For example, no one foresaw the huge impact on biomedical research that has come in the last twenty years from synchrotron-based extended X-ray absorption fine structure (EXAFS) spectroscopy and protein crystallography, even though those techniques had been developed many years previously using laboratory sources. The developing synchrotron source capability has made the techniques qualitatively and unexpectedly more powerful as scientific tools.

This history indicates that although it is very difficult to predict the precise nature of the eventual applications of the LCLS, a source that is more than 10 orders of magnitude brighter than today's synchrotron sources, it is clear that LCLS will make fundamental contributions to our understanding of the structure and dynamics of matter on the atomic scale. Over the past ten years there has been much consideration of the future development and applications of advanced synchrotron radiation sources. A first workshop on "Fourth Generation Light Sources", at SLAC in 1992 [2], concentrated almost exclusively on accelerator technology rather than applications. This workshop served to alert the scientific community to the possibilities for X-ray Free-Electron Lasers (FEL) driven by high energy linacs, such as the SLAC linac. It is interesting to note that a workshop earlier in 1992 on "Applications of X-ray Lasers" [3] did not mention FEL sources at all; only chemical lasers were considered. The SLAC workshop directly stimulated the first workshops on scientific applications of X-ray FELs [4][5]. The next "Fourth Generation Light Sources" workshop, in 1996 at the European Synchrotron Radiation Facility (ESRF) [6], included sessions on both sources and applications. The discussions convinced nearly all the participants that linac-based

FELs would be the most effective machines for continuing to improve the performance of X-ray sources, and in particular, would provide the only viable route to a diffraction-limited hard X-ray source. Subsequent workshops at Deutsches Elektronen-Synchrotron (DESY) in 1996 [7][8] and the Advanced Photon Source (APS) in 1997 [9] have assumed that future fourth generation X-ray user facilities will be based on linac FELs, and have attempted to foresee the new science that these sources will bring. These workshops, as well as more than 20 others, have firmly established the scientific opportunities that LCLS offers.

2.1.2. Summary Project Description

In its vision of the future from 2003, "Facilities for the Future of Science: A Twenty-Year Outlook," the DOE Office of Science placed the LCLS tied for third in near term priorities, and the highest priority for the Basic Energy Sciences (BES) division. The LCLS will be a scientific user facility for the application of XFEL radiation to experimental science. It will bring a completely new dimension to the use of X-rays to study matter through its unique properties never before available. X-rays from synchrotron light sources are currently used to study static atomic structures, but the synchrotron light sources cannot produce ultrashort pulses, so they cannot resolve the ultrafast motions of atoms during dynamical events such as chemical reactions. The LCLS represents a revolutionary advance within the synchrotron radiation world, since it offers the X-rays associated with synchrotron light sources, and the ultra-short, ultra-intense pulses required to study dynamics on the nanoscale. The tremendous brightness of the LCLS X-ray pulse will also be invaluable for creating and probing matter in extreme conditions, and for flash-imaging of nano-objects, such as small clusters of molecules and possibly individual single molecules.

The LCLS Scientific Advisory Committee (SAC) has recommended experiments in five scientific disciplines or thrust areas for the initial operation of the LCLS. These disciplines cover a variety of scientific areas: atomic physics, plasma physics, chemistry, biology and materials science.

Three of the thrust areas establish the basis for the designs of LUSI. They also provide the requirements for sample environments, specialized X-ray detectors, diagnostics, data acquisition and controls. The definition of the required synchronization of external lasers with the LCLS beam is derived from the experimental needs of these first five experiments. In general, these designs are extensions of common practice at synchrotron sources today, but become more demanding due to the unprecedented peak power, short pulse length, coherence, and repetition rate of the LCLS beam. All of these requirements are incorporated into the three instruments within LUSI: optical laser pump/X-ray probe studies in chemistry and materials science, coherent diffraction imaging of single particles and biomolecules, and the application of X-ray photon correlation spectroscopy to the study of nano-scale dynamics.

2.1.3. Project Scope

The scope of the LCLS Ultrafast Science Instruments (LUSI) project is to design, build, and install at LCLS three hard X-ray instruments that will exploit the unique scientific capability of this new facility. As the science programs advance and new technological challenges appear, instrumentation needs to be developed and ready to conquer these new opportunities. These three LCLS instrument concepts are being developed in close consultation with the scientific community through a series of workshops, conferences and focused review committees. In particular, the three LUSI project instruments have been identified as meeting some of the most urgent needs of the scientific community in supplementing the capabilities of the initial LCLS instrument based on the advice of the LCLS SAC.

LUSI plans to build three instruments over a period of six fiscal years (FY2007 - FY2012). One of these instruments will be optimized for hard X-ray studies of ultrafast dynamics at the atomic level, addressing basic problems in chemistry and materials science. The second instrument will concentrate on hard X-ray coherent imaging of nano-particles and large biomolecules. The third instrument will use hard X-rays to study nanoscale dynamics using X-ray photon correlation spectroscopy. This instrumentation will complement the other instrument at LCLS, which is directed towards atomic physics.

A brief description of the three LUSI instruments is as follows:

X-ray Pump-Probe Instrument
The X-ray Pump-Probe Instrument (XPP) will predominantly use a fast optical laser to generate transient states of matter, and use the hard X-ray pulses from the LCLS to probe the structural dynamics initiated by the laser excitation. The laser pump will have the ability to conduct precise optical manipulations, in order to create the desired excited states.

Coherent X-ray Imaging Instrument
The Coherent X-ray Imaging Instrument (CXI) will take advantage of the extremely bright, ultrashort LCLS pulses of hard X-rays to allow imaging of non-periodic nano-scale objects, including single biomolecules or small clusters, at or near atomic resolution.

X-ray Correlation Spectroscopy Instrument
The X-ray Correlation Spectroscopy Instrument (XCS) will take advantage of the unique opportunity provided by the unprecedented brilliance and narrow pulse duration of the LCLS to observe dynamical changes of large groups of atoms in condensed matter systems over a wide range of time scales using X-ray Photon Correlation Spectroscopy (XPCS).

2.2. INSTRUMENTS

2.2.1. Design Goals

In general, the LUSI instrumentation must:

- Fill a scientific need identified by the community, as demonstrated by strong support from a substantial group of potential users;
- Perform better than other existing instrumentation intended for its class of science;
- Be compatible with the characteristics of the LCLS facility, including safety conditions, source performance and physical constraints imposed by other instruments and the existing physical plant.

The principal technical performance parameters that must be met by this instrumentation will be specified in the LUSI Project Execution Plan (PEP) and are given in Table 2-1. Compatibility with the LCLS facility characteristics will be assessed by the LCLS organization, and scientific oversight is provided by the LCLS SAC. Technical advice will come from the LCLS Facilities Advisory Committee (FAC). The LCLS and LUSI also receives additional advice on all detector choices and developments from an external LCLS Detector Advisory Committee (DAC).

Instrument	Parameter	Capable of Achieving	Actual Measurement
X-ray Pump-Probe	Energy Range	4 keV - 25 keV*	
	Energy Resolution	0.1 - 0.002%	
	Imagining Detector		1024x1024 pixels
Coherent X-ray Imaging	Energy Range	4 keV - 25 keV	
	Energy Resolution	0.1 %	
	Imagining Detector		760x760 pixels†
X-ray Correlation Spectroscopy	Energy Range	4 keV - 25 keV	
	Energy Resolution	0.1 - 0.002%	
	Imagining Detector		1024x1024 pixels

Table 2-1. Essential Parameters for LUSI Instruments.

2.3. ALTERNATIVE ANALYSIS

The purpose of an alternatives analysis is to choose the most efficient, cost effective path to the desired goal, the design, construction and installation of state-of-the-art instrumentation at the LCLS facility. Evaluation of alternatives may be made in terms of the three components of a project baseline: technical performance, cost and schedule. The most compelling argument for the construction of the LUSI instruments is the existence of the LCLS itself and the staff and infrastructure at SLAC. There are no technically comparable existing instruments in the U.S. that could be moved to LCLS, and so there is no alternative but to build new ones. The LUSI instrumentation will be optimized to match the characteristics of the LCLS source and to take advantage of the fact that the LCLS facility will be the world's first X-ray free electron laser when it begins early operation in 2009. Therefore, no alternative locations for the instruments were considered.

2.3.1. Cost

The SLAC site is the best choice among alternative sites for the design and construction of the LUSI instrumentation due to the close proximity of the LCLS site and the critical interactions between the LUSI and LCLS staffs on a daily basis. This does not preclude the use of expertise at other laboratories as attested by existing and pending MOU's with BNL and LLNL.

* Using the fundamental and the third harmonic
† Provided by LCLS

2.3.2. Schedule

Early access to the extraordinary capabilities of the LCLS is extremely important in terms of the scientific opportunities that the facility will offer. In order to utilize the LCLS as rapidly as possible, the installation of the instrumentation will be staged over a four year period beginning in FY2009. Studies to examine the possibility of accelerating this schedule are ongoing.

2.3.3. Technical

All instruments are being developed in ways similar to others recently built worldwide. However, throughout the life of the project technological advances will be explored and refinements in design concepts made in order to provide the best state-of-the-art instruments.

2.4. PROJECT SCHEDULE

Major milestones for this project schedule are:

<table>
<tr><td rowspan="2">LUSI Project
CD-0 Mission Need
Approved: Aug. 2005</td><td>CD-1</td><td>CD-2</td><td>CD-3</td><td>CD-4</td></tr>
<tr><td>Cost Range
Approval</td><td>Performance
Baseline
Approval</td><td>Construction
Start Approval</td><td>Start of
Operations</td></tr>
<tr><td>Coherent X-ray
Imaging</td><td rowspan="3">July 2007</td><td rowspan="2">(a) Dec. 2007</td><td rowspan="2">(a) Jul. 2008</td><td rowspan="2">(a) Feb. 2010
(b) Mar. 2012</td></tr>
<tr><td>X-ray
Pump-Probe</td></tr>
<tr><td>X-ray Correlation
Spectroscopy</td><td>(b) Oct. 2009</td><td>(b) Mar. 2010</td><td>(b) March 2012</td></tr>
<tr><td colspan="4">Project Completion</td><td>(b) Mar. 2012</td></tr>
</table>

Table 2-2. Major Project Schedule Milestones. (a) and (b) refer to separate phases of the CD's.

R&D funds totaling $4.9 million (FY2005 - FY2007) have allowed significant development work to begin on two high-performance detectors. However, the schedule is strongly dependent upon contract award dates in the first year of the project.

2.5. COST ESTIMATE

The current estimated total project cost (TPC) range is $51.8 million - $60.0 million, which is portrayed in Table 2-3 below. It is based on a six-year (FY2007- FY2012) construction schedule and is consistent with the funding profile displayed in Table 2-4 below. A separate budget request will be

submitted prior to CD-3 approval for authorization to place long-lead procurements for detectors and optical components.

WBS	Description	Estimated Minimum Cost ($million)	Estimated Maximum Cost ($million)
1.1	Project Management	5.5	5.6
1.2	X-ray Pump-Probe	8.1	10.1
1.3	Coherent X-ray Imaging	7.1	8.6
1.4	X-ray Correlation Spectroscopy	6.2	7.7
1.5	Diagnostics	2.7	3.1
1.6	Controls	6.0	6.8
	Contingency	11.3	13.2
2.0	Other Project Costs	4.9	4.9
LUSI Total Project Costs		51.8	60.0

Table 2-3. Preliminary Estimate by WBS Elements for the LUSI Project.

2.6. FUNDING REQUIREMENTS

The funding profile depicted below is consistent with a six-year construction project beginning in FY2007 and ending in FY2012.

LUSI- Projected Funding Profile ($million)	Fiscal Year							Total
	Prior Years	2007	2008	2009	2010	2011	2012	
Project Costs (WBS 1.0)		0.5	10.0	15.0	15.0	10.0	4.6	55.1
Other Project Costs (WBS 2.0)	3.4	1.5						4.9
Total Project Costs (TPC)	3.4	2.0	10.0	15.0	15.0	10.0	4.6	60.0

Table 2-4. Projected Funding Profile for the LUSI Project.

2.7. RISK ASSESSMENTS AND STRATEGIES

All instrumentation in the LUSI project is being developed in ways similar to other instruments recently built worldwide, for which there are numerous cost benchmarks. The size of the risk is based on an assessment of how much the costs might shift due to refinements in design concepts and improvements in technology. Throughout the life of the project, technological advances will be explored in order to provide the best state-of-the-art instruments. At this time the LUSI project is considered a low-risk investment since the preliminary parameter requirements proposed by the Science Teams are considered achievable within current technical capabilities.

2.7.1. Technical Risks

2.7.1.1. Performance of Optics

The critical X-ray optics within LUSI are the focusing elements and the offset monochromators. Focusing is provided by LUSI for both the pump-probe instrument as well as the coherent imaging instrument. For the larger focal spot sizes, commercial beryllium lens technology has been chosen. This technology has been implemented at many hard X-ray synchrotron beamlines, and is particularly appropriate for the LUSI application due to the fact that beryllium is one of the few materials that can transmit the high peak power of the LCLS beam without damage. This focusing option thus has minimal risk. For the smallest focus required for the coherent imaging application (0.1 micron), a Kirkpatrick-Baez mirror system is the best choice. Because of the grazing-incidence geometry and the source-to-optic distance of ~ 400 meters, the damage issue is not of concern. Though there is some risk to achieving focal spot size and throughput specifications due to stringent requirements for the mirror quality and stability, performance specifications more stringent than those needed here have already been achieved at the European Synchrotron Radiation Facility in Grenoble, France, the SPring-8 facility in Harima, Japan and the Advanced Photon Source at Argonne. Finally there are the offset monochromators, one for the pump-probe experiment and one for the X-ray correlation spectroscopy (XCS) instrument. These systems are conceived as using very thin silicon crystals, to permit multiplexing of the LCLS hard X-ray beam. There is a risk that these crystals will not perform as expected and/or they cannot be fabricated. This risk can be mitigated by using instead somewhat-thicker diamond crystals. These crystals are readily available, but would give a loss in intensity to the pump-probe and XPCS experiments.

2.7.1.2. Performance of Detectors

The LUSI instruments require the development of detectors that are capable of readout rates that match the LCLS pulse rate, 120 Hz. X-ray cameras with this readout rate are not commercially available, so some development will be needed. This development is being carried out by BNL. There is risk associated with achieving the readout rate while maintaining the spatial resolution and noise levels required by the experiments. The required spatial resolution has already been demonstrated with detectors with slower readout rate. The benefit of developing faster detectors will be the efficient use of the LCLS beam. However, commercial detectors with readout speeds of ~ 1 Hz are available that will meet the other requirements for the X-ray pump-probe experiment, and could be employed to mitigate the risk associated with detector development. For the XPCS experiment there is also the need for very small (20-30 μm) pixel sizes, but commercial alternates exist with perhaps a factor of 10 loss in detector efficiency as well as a loss in readout speed. These commercial alternates could mitigate the risk but at a significant loss of performance.

2.7.2. Schedule Risks

Although the schedule is dictated by the funding profile and does not reflect the technological demands of the project, two major drivers will be the design and fabrication of optical components, and the development of fast detectors (currently underway). A request for approval to place long-lead procurements, and discussions about how to reduce the assembly time of these items, are expected to ease the schedule risk and perhaps permit a shortened schedule.

2.7.3. Cost Risks

The cost estimate is judged to be of low risk in terms of completing the project within the budget range. The instrument designs and components are mostly similar to those already developed for other X-ray instruments, and most technical equipment will be ordered from commercial vendors.

No unusual risks are foreseen in providing adequate funding. The project's funding needs have been included in the BES program's out-year funding plans.

During the cost estimate process risk assessments were developed for each major sub-system, usually at work breakdown structure (WBS) element level 4 or lower, using a risk-based contingency approach. This approach provides a consistent, objective analysis procedure across the project. Based on this approach the LUSI cost estimate includes a 31% contingency.

2.8. STAKEHOLDER INPUT

Throughout the planning process for the LCLS and LUSI, every effort has been made to maintain and promote communication with the agencies responsible for science policy in the US, the prospective LCLS user community, and the management of SLAC. Since it was first conceived in 1992, the evolution of the LCLS design has been guided by input from the synchrotron science community. The Basic Energy Sciences Advisory Committee has carried out two formal assessments of the future of synchrotron radiation science in the US, the role of free-electron lasers in general and the LCLS in particular.

The LCLS Science Advisory Committee has provided guidance and input, as have the 34 workshops held since 1992, which have addressed scientific opportunities and challenges of importance to the LCLS.

The SLAC Directorate and Faculty have been actively involved in planning the integration of LCLS operations and science with the rest of the SLAC Scientific Program. The SLAC Science Policy Committee, an advisory body to the President of Stanford University, has received regular updates on LCLS and LUSI activities and planning.

The concept for each LUSI instrument was developed in collaboration with the Science Team for that instrument. Science Teams include scientists from academia, DOE laboratories, other Government laboratories, and industry. The initial choice of instrument concepts was carried out by the LCLS SAC, with a general call for input from the community followed by consideration of compatibility with the LCLS facility. For the selection the SAC was charged to identify instruments that would support the greatest scientific benefit to the U.S. research community and to the DOE mission.

2.9. ACQUISITION STRATEGY

The lead contractor for acquisition of the LCLS Ultrafast Science Instruments (LUSI) is Stanford University, which operates the Stanford Linear Accelerator Center. SLAC will collaborate with two other national laboratories (BNL and LLNL) to design and construct the LUSI instrumentation.

2.10. OVERALL LAYOUT

The overall layout of the LCLS/LUSI experimental area is shown schematically in Figure 2-1, including the Near Experimental Hall (NEH), the X-ray transport tunnel, and the Far Experimental Hall (FEH). The layout of the NEH is shown schematically in Figure 2-2. Hutch #1 is reserved for a future soft X-ray imaging instrument. Hutch #2 has the LCLS AMO instrument and is reserved as well for a future soft X-ray pump-probe instrument. Hutch #3 contains the LUSI hard X-ray pump-probe instrument. The layout of the FEH is shown in Figure 2-3, where Hutch #4 contains the LUSI X-ray correlation spectroscopy instrument. Hutch #5 contains the LUSI coherent X-ray imaging instrument.

2.11. SUMMARY

In summary, this Conceptual Design Report (CDR) describes the design, fabrication and installation of three state-of-the-art instruments that will exploit the unique scientific capability of the LCLS facility. One of the instruments will be optimized for hard X-ray studies of ultrafast dynamics at the atomic level, addressing basic problems in chemistry and materials science. The second instrument will concentrate on hard X-ray coherent imaging of nano-particles and large biomolecules. The third will utilize hard X-rays to study equilibrium dynamics at the nanoscale with XPCS.

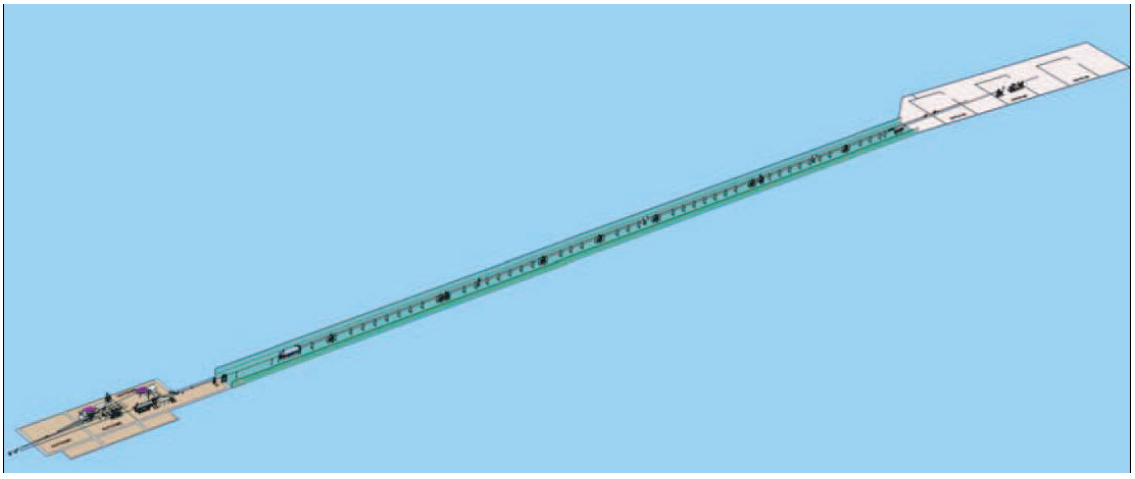

Figure 2-1. Overall layout of LCLS/LUSI Experimental Areas. Included are the Near Experimental Hall on the left, the Far Experimental Hall on the right, and the X-ray transport tunnel connecting the two halls.

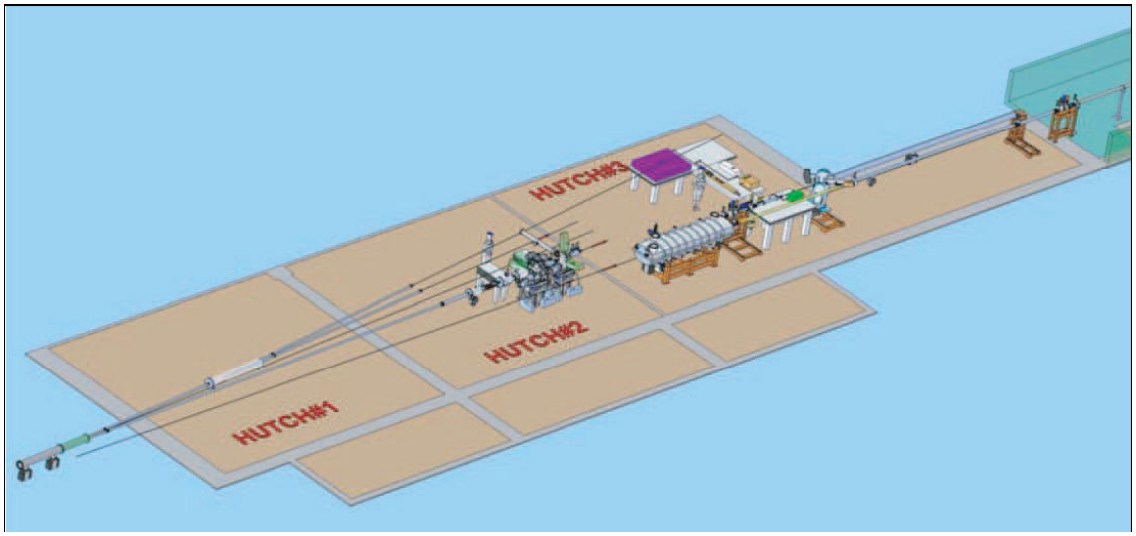

Figure 2-2. Conceptual layout of the Near Experimental Hall showing the LUSI XPP endstation and LCLS AMO endstation. Hutch #1 is reserved for a future soft X-ray imaging instrument, Hutch #2 has the LCLS AMO instrument and is reserved as well for a future soft X-ray pump-probe instrument. Hutch #3 contains the LUSI hard X-ray pump-probe instrument.

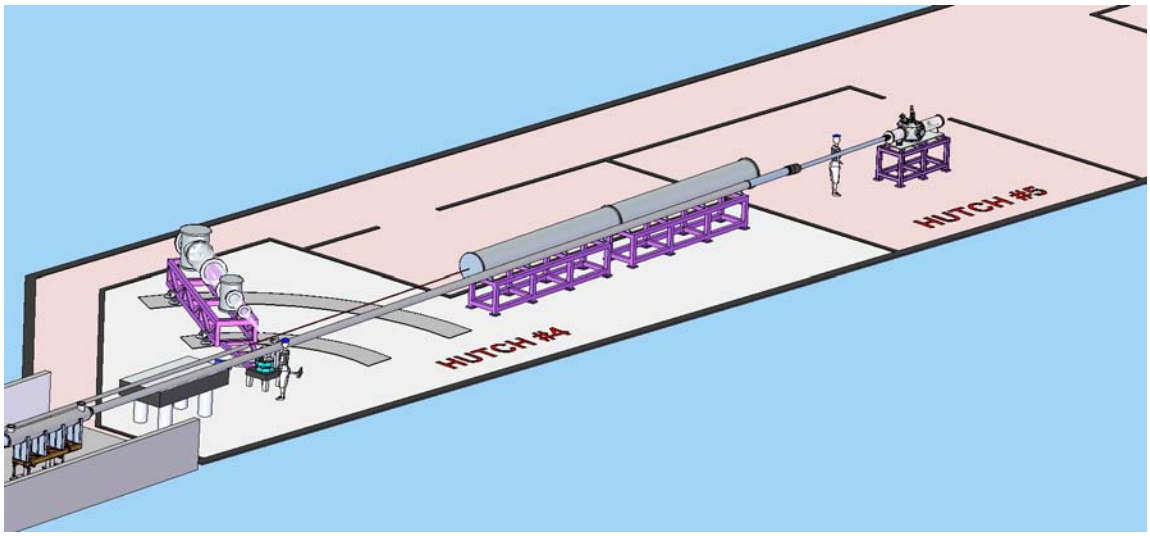

Figure 2-3. Conceptual Layout of the Far Experimental Hall showing the LUSI CXI and XCS endstations. Hutch #4 contains the LUSI X-ray correlation spectroscopy instrument (XCS) and Hutch #5 contains the LUSI coherent X-ray imaging instrument (CXI).

2.12. REFERENCES

[1] For a complete review of DoE facilities see R. Birgeneau and Z.-X. Shen, co-chairs, "Report of the Basic Energy Sciences Advisory Committee, Synchrotron Radiation Light Sources Working Group" (1997).

[2] M. Cornacchia and H. Winick, eds., "Workshop on Fourth Generation Light Sources", SSRL Report **92/02** (1992).
[3] R. London, D. Mathews, and S. Suckewer, eds., "Applications of X-ray Lasers", LLNL (1992).
[4] W. Spicer, J. Arthur, and H. Winick, eds., "Workshop on Scientific Applications of Short Wavelength Coherent Light Sources", SLAC Report **414** (1992).
[5] J. Arthur, G. Materlik, and H. Winick, eds., "Workshop on Scientific Applications of Coherent X-rays", SLAC Report **437** (1994).
[6] J.-L. Laclare, ed., "4th Generation Light Sources", ESRF (1996).
[7] J. Schneider, ed. "X-ray Free Electron Laser Applications", DESY (1996).
[8] G. Materlik, ed., “A Superbrilliant X-ray Laser Facility”, DESY (1997).
[9] M. Knotek, J. Arthur, E. Johnson, and F. Dylla, eds., "Workshop on Scientific Opportunities for Fourth-Generation Light Sources", ANL, 1997.

3 - X-RAY PUMP-PROBE

Biological, chemical, and physical processes involve the time-dependent transformation of matter on the atomic scale. Examples of these processes with technological and environmental significance are the photosynthetic generation of chemical energy, the catalytic production of fertilizer, the chemical degradation of pollutants, and the melting of ice. These structural transformations involve the motion of electrons, atoms, and molecules over very short distances (10^{-9} m) and very short time scales (10^{-12} s). Though much has been learned about these dynamical processes from previous work, particularly studies using X-rays and optical lasers, no existing technology can provide direct observation of atomic motions on ultrafast time scales.

The X-ray pump-probe diffraction (XPP) instrument will enable the study of stimulated changes in the structures of molecules and condensed matter systems. The changes will typically be stimulated by a short pulse of optical laser light, and observed using X-ray scattering techniques. Femtosecond-level synchronization between the optical laser and the LCLS X-ray pulse will allow sub-picosecond time resolution.

3.1. SCIENTIFIC PROGRAMS

The LCLS will provide transversely-coherent hard X-rays with unprecedented flux and time resolution. These attributes of the LCLS have the potential to revolutionize the experimental investigation of structural dynamics with X-ray techniques by directly following the time evolution of the electron density during the course of a photo-induced biological, chemical, or physical transformation. Some examples of the scientific programs that will be pursued by the XPP instrument are described below.

Dynamics of photo-induced phase transitions: Optical manipulation of solids can lead to photo-induced phase transitions on the ultrafast time scale. For many of these materials, a change in crystal symmetry accompanies a magnetic, ferroelectric, or metal-insulator phase transition. These materials have the potential to be utilized as ultrafast switches in magnetic and electro-optic devices and time-resolved X-ray crystallography provides an ideal tool for tracking the changes in atomic structure. For those systems that undergo a 1st-order photo-induced phase transition, time-resolved X-ray scattering has the potential to provide information about the structure and size of the new phase nucleus with previously unachievable detail.

Time-resolved spectroscopic studies of charge and spin dynamics: Charge transfer and spin crossover processes in transition-metal compounds play a critical role in the materials, chemical, and biological sciences. High-temperature superconductivity and colossal magnetoresistivity are among the important materials properties influenced by charge and spin dynamic in transition-metal compounds. These degrees of freedom influence industrial and biological catalysis as well. Transition-metal coordination compounds also show significant potential for solar energy harvesting and photosynthesis. The electronic degrees of freedom prove to be the most critical dynamical properties of these processes, making time-resolved XES, XANES, and RIXS natural tools for studying these systems.

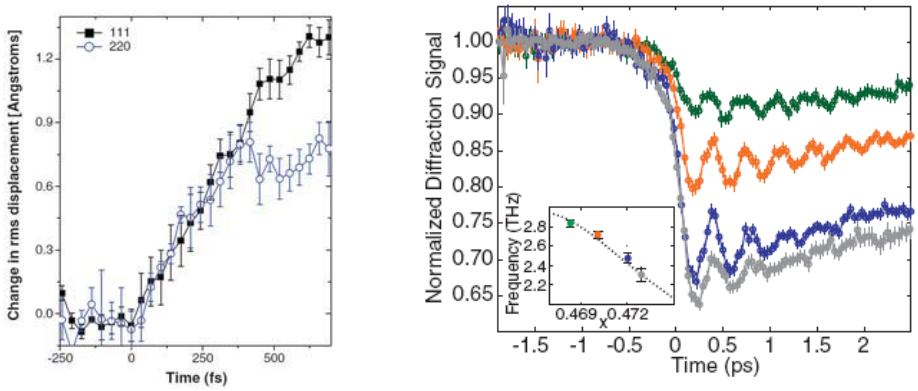

Figure 3-1. Femtosecond atomic displacements generated in InSb and Bi in response to ultrafast photoexcitation of charge carriers. The data sets were measured using time-resolved X-ray diffraction at the Sub-Picosecond Pulse Source [10][11].

Studies of intense laser-matter interactions: The structural response of materials to femtosecond laser excitation differs fundamentally from the response to excitation with longer pulses, because the generation of carriers by linear and nonlinear absorption occurs faster than the time scale for carrier diffusion and carrier-phonon scattering. Consequently, the photon field can deposit enormous quantities of energy into electronic degrees of freedom, while the vibrational internal energy remains comparatively unperturbed. Excitation of carriers can alter the ionic potential energy landscape of a material and can lead to atomic motion [10][11] (see Figure 3-1). Identifying the important distinctions between materials and further correlating the material response with material electronic structure remains an important objective for understanding the light-matter interaction. Further knowledge in this field will enhance our ability to manipulate and control material structure with light.

Time-resolved studies of chemical dynamics in solution: The majority of chemical reactions in biological, environmental, and industrial settings occur in disordered media, with liquid water being the ubiquitous example. The development of methods for studying ultrafast time-resolved diffuse scattering in liquids will be an important component of the LUSI project. Pioneering diffuse scattering experiments have been conducted at ID-9 at the ESRF [12]. While these studies have demonstrated the viability of transient diffuse scattering measurements in liquids, the technique when applied at a synchrotron has insufficient time resolution for studying chemical dynamics. For these studies the improved time resolution of the LCLS will provide a significant advantage over synchrotron facilities.

Dynamics of photoactive proteins: The variability and efficiency of proteins make them powerful molecular foundries. The size, diversity and complexity of proteins also make them challenging to study and understand with atomic detail. X-ray crystallography helped launch the molecular biology revolution and maintains a position of unique prominence in structural biology as the most powerful tool for determining biomolecular atomic structure. While enormously useful, the equilibrium structure cannot capture the full chemical significance of a protein. To understand how a protein functions at a mechanistic level of detail requires measuring in real time the nuclear motion that accompanies its function. Time-resolved protein crystallography represents the most powerful tool for achieving this experimental objective. While time-resolved crystallographic measurements have been conducted with time resolution as short as 150 ps, Figure 3-2 demonstrates that global structural changes have already occurred at the earliest time delay [13]. To observe and understand how a local perturbation propagates from the epicenter of the distortion to points far removed will require X-ray pulse durations and amplitudes only achievable with linac-based sources. By extending the time resolution of these measurements into the femtosecond regime, the ability to observe how a local distortion can be channeled into a concerted global structural change will be possible for the first time.

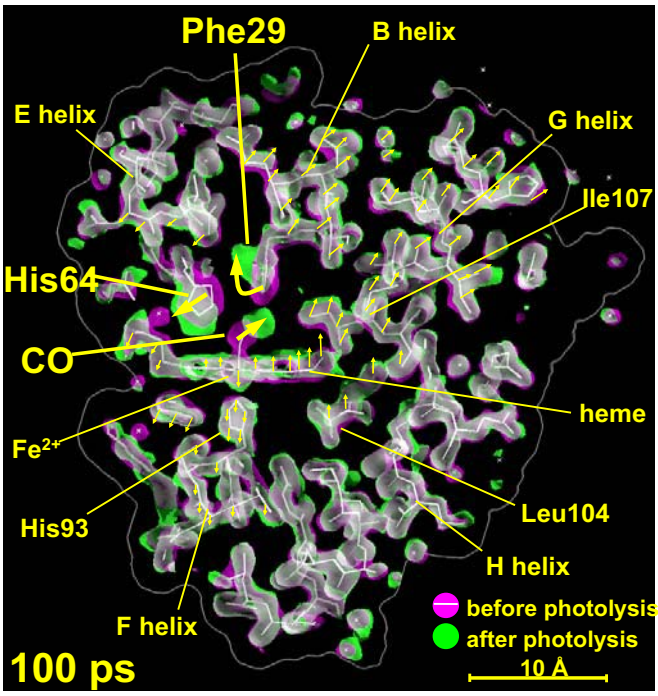

Figure 3-2. Experimentally determined electron densities of the myoglobin molecule before and 100 ps after photolysis [13].

3.2. INSTRUMENT DESCRIPTION

The pump-probe instrument will predominantly use a fast optical laser to generate transient states of matter, and the hard X-ray pulses from the LCLS to probe the structural dynamics initiated by the laser excitation. The laser pump will have the ability to conduct precise optical manipulations, in order to create the desired excited states. The instrument design will emphasize versatility. To maximize the range of phenomena that can be excited, it will be necessary to be able to manipulate the laser pulse energy, frequency, and temporal profile. X-ray scattering will be the dominant tool for probing the laser-induced structural changes, while X-ray absorption and emission spectroscopy will probe changes in electronic structure. These experiments require the union of four experimental capacities: the generation and delivery of X-ray and laser pulses to the sample, the preparation of the excited state in the sample, and the detection of the X-ray scattering pattern or X-ray absorption and emission.

3.2.1. Pump-Probe Techniques

"Traditional" Pump-probe: Traditional pump-probe techniques will be used when the experimental phenomena being probed has a characteristic time scale that is longer than the ~ 1 ps inherent X-ray/laser jitter. For this class of experiments the temporal evolution of the system will be traced by delaying the arrival time of the laser with respect to the FEL radiation with time steps greater than 1 ps. This can be accomplished either by changing the optical path length of the laser system with a mechanical delay line or by changing the RF reference phase that the laser is stabilized to using a microwave phase shifter. Thus, the data is acquired sequentially in a controlled manner. A schematic of this concept is displayed in Figure 3-3. A ~ 1 ps temporal resolution is achievable using this method.

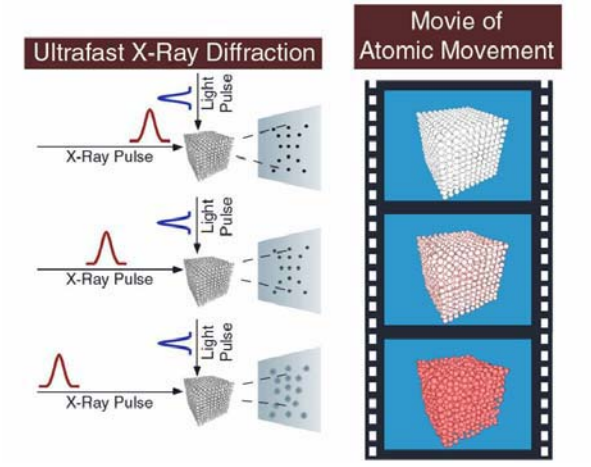

Figure 3-3. Schematic representation of a time-resolved X-ray scattering experiment. The time evolution of the photo-induced process is measured by taking snapshots of the sample as the delay between the laser pump X-ray probe is sequentially varied in a controlled manner [14].

Single Shot Geometry: Femtosecond temporal resolution is needed for many proposed XPP experiments. The temporal resolution can be increased to this level, for some experiments, by implementing a single shot diffraction geometry [10][15][16]. Figure 3-4 displays the general concept of this technique. The X-ray and optical laser pulses impinge on a crystal surface non-collinearly. The incidence angle difference causes the X-ray probe to sweep across the crystal surface at a different rate than the optical laser. Thus, a range of pump-probe delays is imprinted across the crystal surface. The image of the diffraction spot is captured with an X-ray area detector and the temporal information is encoded along a spatial dimension of the spot.

The ability to acquire a range of time points in a single shot is critical for samples that exhibit non-repetitive response to photoexcitation. It is also advantageous to use this experimental technique when the optical laser induces irreversible alterations to the sample. In these instances the sample must be translated after every optical laser pulse and it is beneficial to acquire as much information as possible for each X-ray pulse since there is a limited amount of sample.

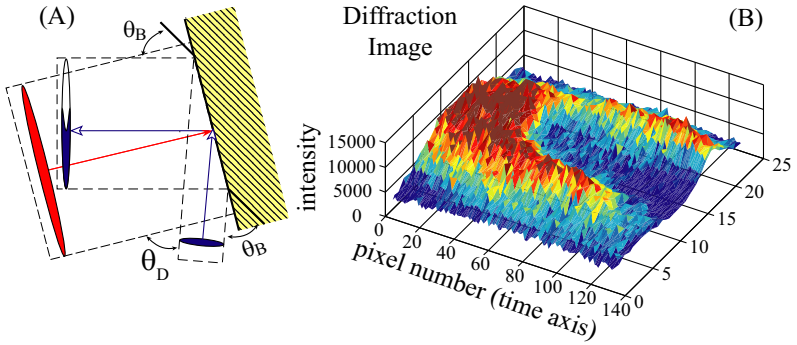

Figure 3-4. Single shot imaging technique used for studying irreversible dynamics in InSb at the SPPS [10]. The path of the laser pulse in red and the X-ray pulse in blue appear (A). The crossed-beam geometry results in a time delay sweep across the surface of the crystal, mapping time delay into a spatial coordinate. By imaging the diffracted intensity, a range of time delays can be measured with a single pulse pair, as shown in (B). The reduction in diffraction intensity in the center of the image resulted from laser induced disordering of the InSb crystal.

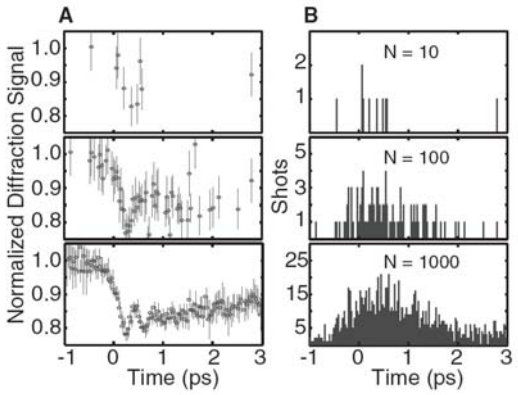

Figure 3-5. X-ray data acquired using non-sequential techniques at the SPPS [11]. Time-resolved X-ray diffraction data is displayed in (A) and corresponding timing histograms in (B) after 10, 100 and 1000 pulse pairs.

Non-sequential Sampling: Many experiments that require femtosecond temporal resolution cannot be performed in single shot geometry due to insufficient signal-to-noise ratio, sample geometry, sample type or X-ray scattering technique used. A diagnostic is required for these situations to cross-correlate a portion of the optical laser pump with the X-ray probe on a shot-by-shot basis. In this manner, the pump-probe timing is measured for every pulse pair and the intrinsic temporal jitter is used to sample the temporal evolution of the studied system non-sequentially (see Figure 3-5). However, a hard X-ray/optical laser cross-correlation technique with sufficient temporal resolution and signal-to-noise ratio appropriate for single shot operation has yet to be realized. Technical advancements are being made in the XUV spectral regime at the FLASH facility but it is unclear if these techniques can be extended into the hard X-ray regime [17],[18]. A robust timing diagnostic was developed at the Sub-Picosecond Pulse Facility (SPPS) facility that measured the relative timing of a femtosecond optical laser with respect to the SLAC electron bunches using electro-optic sampling [19]. A similar diagnostic will be implemented in the LUSI project to obtain femtosecond timing information for all LCLS endstations. The details of the electro-optic timing diagnostic are discussed in Chapter 7.

3.2.2. Overall Concept Layout

Figure 3-6 displays a block diagram of the XPP instrument. The main components are the offset double-crystal monochromator, X-ray optics, X-ray diagnostics, ultrafast laser system, X-ray diffractometer system, detector and small angle scattering beamline. Most of the components will be able to translate between the monochromatic beamline and direct beamline, dependent upon the requirements of a particular experiment. Component specifications are summarized in Table 3-1.

The beamline components will be constructed with a common vacuum interface and working distance, whenever possible, to permit the interchanging of components. This design requirement will maximize the flexibility of the experimental configuration. This capability is important since some experiments will require a particular ordering of the beamline components that may deviate from the normal beamline configuration.

The majority of the components comprising the ultrafast laser system will reside in the laboratory space above the X-ray hutch on the second floor of the NEH. A vacuum optical transport line will deliver laser radiation to the optical tables within the XPP hutch. Pulse compression and frequency conversion optics will reside in the XPP hutch.

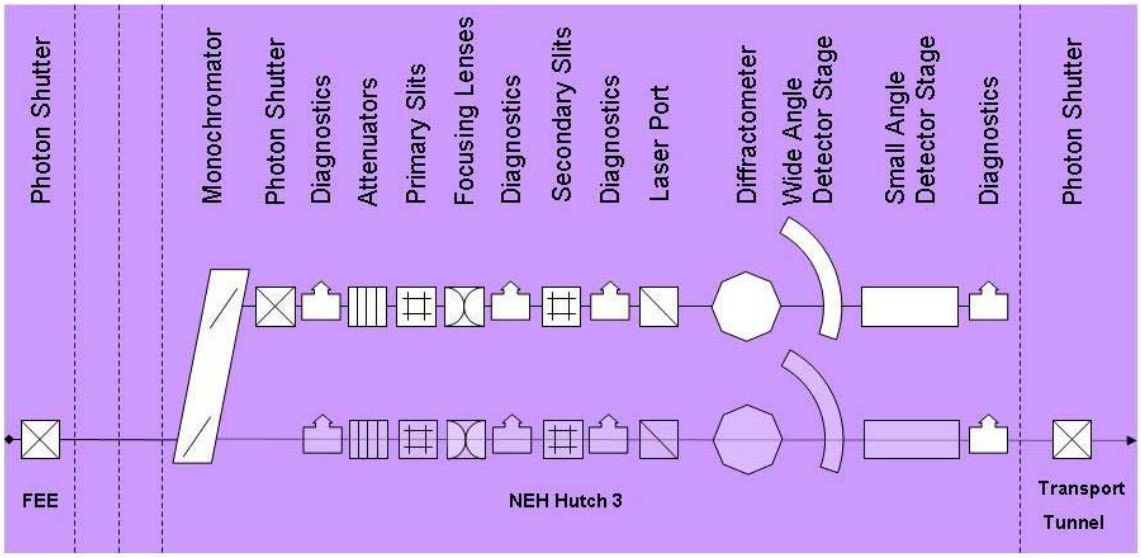

Figure 3-6. Block diagram of the XPP instrument. Transparent blocks represent items that are transferable from the monochromatic beamline to the direct beamline.

Item	Purpose	Specification
Offset Monochromator	Multiplex FEL radiation, narrow FEL spectrum	$\leq 10^{-4}$ spectral bandwidth, 600 mm horizontal offset
Slit System	Define X-ray beam size	5-5000 μm gap, 1 μm accuracy
Attenuator System	Control incident intensity onto sample	Up to 10^6 attenuation at 1.5 Å, 4 steps per decade
Diagnostics	Intensity monitor, position monitor	0.1% relative intensity measurement, < 5% incident X-ray attenuation
Refractive Focusing Lenses	Increase incident X-ray fluence	2-10 μm, 40-60 μm spot size at 1.5 Å, 2-10 μm spot size at 0.5 Å
Laser System	Photoexcitation of samples	Ultrafast pulse duration (≤ 50 fs), Up to 20 mJ pulse energy at 800 nm, 120 Hz repetition rate
X-ray Diffractometer System	Orient samples and move detector in reciprocal space	Spherical detector motion at a 10-150 cm radius, Kappa diffractometer, platform diffractometer
Small Angle Scattering Section	Collect SAXS patterns	2.5, 5, and 10 m sample-to-detector dist., 0.5 m horizontal detector motion
2D X-ray Detector	Provide 2D pixelated detection capability	1024x1024 pixels, 120 frame/s, 10^4 dynamic range, 90x90 μm^2 pixel size

Table 3-1. System specification for XPP instrumentation.

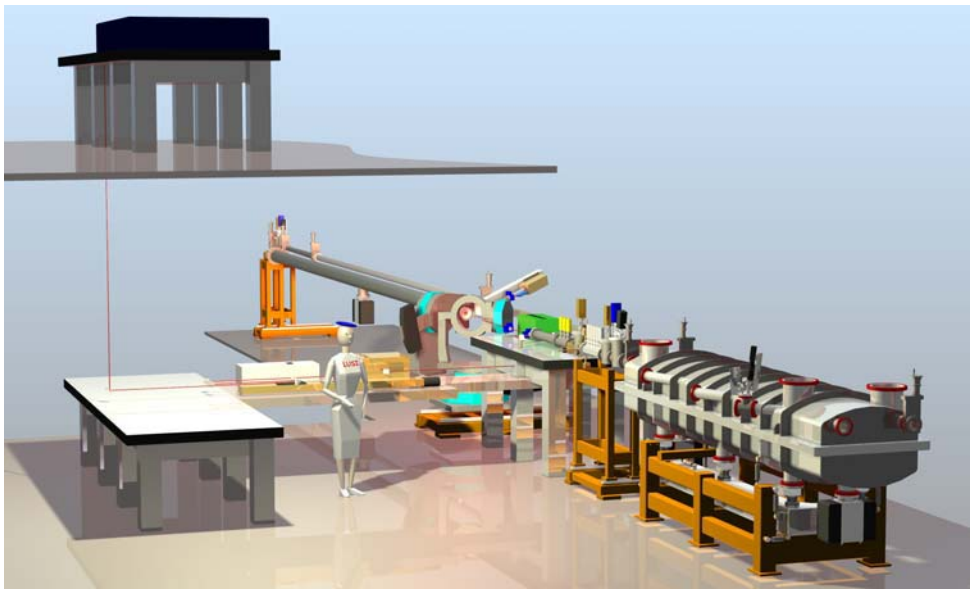

Figure 3-7. Conceptual schematic of the XPP instrument.

3.2.3. XPP X-ray Beam Parameters

X-ray beam parameters such as the beam size, intensity, pulse duration, position, arrival time and wavelength are critical for XPP experiments. These parameters must be either well defined or measured on a pulse-by-pulse basis to ensure experimental success. The X-ray optics and diagnostics described in Chapters 6 and 7 will be used to tailor these parameters to meet the requirements for each XPP experiment.

The nominal FEL beam size at the entrance of NEH hutch 3 is expected to be 170 μm FWHM. Beryllium lens assemblies will be implemented in the XPP instrument to reduce the FEL spot size at the sample. The lens system will be designed with a ~ 4 m working distance and will contain multiple lens assemblies which will allow focusing of multiple FEL harmonics. The design parameters of the lens assemblies are displayed in Table 3-2. Tuning of the X-ray spot size could be achieved by altering the working distance of the lens assembly. A motorized translation of 0.3 m is specified and will permit an order of magnitude spot size variation (see Figure 3-8).

Name	Energy	# of Lenses	Focal Length	Lens-to-Sample distance	Transmission	FWHM Spot Size at Sample
BCRL1	8.3 keV	5	4.1 m	3.95- 4.25 m	41%	1.5 -10 μm
BCRL2	8.3 keV	4	5.2 m	3.95 - 4.25 m	45%	40 - 60 μm
BCRL3	24.9 keV	45	4.1 m	3.95 - 4.25 m	31%	1.5 -10 μm

Table 3-2. Design parameters of the three beryllium compound refractive lens assemblies to be constructed for the XPP instrument. A variable working distance will permit some tuning of the X-ray spot size at the fixed sample position.

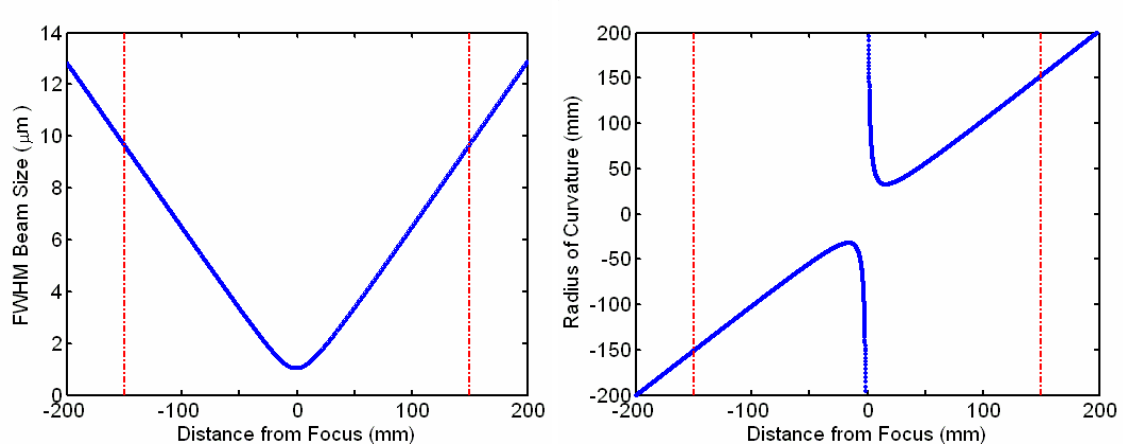

Figure 3-8. FEL beam size with use of a 4 m focus beryllium compound refractive lens and corresponding wavefront curvature as a function of distance from the focus. The red lines represent the tuning range of the lens assembly working distance.

A double-crystal monochromator system, described in Section 6.1, will be installed in the XPP instrument. The XPP monochromator serves three purposes: reduce the spectral bandwidth of the FEL radiation, multiplex a portion of the FEL radiation to allow concurrent experiments to be performed, and produce a diagnostics beam. As described in Section 3.2.1, no X-ray cross-correlation technique currently exists to measure the temporal profile or relative arrival time of the FEL radiation with femtosecond resolution. The development of such a technique will be critical to the long-term success of the LCLS and it is expected that this diagnostic will eventually be fully integrated into the XPP instrument. The cross-correlation diagnostic may be a destructive X-ray measurement or it may require differing X-ray beam parameters than those needed for a particular XPP experiment. Thus, a separate X-ray beam may be required to integrate an X-ray correlation technique into the XPP instrument. This diagnostic beam can be realized by using thin Bragg reflectors within the XPP double-crystal monochromator (see Figure 3-9).

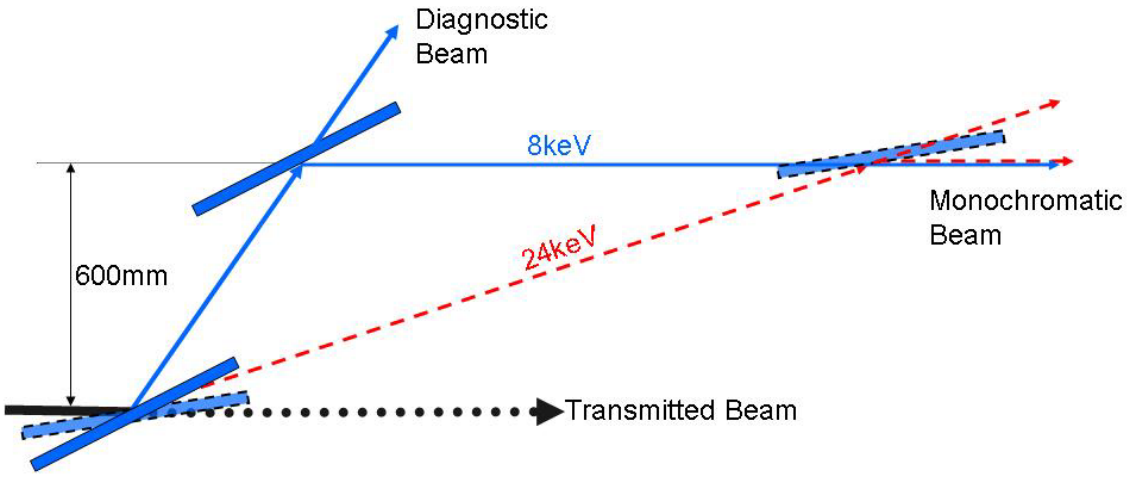

Figure 3-9. Large-offset and fixed-exit thin-crystal monochromator performing at 8 or 24 keV. The offset is 600 mm. The blue and red ray traces represent 8 keV and 24 keV respectively. Thin crystals are used to multiplex the incident beams.

3.2.4. Laser System

Lasers: A chirped pulse amplification laser system will provide the excitation pulse to initiate time-resolved phenomena for the XPP instrument. This system will consist of a Ti:Sapphire oscillator, regenerative amplifier, multipass power amplifier, optical parametric amplifier (OPA), harmonic crystals and temporal pulse shaper. This configuration will permit flexibility of the wavelength, excitation level and temporal profile of the laser pulses used to photo-excite various materials and meets the requirements set forth by the XPP team leaders. Figure 3-10 displays the possible operational configurations of the XPP laser system.

The oscillator will seed a regenerative amplifier, operating nominally at 120 Hz, where the pulse energy is amplified to > 2.5 mJ. The pulse duration shall be < 50 fs and the pulse-to-pulse energy stability shall be < 1% rms. The XPP experimentalists will thus have the option of using the fundamental radiation for sample excitation, or to change the frequency either through parametric amplification or harmonic generation, or to further amplify the fundamental in a multi-pass amplifier.

The performance of the OPA will be limited by the pulse-to-pulse energy stability and spatial mode quality of its input pulses. For example, an input pulse rms energy stability < 1% and M^2 < 1.2 are specified for the TOPAS model OPA distributed by Light Conversion Ltd.[20]. The only commercially-available Ti:Sapphire laser systems that currently meet the rms energy stability requirement are regenerative amplifier based systems [21][22]. However, the mode quality of these systems is specified at M^2 < 1.5 and thus an external spatial filtering system may be required to meet the OPA specification.

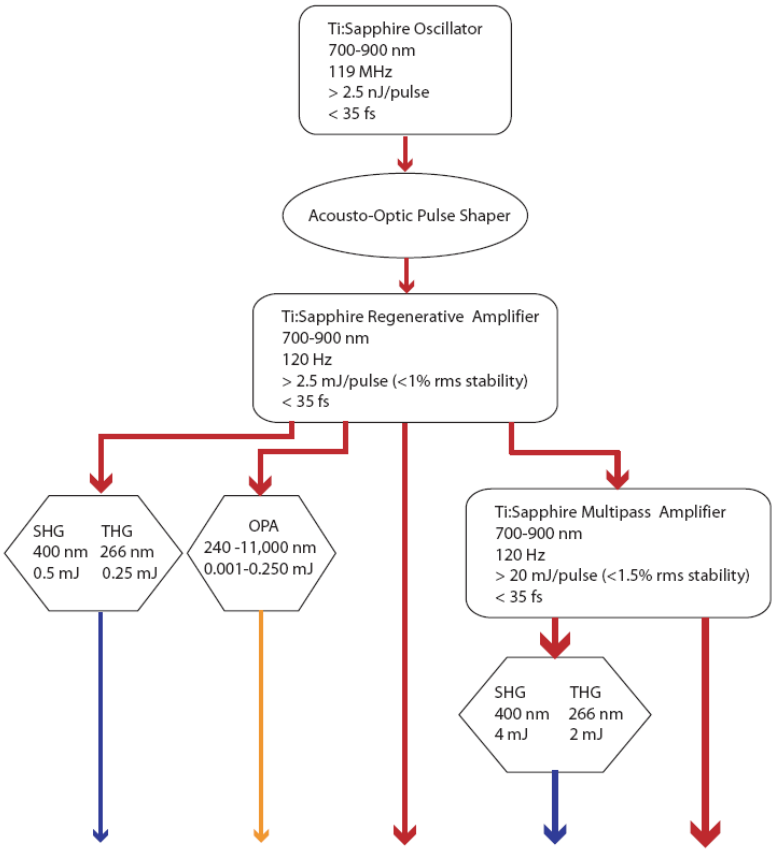

Figure 3-10. Operational configurations of the XPP laser system.

A 2nd stage multi-pass power amplifier, operating at 120 Hz, is included in the XPP laser system. This stage will increase the pulse energy to 20 mJ with a pulse-to-pulse energy stability < 1.5% rms. This level of pulse energy and stability can be achieved through use of the high-energy diode-pumped solid state lasers, as has been demonstrated at the LCLS gun laser [23]. The user then will have the option of exciting the sample with the fundamental wavelength or to convert to a harmonic. This stage will be implemented when high excitation pulse energy is needed.

The ability to shape the temporal profile of the laser pulse in a sophisticated manner was requested by the XPP team in order to perform coherent control experiments. An acousto-optic pulse shaper is specified to allow this capability. This device will be inserted between the Ti:Sapphire oscillator and regenerative amplifier when pulse shaping is required.

Laser Optics and Optomechanics: Ultrafast-grade optics (mirrors, waveplates, polarizers, lenses, windows and beamsplitters) spanning the wavelength range of 240 nm - 11 μm are required to deliver laser radiation to the XPP samples and to the various laser diagnostics. Automated control of a portion of the laser optics will allow remote user control of the intensity, position, polarization and temporal profile of the excitation pulse. Additionally, a 3-meter retro-reflecting delay line is specified that will allow any arbitrary pump-probe time delay to be achieved. The stage will provide 10 fs step precision and repeatability (1.5 μm in the retro-reflecting geometry).

Layout: It is advantageous to house the lasers in the designated laser room on the 2nd floor of the NEH (directly above the experimental hutches) due to the complexity of these systems. This will permit tuning and maintenance to be performed without interruption of X-ray operation in the experimental hutches as well as all-optical experimentation. A transport system that delivers the beam from the laser room to the experimental hutch must be designed to accommodate this configuration. A relay imaging system will be implemented to preserve the spatial mode quality of the beam. Since the beam must go through a focus in such a relay imaging system, a portion of the transport must be performed in vacuum to prevent the occurrence of non-linear effects that may degrade the laser characteristics. In addition, the compression stage of the amplifier will be replicated in the experimental hutch to allow the pulses to be transported uncompressed. A pointing stability feedback system, identical to the system designed for the LCLS gun laser transport, will be installed to mitigate the effects of laser pointing instabilities that occur when transporting the beam over long distances.

The OPA will be housed in the experimental hutches since compressed fundamental pulses are required to seed the OPA. This configuration limits the transported laser wavelengths to the Ti:Sapphire fundamental (700-900 nm) and has the advantage that the transport optics do not need to be altered when a wavelength other than the fundamental is required for the experiment. However, the difficulty of pumping an OPA system at a distance of 10 m from the pump laser is a primary concern. An optical table assembly that can accommodate the entire laser system has been specified for the experimental hutch to mitigate this risk associated with OPA operation.

Laser enclosures will be implemented throughout the optical system and will contain all of the laser optics and diagnostics. The enclosures will serve the purpose of reducing the risk of accidents as well as providing an environment for the optics and optomechanics that is shielded from air currents, acoustic noise, dust and unintended bumping.

Laser Timing: The Ti:Sapphire laser oscillator, operating at a 119 MHz repetition rate, will be actively stabilized to the RF signal used to synchronize the accelerating components of the SLAC linac. A 100 fs rms phase jitter between the laser pulse train and the RF, integrated from 1 Hz to 10 kHz, is desired. This phase jitter, along with the X-ray pulse phase jitter with respect to the RF, will determine the ultimate temporal resolution of the majority of the XPP experiments without the use of advanced timing techniques.

An electro-optic timing diagnostic will be used to improve the temporal resolution of the XPP instrument below the jitter limit. This diagnostic was used successfully at SPPS [12]. The details of the diagnostic are described in Section 7.2.5.

Laser Diagnostics: Diagnostics that monitor and record the pulse temporal profile, pulse energy, and spectrum on a shot-by-shot basis are included in the XPP laser system. Additional diagnostics to characterize the spatial profile and the contrast ratio (for pulse pedestal, pre-pulses and post-pulses) are included as well. This suite of laser diagnostics will be critical to the operation of these laser systems and thus to the overall performance of the experimental station.

3.2.5. Diffractometer System

The XPP diffractometer system, consisting of a sample manipulator and detector mover, will be the primary piece of instrumentation used to acquire data for the XPP station. The diffractometer will be designed to operate in both the direct beam and monochromatic beam. A precision translation platform will move the diffractometer system between the two beamlines.

Detector Motion: Most experiments performed at the XPP instrument will require the movement of an X-ray detector about the sample. In particular, it will be necessary to remotely move a detector along a spherical surface centered at the sample region. The radius of the detector sphere must be optimized on a per experiment basis and thus a variable radius spanning 10 cm to 1.5 m is needed. The precision and repeatability of this motion is set by the pixel size of the XPP detector (90 μm).

Two solutions are being considered to satisfy the detector motion requirements. The first solution utilizes a pair of orthogonal rotation stages and a translation stage. These devices are typically integrated with the sample manipulation instrumentation to create a '6-circle' diffractometer (see Figure 3-11). A second solution that implements a robotic arm to move the detector is also under consideration. Unique strengths for each solution exist and will be investigated before the final technological decision is made.

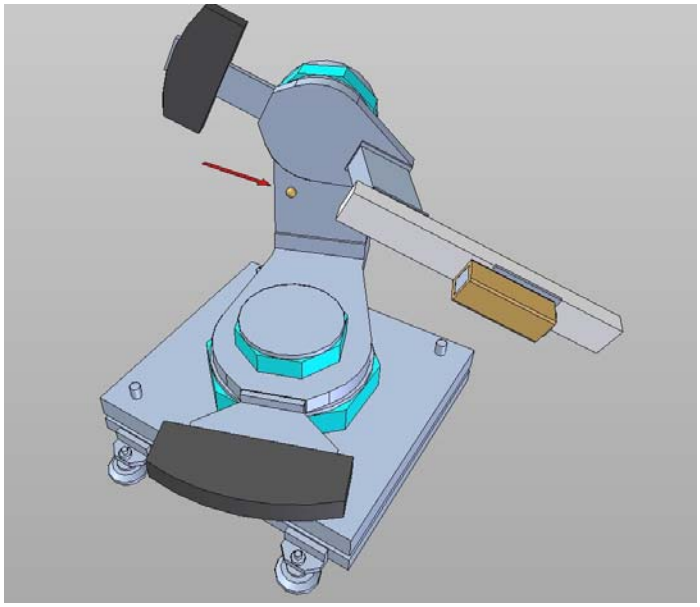

Figure 3-11. Conceptual image of the detector arm of the XPP diffractometer system.

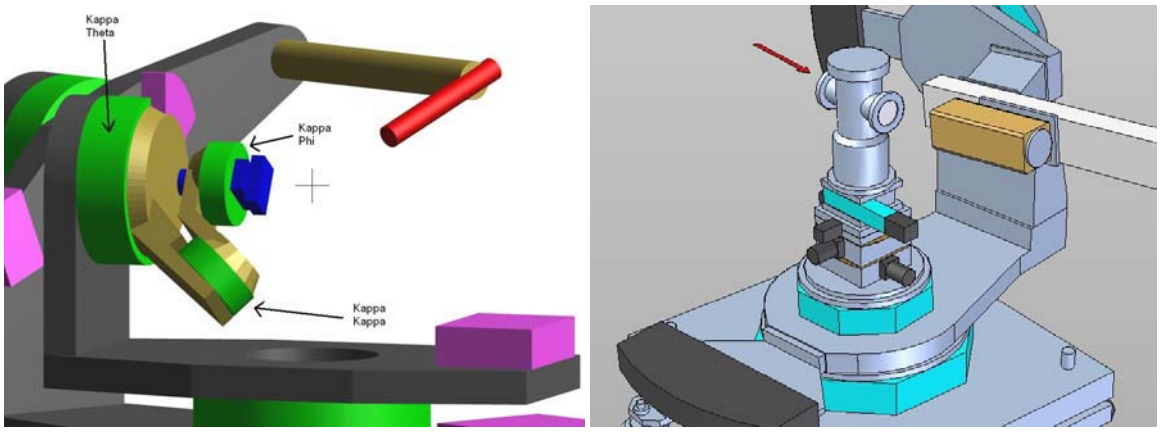

Figure 3-12. Conceptual image of the kappa and platform difractometer configurations for the XPP instrument. The kappa is on the left and the platform on the right. The image of the kappa diffractometer was acquired from the ID32 surface scattering beamline website of the ESRF [24].

Sample Manipulation: The types of samples that will be studied with the XPP instrument include, but are not limited to, single crystals, organic crystals and liquids. The manipulation requirement for each type of sample varies dramatically. Thus, the ability to accommodate a wide variety of samples, sample geometries and sample environments is a primary design criterion for the sample diffractometer.

Some of the studies that will be performed at the XPP instrument will involve the measurement of Bragg reflections from single crystal samples. Thus, precise control of the complete sample orientation in the rotational degrees of freedom is required. Further constraints are placed on the sample orientation when the laser excitation pulse is introduced since it may be necessary to maintain a particular X-ray and/or laser incidence angle while accessing a region in reciprocal space. In addition to providing the rotational motions for sample orientation, the XPP sample manipulator will have the capability to precisely translate the sample along the two axes perpendicular to the incident X-ray beam. This capability is critical for experiments performed at high photoexcitation densities where the sample is permanently damaged by a single excitation pulse. When performing studies in this excitation regime the sample must be translated so the subsequent excitation pulse is incident upon a previously un-excited region of the sample. This translation must maintain the sample orientation with respect to the X-ray beam.

The current XPP sample diffractometer concept employs a modular approach to meet this requirement. Two separate components are designed to interface onto a rotation stage: a kappa goniometer and a platform. Figure 3-12 displays a conceptual schematic of the two possible configurations of the XPP diffractometer. The configuration choice will be made based of the requirements of a particular experiment and will largely be determined by the accessibility of reciprocal space needed, the proximity of other equipment to the sample, size of the sample, and environment of the sample (vacuum, temperature, pressure, etc.).

Small Angle Scattering Capability: The XPP instrument will have small-angle X-ray scattering (SAXS) capability. An alcove in the XPP hutch will permit a sample-to-detector distance of 10 meters, along with two discrete intermediary distances (2.5 m and 5 m). A translation platform will be constructed to remotely move the detector at these locations perpendicular to the X-ray beam propagation direction. A large diameter vacuum beam pipe will allow scattered radiation to reach the detector without significant attenuation. The entire SAXS assembly will be capable of operating in both the monochromatic and direct FEL beam path. Figure 3-13 displays a conceptual image of the SAXS alcove.

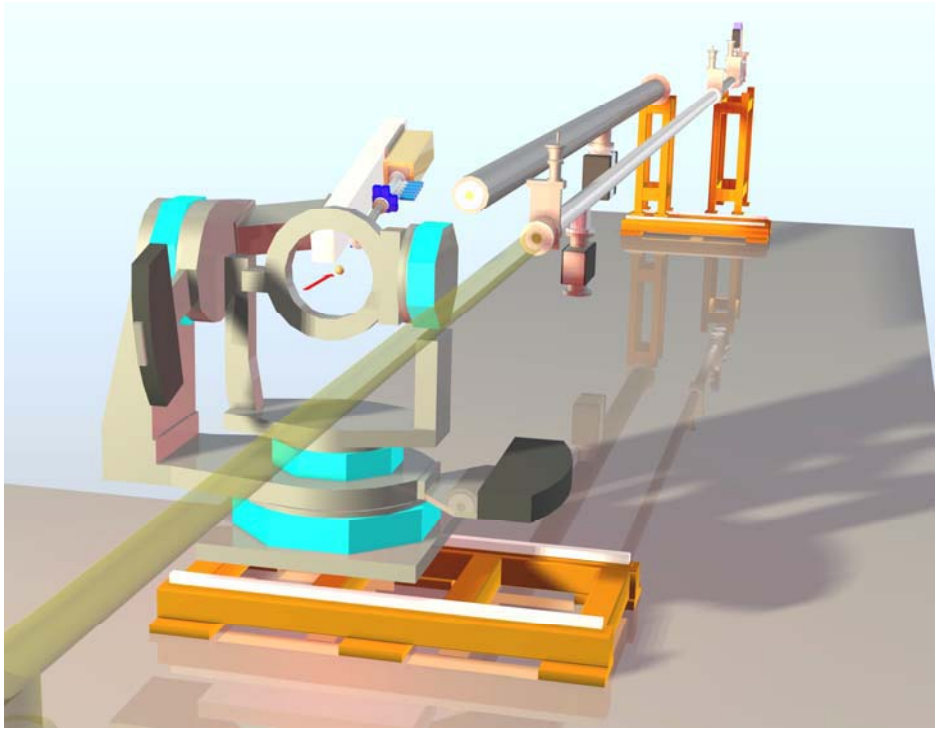

Figure 3-13. Conceptual schematic of the small angle scattering alcove for the XPP instrument.

Temperature-Controlled Sample Environment: Two separate temperature regulating devices are envisioned for the XPP instrument. The first is a vacuum cryostat system. This device will be used in conjunction with the platform configuration of the XPP diffractometer and will have cooling capability down to 20 K with a 7 W capacity. However, some restrictions will be placed upon the accessible reciprocal space solid angle since the cryostat will operate in a vacuum environment and windows must be used. Certain experiments, in particular experiments involving organic samples, require a large reciprocal space access in addition to modest cooling capacity. A cryostream will be used for this class of experiments with the kappa goniometer.

3.2.6. XPP 2D Detector System

2-Dimentional Detector System: An X-ray active matrix pixel sensor (XAMPS) is being developed by Brookhaven National Laboratory for the XPP instrument since a detector system with the required characteristics is not commercially available. It will include an array of 1024 x 1024 pixels with a pixel size of 90x90 μm^2. To support the breadth of experiments that will be performed at the XPP station, the detector must have the ability to detect a single X-ray photon with high efficiency as well as measure a slight change in an intense Bragg reflection. To accommodate these requirements, the detector will have high quantum efficiency (approaching unity at 8 keV) and a 10^4 dynamic range per pixel. A summary of the detector parameters is presented in Table 3-3.

The LCLS will be a highly fluctuating source even when maturely commissioned. The successful execution of the experiments at the X-ray pump-probe instrument will be limited by the ability to mitigate these source fluctuations through diagnostics. It is therefore necessary that both the pixel array detector and the diagnostics operate on a pulse-by-pulse basis, since integration over the source fluctuations cannot be performed. Thus, the readout rate of the detector must accommodate 120 Hz operation to take advantage of

the full LCLS repetition rate. The expected readout rate of 1 kHz for the XAMPS detector meets this requirement.

The XAMPS detector is a semi-monolithic device. A pixelated high-resistivity silicon sensor, 500 μm thick, serves as the detection volume where incoming X-rays are converted into electrons. The number of detected X-rays is deduced from the integrated charge per pixel. A switching transistor is integrated on the silicon bulk in each pixel to release the charge for readout. A separate readout ASIC contains a charge-sensitive amplifier with two gain settings to accommodate the large dynamic range. The analog signals coming from the readout chip are multiplexed and digitized in a 12 bit ADC. The XAMPS is read out one row at a time (1024 pixels), resulting in a total readout time of ~1 ms per frame.

The following technical challenges will be addressed by the XPP detector development team:

- Engineering the readout ASIC to have a large dynamic range while maintaining single photon sensitivity.
- Overcoming the fabrication complexities associated with integrating a switching transistor into each pixel.
- Sustaining a 2 Gbit/s peak data rate throughout the readout and storage process.
- Engineering a data acquisition board that will merge beam diagnostics data and perform real time data processing.

Parameter	Specification
Energy Range	4-24 keV
Well-depth/pixel	10^4
Readout Frame Rate	> 120 Hz
Quantum Efficiency	> 90% at 8 keV
Noise	< 1100 electrons rms per pixel
Pixel Size	90 μm x 90 μm
Detector Area	1024x1024 pixels

Table 3-3. Detector specifications for the XPP instrument.

Dispersive X-ray Spectrometer: A dispersive X-ray spectrometer will be constructed for time-resolved X-ray emission (XES) and resonant inelastic X-ray scattering (RIXS) experiments. A conceptual design is displayed in Figure 3-14. This spectrometer will have an energy resolution of ~ 1 eV FWHM and spectral dynamic range of 50 to 100 eV, sufficient to observe the K_β or the K_α emission lines [25]. Current non-dispersive X-ray emission analyzers have collection efficiencies of better than 10^{-6}. Given the high flux of the LCLS, the potential exists for measuring a full spectrum with a single pulse.

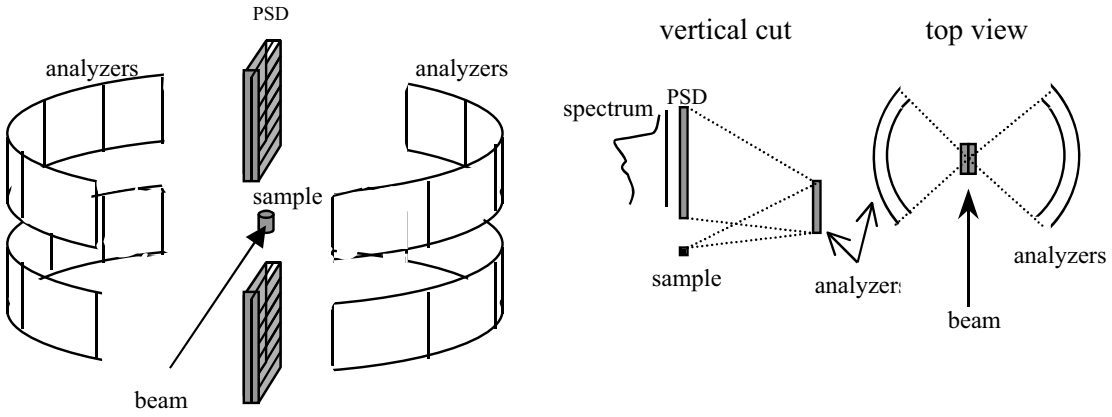

Figure 3-14. Schematic setup of a dispersive X-ray spectrometer for the XPP instrument. Four arrays of cylindrically curved crystals sagitally focus the X-ray emission onto position sensitive detectors [25]. The emission spectrum is dispersed along the vertical axis of the detectors. The apparatus will be rotated by 90° for RIXS experiments.

3.3. REFERENCES

[10] A. M. Lindenberg et al., *Science*, **308**, 392-395 (2005).
[11] D. M. Fritz et al., *Science*, **315**, 633-636 (2007).
[12] H. Ihee, M. Lorenc, T.K. Kim, Q.Y. Kong, M. Cammarata, J.H. Lee, S. Bratos and M. Wulff, *Science*, **309**, 1223-636 (2005).
[13] F. Schotte, M. Lim, T.A. Jackson, A.V. Smirnov, J. Soman, J.S. Olson, G.N. Phillips, M. Wulff and P.A. Anfinrud, *Science*, **300**, 1944-1947 (2003).
[14] Credit, C.W. Siders, http://www.sciencemag.org/cgi/content/full/286/5443/1310.
[15] R. Neutze and J. Hajdu, *Proc. Natl. Acad. Sci. U.S.A.*, **94**, 5651-5655 (1997).
[16] O. Synnergren, M. Harbst, T. Missalla, J. Larsson, G. Katona, R. Neutze and R. Wouts, *Appl. Phys. Lett.*, **80**, 3727-3729 (2002).
[17] S. Cunovic, N. Muller, R. Kalms, M. Krikunova, M. Wieland, M. Drescher, Th. Maltezopoulos, U. Fruhling, H. Redlin, E. Plonjes-Palm and J. Feldhaus, *Appl. Phys. Lett.*, **90**, 12112 (2007).
[18] P. Radcliffe et al, *Appl. Phys. Lett.*, **90**, 131108 (2007).
[19] A. L. Cavlieri et al, *Phys. Rev. Lett.*, **94**, 114801(2005).
[20] Datasheet HE-TOPAS by Light Conversion Ltd. (2007).
[21] Datasheet Legend Elite USP by Coherent, Inc. (2007).
[22] Datasheet Spitfire® Pro by Spectra-Physics (2007).
[23] Datasheet Jedi by Thales Laser (2007).
[24] http://www.esrf.eu/UsersAndScience/Experiments/SurfaceScience/ID32/
[25] U. Bergmann and R. Frahm, TDR XFEL workshop series "Methods and Instrumentation for the XFEL", J. Hastings and Th. Tschentscher, eds., **52**, (2001).

4 - COHERENT X-RAY IMAGING

X-ray scattering has long been used to determine atomic structures of biomolecules. The X-ray dose needed to achieve a given resolution for a particular sample can be calculated. It is easy to show that the dose required to image a single molecule is much larger than the dose required to completely destroy the molecule through radiation damage processes. X-ray crystallographers mitigate this problem by spreading the damage over billions of molecules in a single crystal, greatly enhancing the diffraction signal. Since the molecules are all identical and precisely aligned in the crystal, the X-ray scattering information is preserved and the structure can be determined.

LCLS offers another way around the damage problem. Since the FEL X-ray pulse is very intense and very short, it is possible in principle to deliver the required dose to a nano-scale sample and record the scattered X-ray information before the damage processes have time to destroy the sample. In other words, an LCLS X-ray pulse could be focused onto a single molecule, which would be destroyed – but not before the scattered X-rays are already on their way to the detector carrying the information needed to deduce the image [26]. The Coherent X-ray Imaging (CXI) Instrument will offer the possibility of determining structures at resolution beyond the damage limit for samples which do not form crystals, including important classes of biological macromolecules.

4.1. SCIENTIFIC PROGRAMS

The unique characteristics of the photon beam provided by LCLS, such as the unprecedented peak brightness at hard X-ray wavelengths will present new possibilities to the field of X-ray imaging. The CXI instrument is designed to make optimal use of the LCLS FEL beam to allow for imaging of scientifically and technologically relevant nano-scale samples which cannot be imaged using currently available technology.

Reproducible biomolecules: Only a two-dimensional diffraction pattern will be collected from a single biomolecule before it is destroyed by the LCLS beam. Such a two-dimensional pattern encodes information about a projection image of the object onto a plane parallel to the detector plane. Three-dimensional structural information about highly-reproducible molecules such as viruses, large proteins or molecular complexes could be derived if a series of the molecules were delivered into the LCLS beam one after the other using a particle injector. Each injected molecule would have a different orientation and a full 3D diffraction data set could be obtained from a large number of identical copies of the molecule, complex or virus. Atomic or near-atomic resolution structures could be obtained for difficult to crystallize biomolecules. One of the challenges will lie in properly classifying each diffraction pattern in order to orient the patterns relative to each other in three dimensions. It would greatly reduce the data collection time and the signal level requirements if one could produce an aligned beam of particles. This might be achieved by hitting the particles with a non-resonant laser in the infrared range to align the particles along the polarization direction of the laser [27].

Small biomolecules attached to large known structures: Very small proteins, on the order of 10 nm or less will scatter only weakly which may lead to a signal-to-noise ratio (SNR) below what is necessary

for imaging. It is possible to attach such small proteins of unknown structure to larger known biomolecules such as large viruses. By binding each sample protein to a specific site on the large biomolecule, one could obtain a set of reproducible objects suitable for 3D imaging at LCLS. The large structure could act as a holographic reference and would be used to boost the SNR. The structure of the small protein could be recovered from the interference between the diffracted waves of the two objects.

Nanocrystals of proteins: It is often the case that large crystals of a certain protein cannot be grown but a large number of very small crystals can readily be obtained. These sub-micron crystals do not scatter enough X-rays to yield an atomic structure using conventional protein crystallography techniques. The high flux of LCLS will allow these to be used for structure determination. Assuming all the nanocrystals possess the same crystal symmetry, a series of nanocrystals could be illuminated by LCLS X-ray pulses and the diffraction patterns recorded. The variations in alignment of the crystal axes from sample to sample will be relatively straightforward to determine from the Bragg peaks in the diffraction patterns. A full 3D set similar to conventional protein crystallography will be built up and standard crystallography phasing methods will yield the protein structure. It will be possible to inject these nanocrystals directly into the beam and size-select them using a differential-mobility analyzer to select a set of similar crystals.

Nanoparticles: Technologically relevant nanoparticles such as quantum dots are difficult to image using existing X-ray sources due to their weak scattering. LCLS will make it possible to obtain two-dimensional projections of any non-reproducible nanoparticle and three-dimensional images of reproducible objects. Furthermore, the LCLS beam could be attenuated to a level slightly below the damage threshold of an inorganic nanoparticle and a full 3D reconstruction could be obtained from a single particle using multi-image tomographic techniques. The large transverse coherence length of the LCLS, coupled with a large detector area, will allow large particles to be imaged in 3D at near-atomic resolution.

Hydrated cells: Living cells are all unique at the atomic level. It will therefore not be feasible to obtain a full three-dimensional image of a cell at atomic resolution at LCLS since damage would occur to the single cell with a single exposure. However, LCLS will offer the capability to study fully hydrated cells beyond the damage limit in two dimensions. The cells will be injected sequentially into the X-ray beam and a 2D diffraction pattern will be collected from each LCLS shot. The rapid injection of the cell into vacuum would prevent them from drying out and they would remain fully hydrated during the measurement. The high peak flux of LCLS will make this measurement possible, since the cell will fly through the beam very quickly at speeds of up to 200m/s using the aerodynamic lens injection technology. The ability to image multiple similar copies in a short time will allow 2D high resolution structural information to be obtained about the main reproducible parts of the cell. High-resolution information will be obtained on important structural cellular transformations by injecting cells into the beam at different stages of a biological process. For example, a single cell organism being infected by a large virus could be studied by injecting cells directly into the LCLS beam at various times after the virus is introduced into the sample.

Radiation damage studies: The LCLS source will produce hard X-ray fields of unprecedented high intensity. It will allow for the first time tests of radiation damage models under such extreme conditions. These models [28][29], are directly relevant to atomic-resolution imaging since the damage suffered during a pulse must be limited or the reconstruction will suffer. Objects such as viruses of known structure or well-characterized nanoparticles will be mounted on X-ray transmissive substrates or attached to thin fibers produced by electrospinning [30] to minimize unwanted scatter. Single pulse diffraction patterns from a sample containing multiple copies of the same virus will be measured at different fluence and pulse length values to gain a better understanding of the damage process and determine the necessary conditions for single-molecule imaging. These experiments will require a pulse picker to select a single FEL pulse to illuminate the sample.

Pump-probe imaging: It will be possible with the use of an optical pump laser to image scientifically relevant photo-induced changes in non-crystalline samples. For example, the explosion of a single particle such as a virus induced by a high power optical laser beam will be measured by hitting the particle, either mounted on a substrate or injected into the vacuum chamber with the laser beam at different time delays before the FEL pulse. The laser ablation of silicon is also technologically relevant and the explosion of thin silicon foils will be imaged in the same way.

Time-delay holography: How a biological sample explodes after interacting with the LCLS beam is not fully understood and will be studied using a new technique called time-delay holography [31]. In these experiments, a single FEL pulse will interact with the sample producing a prompt scattering pattern. Just beyond the sample, at a controllable distance, a mirror will be used to reflect the direct beam so it interacts with the sample a second time, producing a delayed scattering pattern. During the second pass, the sample will be undergoing a Coulomb explosion which we wish to study. The mirror will reflect the prompt scattering, as well as all the plasma emissions and Compton scattered photons from the first pass, although inefficiently. The samples will be mounted on a thin (20 nm) X-ray transmissive silicon nitride window attached to a silicon wafer. By using a very small window size (10-20 μm) most of the prompt scattered photons reflected from the mirror will be blocked by the wafer. In effect, only the back-reflected direct beam will come back through the window and onto the sample. One will thus measure only the delayed diffraction pattern from the exploding particle. For these experiments, the incident beam must first pass through a hole in the detector before impinging on the sample. The detector that will be used in the CXI instrument (shared with LCLS) will have a hole in the middle to let the damaging direct beam pass (see Section 4.2.5). The instrument will be designed to allow enough space for the detector assembly to be mounted upstream of the sample chamber to make these experiments feasible.

4.2. INSTRUMENT DESCRIPTION

Diffraction imaging is elegant in its experimental simplicity: a coherent X-ray beam illuminates the sample and the far-field diffraction pattern of the object is recorded on an area detector. The experiments performed on the CXI instrument are based on this simple geometry. With the full flux of LCLS impinging on it, the sample gets completely destroyed a short time after the pulse. The diffraction pattern can be recorded before the damage occurs with suitably short pulses. This is called flash imaging and was recently demonstrated at low resolution using longer-wavelength (32 and 13 nm) FEL radiation [32]. Since the goal of these experiments is to measure the diffraction from small weakly scattering samples, it becomes imperative to minimize the noise. Some experiments therefore require a container-less sample delivery to the LCLS beam. A particle injector which sends the particles into vacuum as a focused particle beam that intersects the FEL beam is a vital component of the instrument.

4.2.1. Coherent Imaging Technique

Figure 4-1 displays the envisioned experimental geometry for three-dimensional structure determination using coherent diffraction imaging. The fully-coherent pulse of X-rays from LCLS illuminates the sample, which is smaller than the beam, producing a continuous diffraction pattern. The particles are injected into the FEL beam (see Section 4.2) and are then destroyed in a Coulomb explosion. The diffraction pattern is recorded by a pixel array detector (see Section 4.2.5), which has the high quantum efficiency and dynamic range required to measure simultaneously the very high intensities near the center and the very weak intensities at high angles.

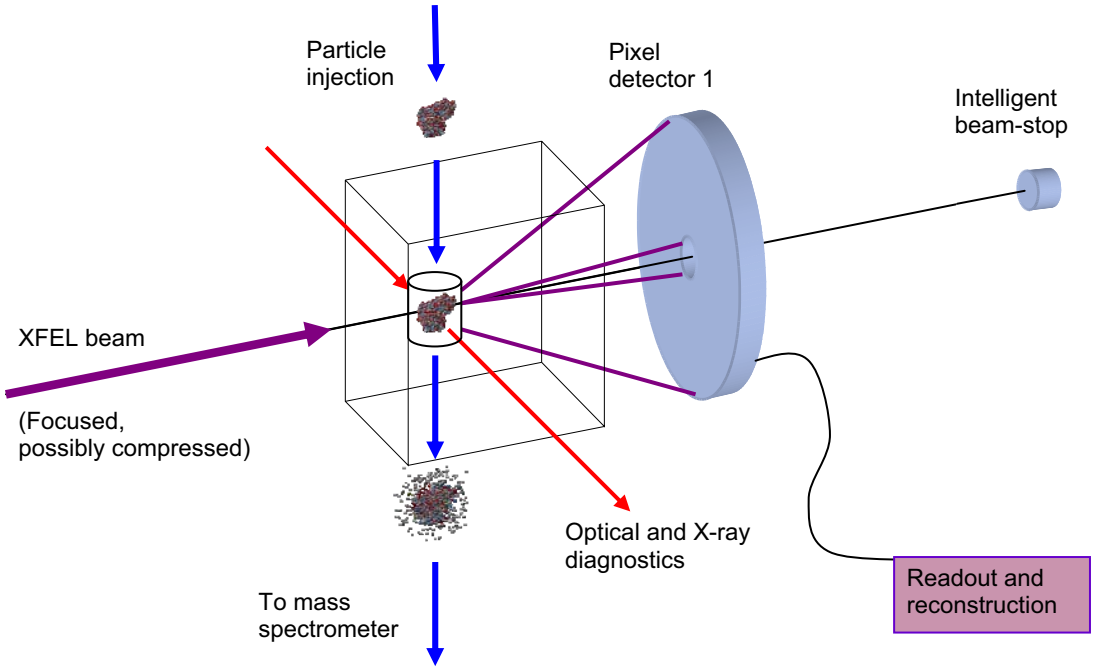

Figure 4-1. Schematic diagram of the single-particle diffraction imaging experiment at LCLS. Copies of a reproducible sample are exposed to the beam one by one in random orientations. A 2D detector records the coherent X-ray diffraction pattern. A 3D image of the sample can be reconstructed from the diffraction patterns

Oversampling: Each measured 2D diffraction pattern gives, within reasonable approximations, the square modulus of the Fourier transform of the projection of the electron density of the illuminated object onto a plane parallel to the detector plane. In order to retrieve the image of the object, the phases of the diffracted wave, which are not measured, must be recovered. To make this possible, all the necessary information about the object must be present in the diffraction pattern, which means all the spatial frequencies present in the object must be adequately sampled. The highest spatial frequency corresponds to the overall size of the object. Oversampling the signal relies on the knowledge of the presence of a zero density area around the object. With higher oversampling, the zero-density area becomes larger and this constrains the possible structures that can produce the measured diffraction pattern, leading to a unique possibility in the absence of noise for two and three dimensions [33].

Phase retrieval and image reconstruction: In principle (and this has been demonstrated multiple times [34][35][36]), the oversampled diffraction pattern can be inverted to obtain an image using phase retrieval computer algorithms. These algorithms solve the phase problem by iteratively projecting from the image plane to the diffraction plane, imposing known constraints at each step. The constraint in the diffraction plane is that the calculated diffracted amplitudes match the measured amplitudes. At the image plane, the simplest constraint arises from the oversampling, which creates a support where the object is non-zero, with everything outside the support equal to zero. Many variations of the algorithms exist, differing in the way the constraints are imposed [38]. The algorithms converge to a unique solution in the absence of noise for dimensions greater than 1, except for some pathological cases in two dimensions [33]. In the presence of noise, a set of often similar solutions can satisfy the set of constraints. The quality of the solution is determined by an error metric measure and when available, using prior knowledge about the sample.

Classification, averaging and orientation: Each 2D diffraction pattern can be inverted to yield a 2D projection of the object (and this may provide sufficient information for some applications). Three-dimensional imaging requires more than one view of the sample. Multiple 2D patterns with different orientations can be combined to create a 3D data set, which when inverted produces a full 3D image of the object. The 3D set will be obtained by recording the diffraction pattern from a different molecule with every pulse, at 120 Hz. The large number of images will then be post-processed and classified by grouping sufficiently similar images. Computer algorithms are being developed to identify images from similar orientations and average them together in order to increase the signal-to-noise ratio, which may be insufficient from a single shot. The storage and post-processing of a very large number of images will require very powerful computers and software development. The relative orientation of each set of averaged image will be determined from common lines between intersecting planes [37]. The phase retrieval for a 3D diffraction data set obtained through proper averaging of multiple images is performed in the same way as for two dimensions and has been demonstrated. The only difference is the longer computing time required to reach a solution with the larger data set. Practical algorithms exist that are very robust and allow *ab initio* reconstruction of 3D structures.

Resolution: Resolution in these diffraction experiments does not depend on sample quality in the same way as in conventional crystallography. Though the resolution is determined by the highest scattering angle at which there is a measurable signal, as in the case of conventional protein crystallography, this angle is not determined by the sample quality. The resolution of the reconstructed image is a function of radiation intensity, pulse duration, wavelength, and the extent of ionization and sample movement during the exposure [26][28][29]. The detector must be designed to allow for an acceptable compromise between oversampling and resolution.

4.2.2. Overall Concept Layout

Figure 4-2 displays a block diagram of the CXI instrument. The main components are the pulse compressor, pulse picker, Kirkpatrick-Baez (KB) mirror system, X-ray diagnostics and sample chamber including the particle injector, detector and post diagnostic wavefront sensor. Component specifications are summarized in Table 4-1.

The sample chamber will be flexible enough to accommodate a variety of sample supports and manipulators. It will also permit pump-probe studies by providing a port for the introduction of a laser pump pulse. A port for a laser alignment of particles is included.

The coherent X-ray imaging instrument is simple in concept: it will focus the LCLS beam onto the sample and then collect the diffraction patterns. Figure 4-3 shows a 3D drawing of the instrument concept. The focusing will be varied using one of two options. The first is to use three separate optical elements giving nominal beam focus sizes of 10, 1 and 0.1 μm. The second option is to use only the optical element producing a 0.1 μm focus, and to move the sample in and out of the focus to vary the beam size. The sample chamber will be evacuated to a pressure sufficiently low to reduce the background from the residual gas to a small fraction of that coming from the sample itself. The detector distance will be adjustable to accommodate a range of sample dimensions and resolutions. In addition various diagnostics including electron and ion time-of-flight detectors and an optical microscope will permit the observation of the results of the FEL-sample interaction and the subsequent Coulomb explosion. Diagnostics for the X-ray beam will be provided in order to characterize the incident beam on a pulse-by-pulse basis.

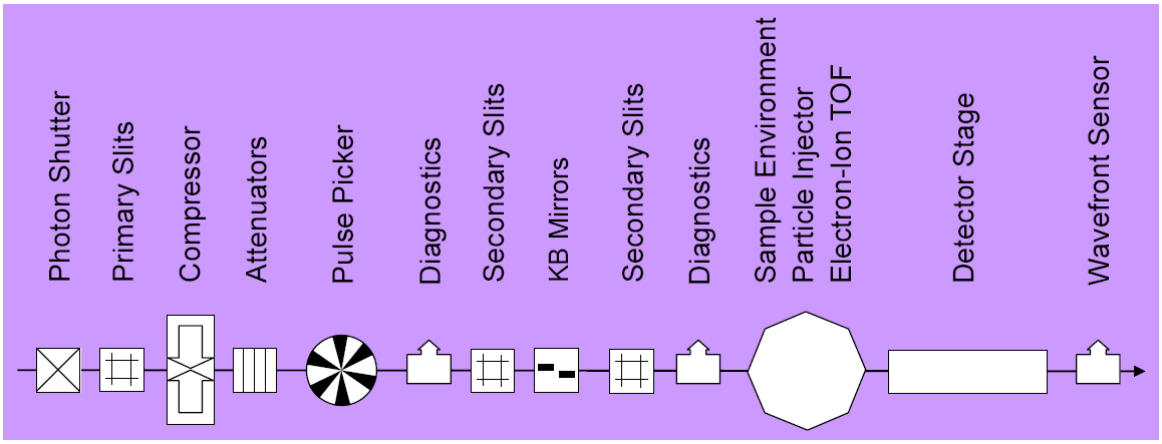

Figure 4-2. Block diagram of the CXI instrument.

Item	Purpose	Specification
Slits/Apertures	Beam definition, Beam halo cleaning	0.25 μm accuracy 1 μm repeatability Resistant to beam damage
KB mirrors	Provide small beam sizes at the sample location	KB 0.1 μm: Focal length, 0.4 m KB 1 μm: Focal length, 4 m
Attenuators	Provide variable attenuation for alignment	Variable, up to 10^6 reduction
Sample Environment	Provide vacuum environment for reduction of background scatter and sample holders, injector	Base pressure < $1x10^{-7}$ torr
Electron, Ion TOF	Sample diagnostic	Ions: 1 AMU resolution up to mass 100 Electrons: resolving power 1000
Detector Stage	Move the detector	1.5 m of travel Distance to detector from 50 mm to 1.55 m
Wavefront Sensor	Determine the wavefront at the sample position	Measure the wavefront in the far field and reconstruct the wavefront at the sample at 120 Hz.
2D Detector	Provide 2D pixelated detection capability	760x760 pixels, 120 frame/s, dynamic range 1000, pixel size 110x110 μm^2

Table 4-1. System specification for CXI instrumentation

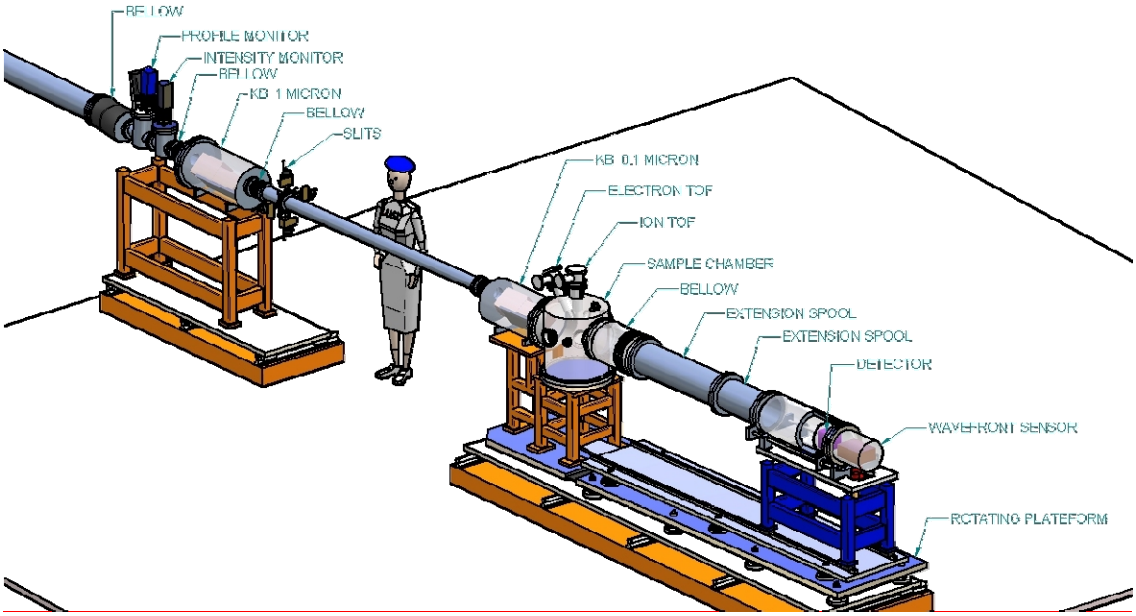

Figure 4-3. Conceptual schematic of the CXI instrument with 3 focusing optics.

4.2.3. X-ray Beam Parameters

X-ray beam parameters such as the beam size, intensity, pulse duration, position and wavelength are critical for CXI experiments. These parameters must be either well defined or measured on a pulse-by-pulse basis to ensure experimental success. The X-ray optics and diagnostics described in Chapters 6 and 7 will be used to tailor these parameters to meet the requirements for each CXI experiment.

Single focusing optic: The nominal FEL beam size at the entrance of NEH hutch 5 is expected to be 350 μm FWHM. A Kirkpatrick-Baez (KB) mirror system will be implemented in the CXI instrument to give a nominal 0.1 μm focus. The beam size at the sample can be adjusted to its required size by moving the sample slightly away from the minimum focus. The KB system will be designed with a ~ 0.4 m working distance which will provide a waist of 60 nm. The design parameters of the KB system are displayed in Table 4-2.

Name	Energy	Focal Length	KB-to-Sample distance	FWHM Spot Size at Sample
KB-0.1	8.3 keV	0.40 m	0.400 m	0.06 μm
KB-1	8.3 keV	0.40 m	0.407 m	1.0 μm
KB-10	8.3 keV	0.40 m	0.470 m	10 μm

Table 4-2. Design parameters of the KB system to be constructed for the CXI instrument. A variable KB to sample distance will permit tuning of the X-ray spot size at the sample position.

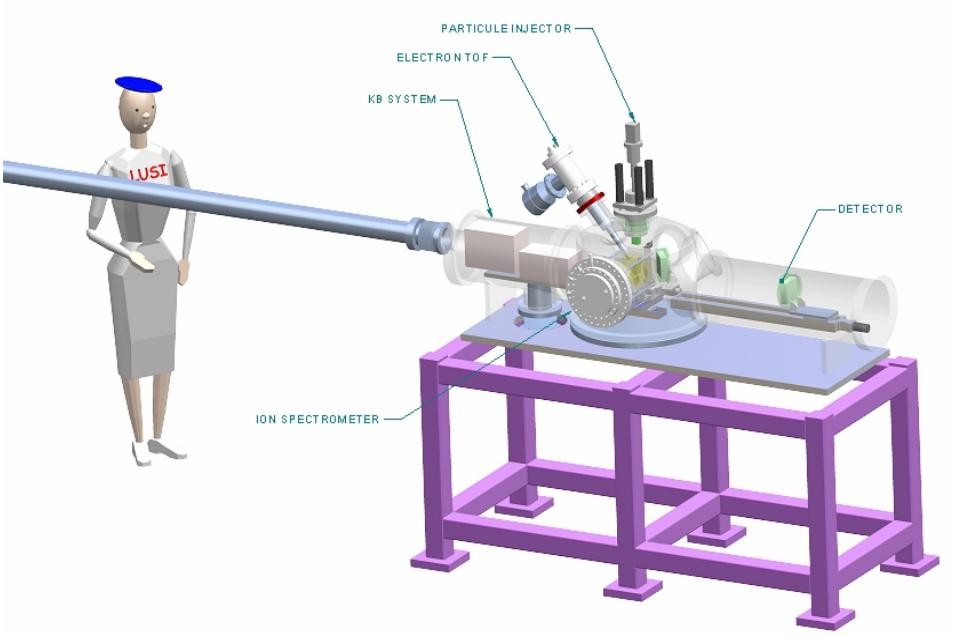

Figure 4-4. Schematic of the CXI instrument with a single focusing optic.

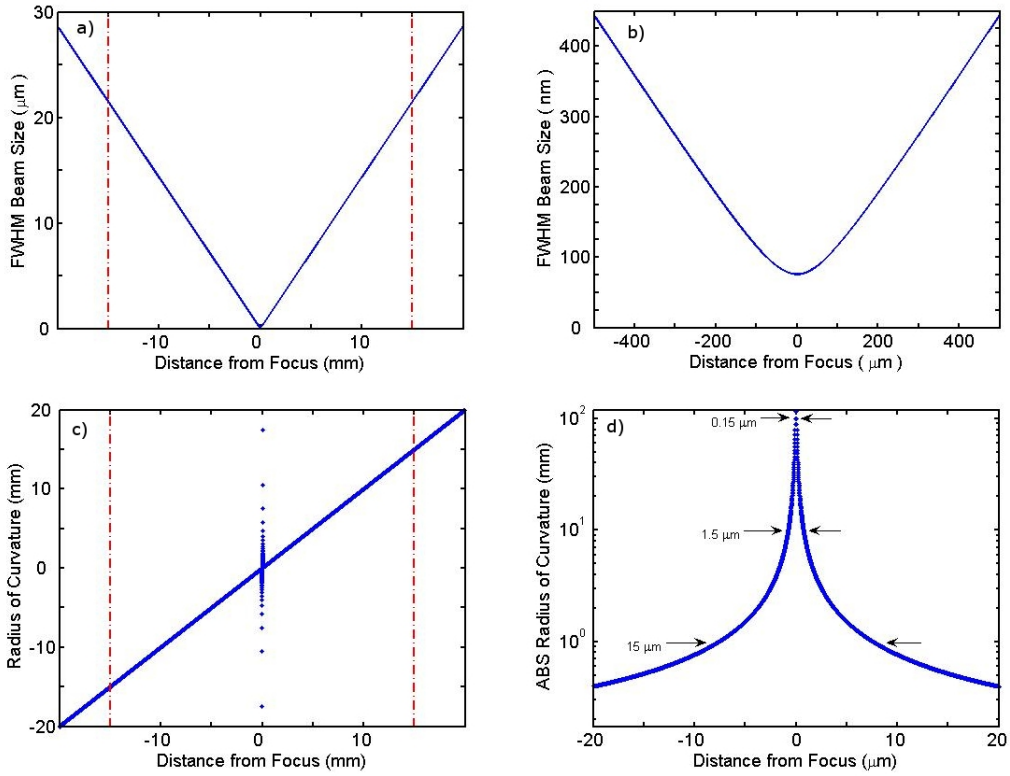

Figure 4-5. FEL beam size with use of a 0.4 m focus KB system and corresponding wavefront curvature as a function of distance from the focus. The red lines represent the tuning range of the lens assembly working distance. (a) FWH beam size as a function of distance from the waist, (b) a zoom showing the theoretical 60 nm focus, (c) wavefront curvature as a function of distance from the waist, (d) zoom of the absolute value of the radius of curvature near the waist.

Multiple focusing optics: An alternative focusing approach has also been considered. The system would consist of separate fixed-focal-length optics for 10, 1.0 and 0.1 micron focus sizes. The 10 micron focus would be achieved with a Be lens, and two KB systems would provide 1.0 and 0.1 micron foci respectively. While this concept avoids relative sample motion, the complication of several different optical arrangements makes this a less desirable approach. Nevertheless, it may be the necessary approach if the single KB mirror cannot be made with sufficiently low roughness. The roughness leads to distortions of the wavefront away from the focus.

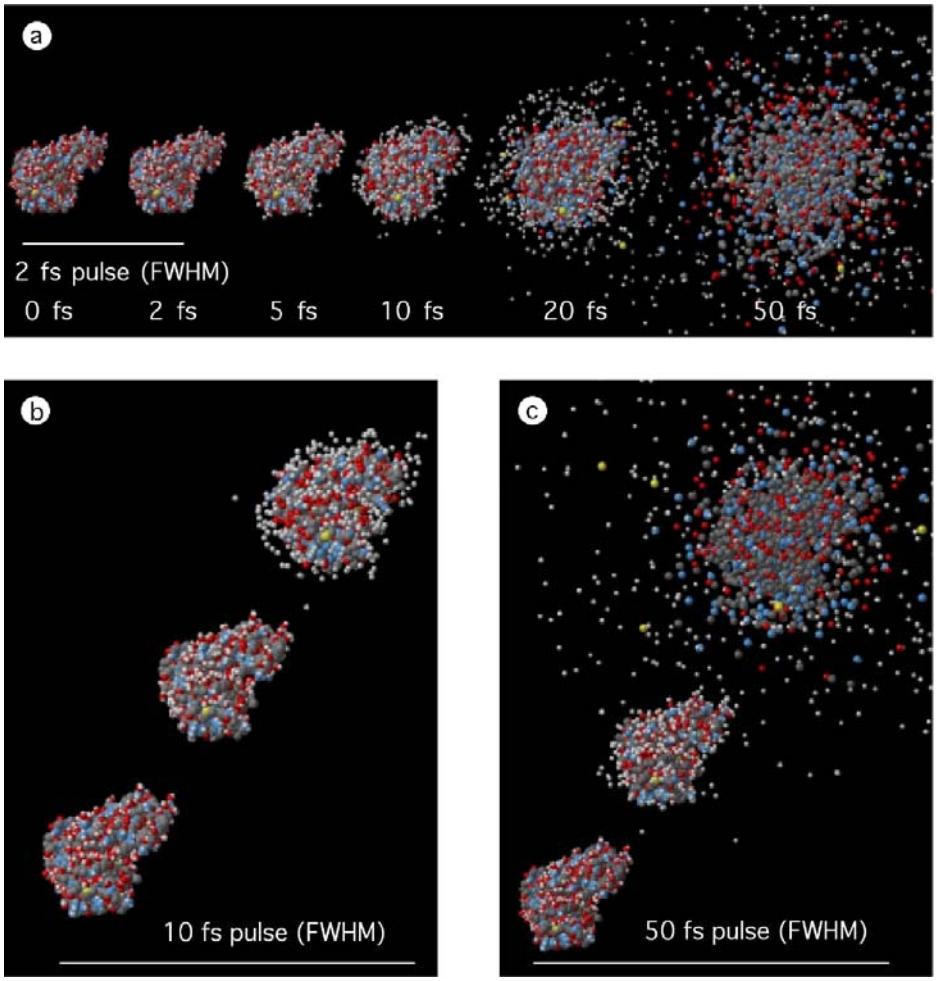

Figure 4-6. MD simulation of radiation-induced Coulomb explosion of a small protein of lysozyme. Results shown are based on [26]. White balls: H, Gray: C, Blue: N, Red: O, Yellow: S. Integrated X-ray intensity: $3x10^{12}$ (12 keV) photons/100 nm diameter spot (corresponding to $3.8x10^{8}$ photons/nm^2, or $3.8x10^{6}$ photons/Å^2 on the sample) in all cases. (a) Protein exposed to a 2 fs FWHM X-ray pulse, and disintegration followed in time. The atomic positions in the first two structures (before and after the pulse) are practically identical at this pulse length due to an inertial delay in the explosion. (b) Lysozyme exposed to the same number of photons as in (a) but the pulse FWHM is now 10 fs. The images show the structure at the beginning, in the middle and near the end of the X-ray pulse. (c) Behavior of the protein during a 50 fs FWHM X-ray pulse. It is also apparent from the figure that during the Coulomb explosion, hydrogen ions and highly ionized sulphurs are the first to escape the immediate vicinity of the protein (at 12 keV, the photoelectric cross section for sulphur is about fifty times larger than that of carbon).

Pulse compressor: Beam optics will be provided to compress the LCLS pulse. The baseline LCLS pulse will have duration of ~ 100 fs with nominally a few x 10^{12} photons per pulse. While this will provide an ideal beam for initial studies, as the technique of coherent X-ray imaging matures there will be a desire to produce shorter pulses containing the same per-pulse energy. The need for shorter pulses is shown in Figure 4-6, where MD simulations of the response of a lysozyme protein to pulses containing 3x10^{12} photons and durations of 2, 10 and 50 fs respectively are shown. It is clear that by 50 fs significant distortion of the molecule has occurred during the pulse [26]. As with optical lasers, if one can chirp the LCLS beam then in principle one can optically compress it. The optical scheme to compress the pulse is shown in Figure 4-7. Here the intrinsic dispersive nature of Laue diffraction is used to produce a wavelength-dependent path length difference. With proper conditions, one can achieve an order of magnitude reduction in pulse length with, in a best case, a 2-4 fold loss of intensity depending on the performance of the multilayers. The specifics for the LCLS are given in Table 4-3. The parameters are those shown in the compressor schematic. The LUSI project will provide the precision rotation stages and translations required as well as the multilayers.

Pulse picker: One additional beam-conditioning component will be provided. The coherent imaging station will be used to investigate a wide variety of sample ranging from injected single bio-molecules to arrays of bio-molecules and other nanoscale objects. When the background scattering is low enough these will be placed on substrates for support. Under these circumstances, with the LCLS operating at 120 Hz, it will be required to isolate a single LCLS pulse, translate the substrate, and illuminate another object. In order not to require changes in the machine operating frequency a 'pulse picker' will be provided that can isolate a single LCLS pulse or provide a reduced repetition rate. This can easily be accomplished with rotating discs that are phase locked to the linac and a simple shutter that can close in a time ~ 0.5 s once the LCLS rate has been reduced to 1 Hz. Rotating choppers operating at much higher speeds are in routine operation at ESRF and elsewhere.

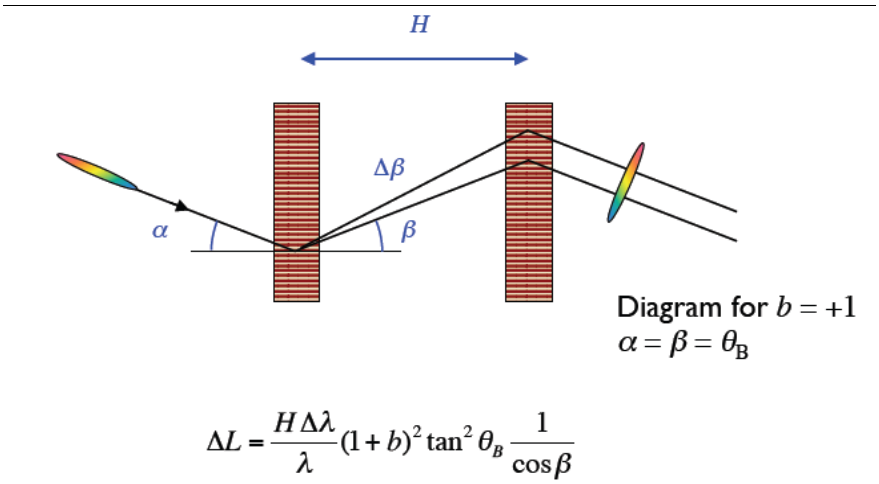

Figure 4-7. A Laue pulse compressor based on 'sliced' multilayers.

λ (nm)	d (nm)	θ_B	b	Sin β	H (mm)	Δλ/λ (%)
0.15	2.0	2.1°	+1	0.03	2600	0.5%

Table 4-3. Parameters for a Laue case pulse compressor for the LCLS.

4.2.4. Sample Environment

4.2.4.1. Vacuum Requirements

The background signal level will be an important concern in these imaging experiments. Since the size of a single bio-molecule is so small there must be very little else in the beam to cause scattering that arrives at the detector. When imaging single molecules, the sample cannot be held on a substrate, since the scattering from the atoms of the substrate will overwhelm the signal of the molecule itself. For similar reasons, one must minimize the number of scattering atoms along the entire beam path. Therefore, the sample (and indeed the entire optics and experimental apparatus) must be in high vacuum to reduce air scatter as much as possible. The required background pressure can be estimated simply. Assume one is imaging a bio-molecule of weight ~ 500 kDa, typical of the smallest molecules of interest at LCLS. Suppose there are sufficient scatter guards to eliminate the background noise coming from everywhere along the beam path except for within 10 cm of the sample. Then for a 1 μm^2 beam traversing a 10 cm path just in front of the molecule, a pressure of $1x10^{-7}$ torr will contribute a background signal of ~ 1% of the scattering from the sample. This sets an upper limit on the pressure requirements inside the sample chamber.

4.2.4.2. Particle Injection

The apparatus to extract nanoscale biomaterials from solution and inject them into vacuum to interact with a focused X-ray beam is a key and enabling technology for biological imaging at free-electron lasers. For LCLS, an injection process that can bring a purified stream of biomolecules, nanoparticles, viruses and cells into vacuum in a known orientation to interact with the highly focused pulses for single-particle imaging is required. Injector development has been funded at Lawrence Livermore National Laboratory (LLNL) through a Laboratory Directed Research and Development Strategic Initiative (LDRD-SI) project titled “Biological Imaging with 4th Generation Light Sources”. Major milestones achieved during this project include the first experimental demonstration of the concept of diffraction imaging of free (injected) particles using individual femtosecond-length pulses from the free electron laser in Hamburg (FLASH).

A schematic of the container-less or substrate-free sample delivery approach designed to maximize ‘first-results’ potential at LCLS is shown in Figure 4-8. A continuously refreshed beam of electrosprayed biomolecules, nanoparticles, viruses and cells is created through a differentially pumped aerodynamic focusing interface. The beam, ca. 250 μm in diameter, consists of the electrosprayed particles positioned randomly in space and time. Particles are only imaged during coincidental overlap of the FEL pulse, with particles in the interaction region. Samples can be changed at atmospheric pressure, contributing to the ease of operation and adaptability of the technology. This particle injection approach has proven to be a resounding success during two experimental campaigns at FLASH using 13.5 nm light. For example, during a shift in March 2007 the injector was operated continuously for 18.7 hours, performing 26 sample changes with 14 different samples (Figure 4-9). The CCD collected images continuously for almost all 18.7 hours and 11.6 % of images contained particle scattering information (1873 out of 16639 images), giving an average hit rate of 0.05 particles/s (including all sample change down time). Injected particles from which coherent diffraction patterns have been recorded and images have been reconstructed include megadalton DNA complexes in ~150 nm sucrose droplets, 75-700 nm diameter spherical nanoparticles and intact marine microorganisms (~1μm x 700 nm). This data set demonstrates the adaptability, stability and data richness of the particle injection experiment. Most importantly, it confirmed estimates of the hit rates achievable.

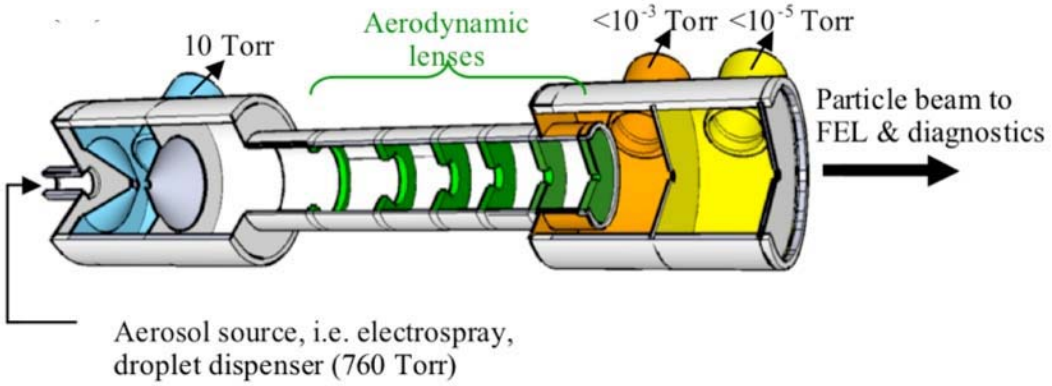

Figure 4-8. Schematics of the Particle Injector for container-less sample delivery to LCLS. The differentially pumped interface is equipped with aerodynamic focusing. Aerosol produced by charge-reduced electrospray sampled at the inlet is focused into a narrow particle beam at entry to the FEL high vacuum. The entire system translates out-of vacuum to steer the particle beam to the FEL focus.

LCLS bioimaging requires operation in free-fire mode with this injection strategy because the FEL cannot be triggered to coincide with random particle arrival. To compensate, experimental injection parameters must be optimized so that the hit rate with the FEL beam is maximized. The most easily controlled parameters independent of the FEL are the aerosol concentration and the inlet transmission efficiency, which must be maximized and the particle beam transverse area, which must be minimized. Advanced diagnostics have been developed at LLNL that, coupled with standard particle samples, enable characterization of the performance of the injection system without FEL (i.e., at LLNL). The injector is designed to use spherical nanoparticles as a set of standards that allow the injector to be tuned for specific particle sizes, i.e. for viruses vs. cells. Accurate measurements of the hit rates expected for a sample can be made off-line of the LCLS with a pulsed Nd:YAG laser and a time-of-flight mass spectrometer.

The injection system for LCLS will have several key upgrades to improve performance over the current injector to meet the stringent standards required for LCLS operation and to ensure single particle imaging ‘first results’. Efficiency gains will be achieved in the inlet transmission and aerodynamic focusing design. Reduced beam divergence will be achieved by closer proximity of the injector nozzle to the interaction region, decreasing the particle beam diameter. Coupling these efficiency gains with the use of microfabricated multiplexed electrospray nozzles or droplet dispensers and highly pre-concentrated samples to increase the aerosol concentration sampled into the injector will increase the hit rate by orders of magnitude for the ‘free-fire’ mode of operation. Furthermore, the mechanical interface to align the injected particle beam to the FEL beam is modular in design and can also accommodate a Rayleigh droplet source injector designed in collaboration between LLNL and Arizona State University (ASU). This injector operates with in-vacuum droplet dispensing technology that creates equally spaced submicrometer-sized droplets that could be timed with the FEL pulses.

Once particles are imaged, it is important to understand the effects of transfer of the biomolecule, virus, or cell on activity or viability. To address this problem, the injector is designed to have a collection or ‘soft landing’ module after the interaction region to facilitate off-line characterization of injected biomaterials.

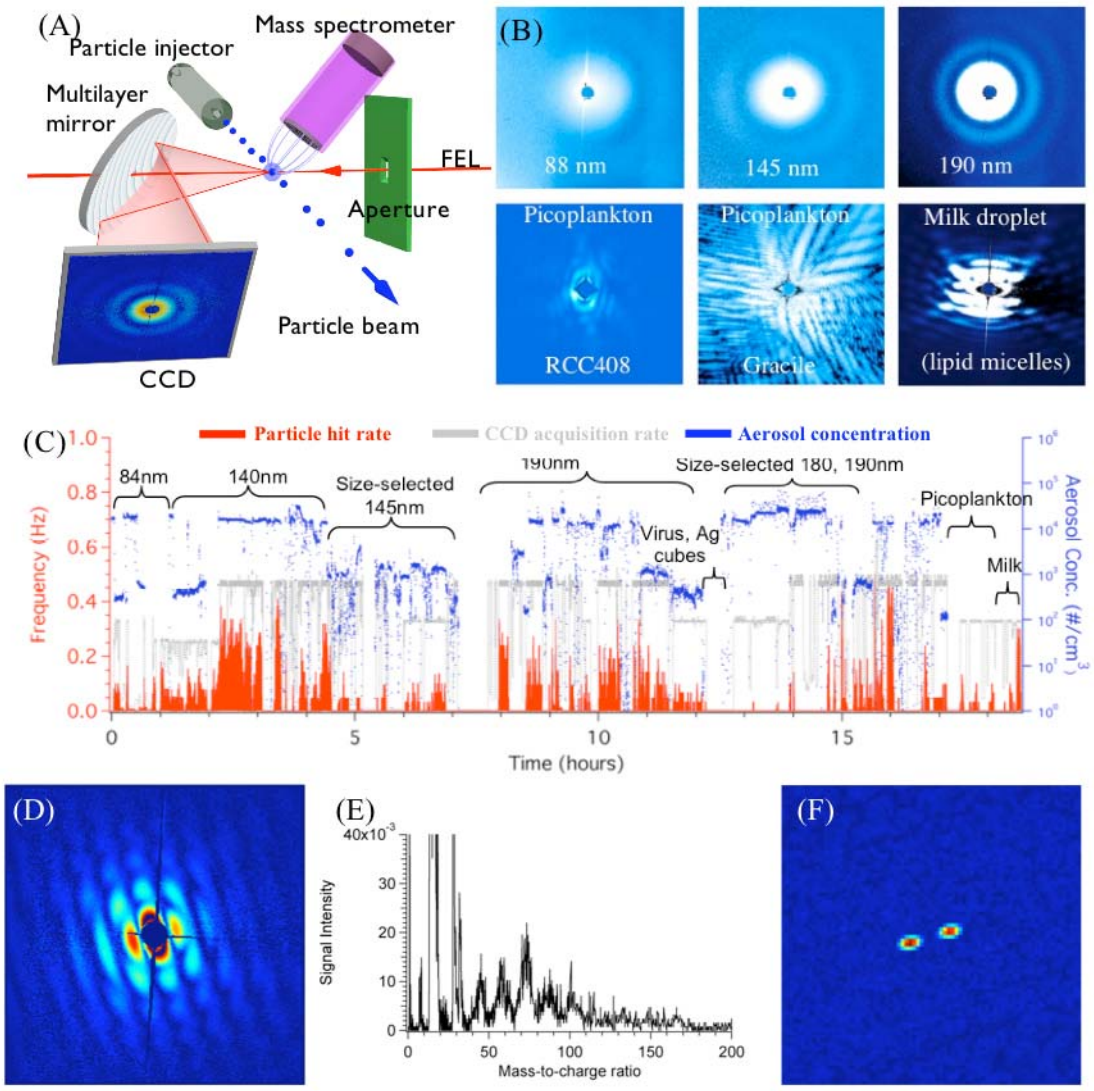

Figure 4-9. Experimental measurement and analysis of coherent X-ray diffraction of injected particles. (A) A schematic of the diffraction camera for FLASH in particle injection mode (note at LCLS the detector will be on the FEL axis). (B) Example images of spherical nanoparticles and complex biological samples such as single cells and milk droplets. (C) Data stream from a particle injection shift in March 2007 at FLASH. (D) Diffraction pattern collected during injection of megadalton scaffolded DNA complexes with a tamper of sucrose. (E) Time-of-flight mass spectrometer detected ions specific to this type of particle. (F) The image reconstruction showed that two particles were irradiated simultaneously by a single FLASH pulse.

Tamper layers: The particle injector has been designed to accommodate a key question associated with single particle imaging: Is the molecular structure preserved as it is delivered from solution into sprayed drops, which are then introduced into vacuum? This question is being examined at LLNL through molecular dynamics simulations. These simulations also revealed that the presence of a tamper layer around the molecule, be it water or any other material can slow the damage to the molecule, allowing the

use of longer pulses. The charge-reduced electrospray of biomolecules allows for in-situ synthesis of nanoscale tampers through control of solute concentration in the starting solution.

Overall, the particle injector is designed to be a highly adaptable and modular system capable of highly efficient transfer of biomolecules, nanoparticles, viruses and cells to the interaction region of the FEL. The success of this particle injection approach at FLASH has provided a window into the potential power of LCLS imaging of free nanoscale biomaterials in the future. LUSI will provide, through a contract with LLNL, the particle injector for the CXI instrument.

4.2.4.3. Laser Alignment of Particles

The classification of the 10^5 or more diffraction patterns may prove difficult due to the low signal-to-noise ratio at the high resolution. This task could be made significantly easier and the single shot intensity requirements can be reduced by injecting pre-aligned particles in the LCLS beam. This could be achieved by hitting the particles with a short pulse from a non-resonant laser a short time before they interact with the FEL beam. The planned experiments do not require pre-alignment but would be greatly simplified by it. A line of sight to the particle stream will be made available for a future addition of an alignment laser to the system.

4.2.4.4. Fixed Target Samples

The initial experiments to be performed on the CXI instruments will be on fixed targets rather than injected particles for simplicity during the commissioning phase. Beyond these initial tests, many other samples will be better suited to fixed targets due to a limited sample size for example. A three-axis translation stage will allow the positioning of individual samples mounted on a large holder into the FEL beam for two-dimensional imaging. The samples will also be moved along the FEL beam to vary the focal size to study X-ray fluence dependence on the damage process for example.

4.2.4.5. Cryo Goniometer

Electron microscope goniometers could be useful for studies where a controlled sample rotation is necessary, e.g. for coherent diffraction experiments on nano-crystals, intact cells and cell organelles, and other non-reproducible samples using the unfocused, coherent beam of the LCLS. For example, cryo-electron -microscopy (cryo-EM) performs structural studies on hydrated samples at low temperatures in a high vacuum environment. Existing cryo-EM equipment can be adopted for similar studies in an X-ray beam. Sample molecules and particles may be embedded in a thin layer of vitreous ice of a few hundred Å in thickness. Such a technique will require good pointing stability from the LCLS, with minimal pulse-to-pulse jitter. If this can be achieved, the complete repertoire of methods used in cryo-EM will become available for X-ray experiments. Rotating the sample will be required for 3D imaging of non-reproducible samples, though it will not allow measurements beyond the damage limit and would be most appropriate for radiation-resistant inorganic samples. Figure 4-10 shows a schematic diagram of a JEOL three-axis goniometer and sample holder. All motors, encoders, gears and switches are outside the vacuum. The horizontal drive provides motion along the X-axis. The main drive provides motion along the Y- and Z-axis and rotation around the X-axis. The samples can be maintained at liquid nitrogen temperatures to reduce radiation damage and can be easily changed without breaking the vacuum system. An optical microscope with a long focal length will be used to align the samples and position the rotation axis to the LCLS beam.

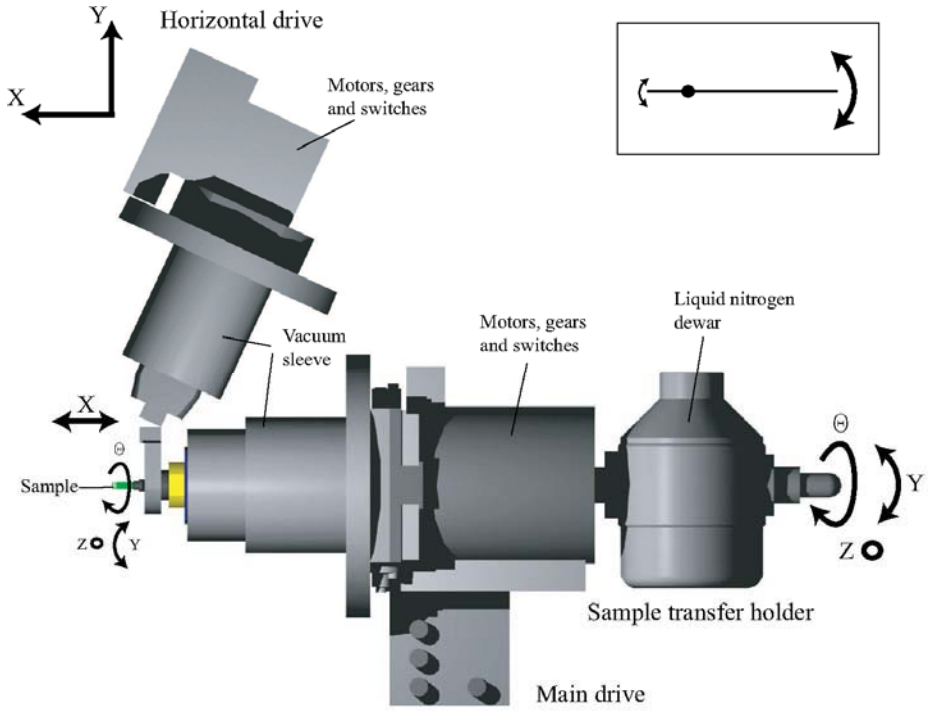

Figure 4-10. Engineering concept of the Cryo-EM goniometer stage for the CXI instrument.

4.2.5. Detector Considerations

The diffraction pattern will be recorded on a pixellated detector, shared with LCLS, subtending a solid angle dependent on the desired resolution with a hole in the middle to avoid the direct beam. There must be sufficient pixels in the detector to oversample the diffraction pattern, which depends on the sample size and desired resolution, as described below. The scattering from the sample covers a large dynamic range: it is strong very close to the central core, and at high angles there will be much less than one photon per pixel, on average. Since the technique relies upon classifying and averaging a large number of patterns, the read noise must be considerably less than the photon count per pixel averaged over these patterns. Estimates of the noise level and dynamic range are given below, after first listing the requirements of pixel count and sampling. For larger structures, e.g., virus particles, and single cells, a finer sampling will be needed than for smaller objects.

The detector size should not be larger than approximately 100 mm x 100 mm, in order to reduce the beam path from sample to detector. At better vacuum levels, this distance could be increased without increasing the background. Other desired parameters are a read-out speed matching the pulse rate of the LCLS and an overall dynamic range on the order of 10^3. Diffraction data may be supplemented by a lower-resolution image of the sample obtained with a wave-front sensor as it could prove valuable in enhancing the robustness of the oversampling phasing algorithms by providing information about the missing central part of the data.

The pixel requirements simply depend on the number of resolution elements to sample an object of a given size at a given resolution, as described in [37]. To achieve a resolution $f_{max} = 1/d$ requires a maximum scattering angle 2θ given by $\sin\theta = \lambda f_{max}/2$. For an object of finite extent of width D, its Fourier transform is band-limited. The Nyquist sampling rate of the transform is 1/D in each dimension. To measure this transform to a resolution 1/d, in one dimension, requires samples from -1/d to +1/d or 2D/d samples. In

real space this corresponds to samples at intervals $\Delta x = d/2$, which is the largest sufficient interval to measure periods larger than d. The detector measures the diffraction intensities, which are the modulus squared of the molecular transform, or equivalently, the Fourier transform of the object's autocorrelation function. For an object of extent D the extent of its autocorrelation is 2D, which means that the diffraction intensities are band-limited with a Nyquist rate of 1/(2D). Note that sampling at a higher rate than 1/(2D) does not add any information to the measurement, but may improve the signal to noise ratio of the measurement. However, pixellated detectors do not sample at points but integrate over the active area of the pixels. This corresponds to a Modulation Transfer Function (MTF) that may decrease to zero at spatial frequencies (at the detector) of period 2p, where p is the pixel width. The effect of the MTF is to apply an envelope to the reconstructed real-space image, which should be no less than 0.7 at the largest radial extent of the object. Thus, the detector's MTF influences the required pixel count. The number of pixels along the width of the detector is given by $N = 2 D s / d$, where s is a sampling ratio per dimension (relative to the molecular transform Nyquist rate), with $s = 2$ in the case of minimum required sampling (for which the 0.7 MTF level should occur for pixel frequencies no lower than 1/(4 p)).

Based on these considerations, the LCLS detector with 760 pixels placed 84 mm from the sample can provide a resolution of 0.3 nm for an object with a diameter of 57 nm with the minimum oversampling of 2. This detector does not have sufficient pixels to image larger objects at the same resolution. For a 1 micron object, moving the detector back to 1450 mm from the sample gives 5.2 nm resolution, again with an oversampling of 2. In the experimental chamber for imaging translation will be provided to cover the sample to detector distance illustrated here. Since the detector is tiled, as the method of lensless imaging matures additional tiles can be added as needed.

Finally, a central hole in the detector will be required. This will permit the central beam to pass through the pixel detector, and expands as a function of distance from the beam waist until it reaches sufficient dimensions that it can be analyzed by a wavefront sensor. Since the detector sensor requires guard rings, the physical 'hole' must be smaller than the 'dead region' in the 760x760 pixel detector. Image reconstruction can be achieved even with considerable missing data due to this dead region in the middle of the detector. However, the larger this region, the larger the uncertainty of various components of the image, and the less quantitative the image becomes. The size of the hole will therefore be optimized so that the downstream wavefront sensor detector will also capture the scattered beam in the nearly forward direction and will be optimized based on simulations to give the most robust constraints for the reconstruction of the observed scattering patterns.

We estimate the maximum requirement for the number of pixels is $N = 2000$, which corresponds to a particle size of 100 nm at a resolution of 0.3 nm and a sampling ratio of $s = 3$, or a particle size of 200 nm at the same resolution and a sampling ratio of $s = 1.5$. The larger sampling would be required if the detector MTF at 1/(2 p) were about 50%. These are likely parameters for imaging of nanoparticles, and for the imaging of arrays of biological particles. For the cow-pea mosaic virus (CPMV) test object described below, which has D = 32 nm, we require $N = 450$ pixels for $s = 2$ and a resolution of 1/(0.3 nm). Thus the LCLS shared detector with $N = 760$ pixels will be more than sufficient for early studies. This reduced pixel count will be sufficient for most small biological samples, and a larger pixel count detector will be needed for larger objects (Figure 4-11).

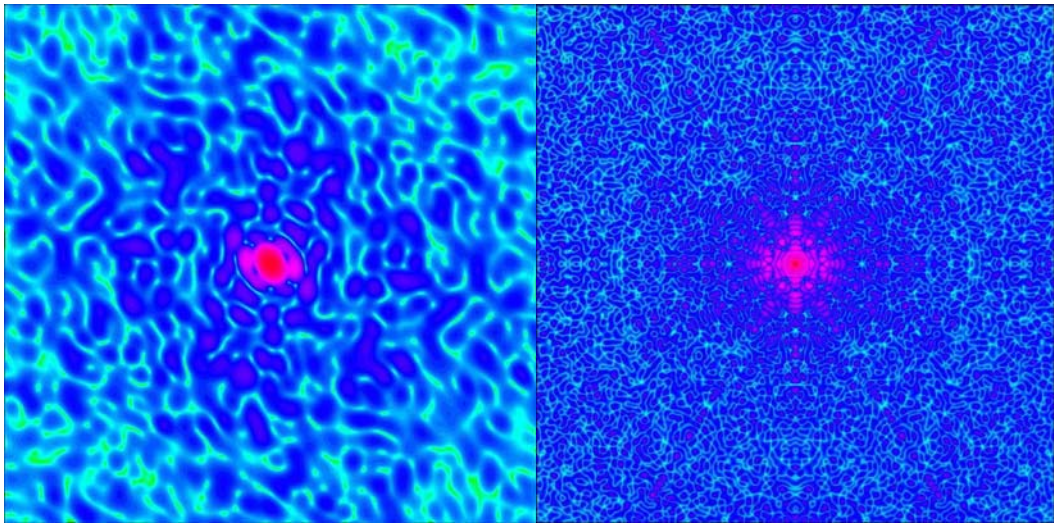

Figure 4-11. Planar section through the center of the molecular transform of a small protein molecule lysozyme and of a larger virus capsid at similar maximal resolutions. The lysozyme is shown on the left and the capsid (tomato bushy stunt virus) on the right. The level of detail is significantly different in the two pictures, and detectors should be able to resolve details in the patterns of even larger objects than a virus particle.

4.3. REFERENCES

[26] Neutze, R. Wouts, D. van der Spoel, E. Weckert, and J. Hajdu, *Nature*, **406**, 752-757 (2000).
[27] Larsen, J. J. et al., *Phys. Rev. Lett.*, **85,** 2470, (2000)
[28] Bergh, M., Timneanu, N., van der Spoel, D., *Phys. Rev. E*, **70**, 051904 (2004).
[29] Hau-Riege, S.P., London R.A., Szöke, A., *Phys. Rev. E*, **69**, 051906 (2004a).
[30] Teo, W.E., Ramakrishna, *Nanotech*., **17**, R89-R106, (2006).
[31] Chapman et al., accepted by *Nature*, (2007)
[32] Chapman, et al., *Nature Physics*, **2**, 839-843 (2006).
[33] Bates, R.H.T., *Optik*, **61**, 247-262, (1982).
[34] Pfeifer, M.A., Williams, G. J., Vartanyants, I. A., Harder, R., Robinson, I. K., *Nature*, **442**, 63-66 (2006).
[35] Miao, J. et al., *Proc. Natl. Acad. Sci. USA*, **100**, 110-112, (2003).
[36] Chapman, H.N. et al., *J. Opt. Soc. Am. A*, **23**, 1179-1200, (2006).
[37] Huldt, G., Szöke, A., Hajdu, J., *J. Struct. Biol*., **144**, 219-227, (2003).
[38] Marchesini, S, *Rev. Sci. Instrum.,* **78**, (2007).

5 - X-RAY CORRELATION SPECTROSCOPY

Coherent X-rays are particularly well suited for studying disordered system dynamics on nanometer length scales, using X-ray Photon Correlation Spectroscopy (XPCS) [39]. XPCS measures the temporal fluctuations in speckle patterns produced when coherent light is scattered by a disordered system. Figure 5-1 shows a speckle pattern taken from Vycor porous glass [40] . XPCS is complementary to Dynamic Light Scattering (DLS) or Photon Correlation Spectroscopy (PCS) with visible coherent light, techniques that probe slow dynamics ($\omega < 10^6$ Hz) but can only access the long wavelength regime ($Q < 4 \cdot 10^{-3}$ Å^{-1}). Neutron-based techniques (inelastic, quasi-elastic neutron scattering and neutron spin-echo) and Inelastic X-ray Scattering (IXS) can access the same Q range as XPCS, but these techniques only probe the dynamic properties of matter at high frequencies (from typically 10^8 Hz to about 10^{14} Hz) [41]. The peak coherent flux of the LCLS FEL radiation will be 9 orders of magnitude larger than 3rd generation synchrotron light sources and will allow, for the first time, the studies of dynamics up to about 10^{13} Hz at large Q. This is illustrated in Figure 5-2, which displays the frequency-wavevector space covered by a selection of relevant methods. There is a wide variety of problems to be addressed [44] and some prominent examples are summarized in the proposed experimental program described below.

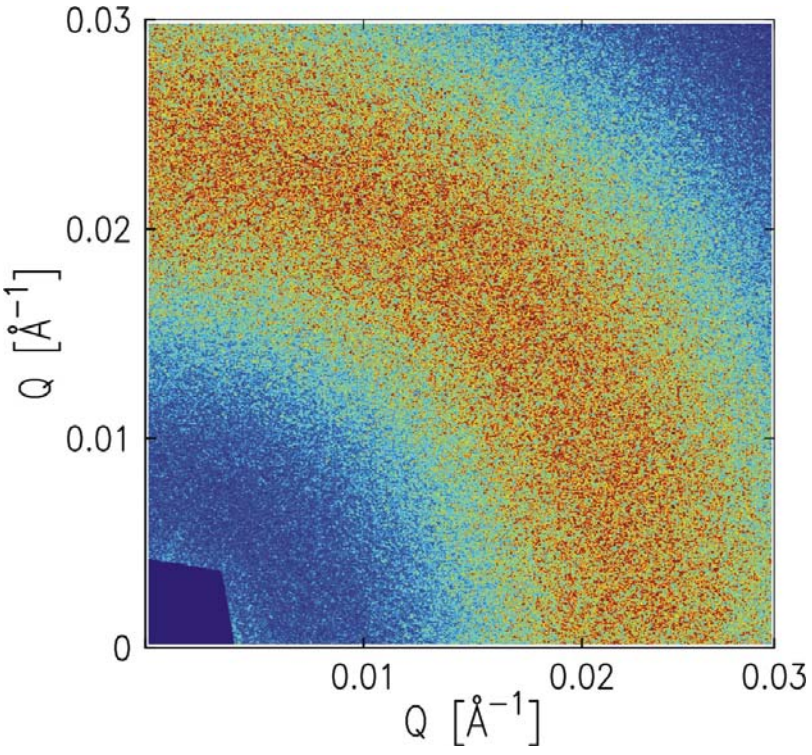

Figure 5-1. Speckle pattern measured at 8 keV of a porous silica static sample of Vycor. The pattern presents a correlation ring located at Q = 0.023 Å^{-1}.[40].

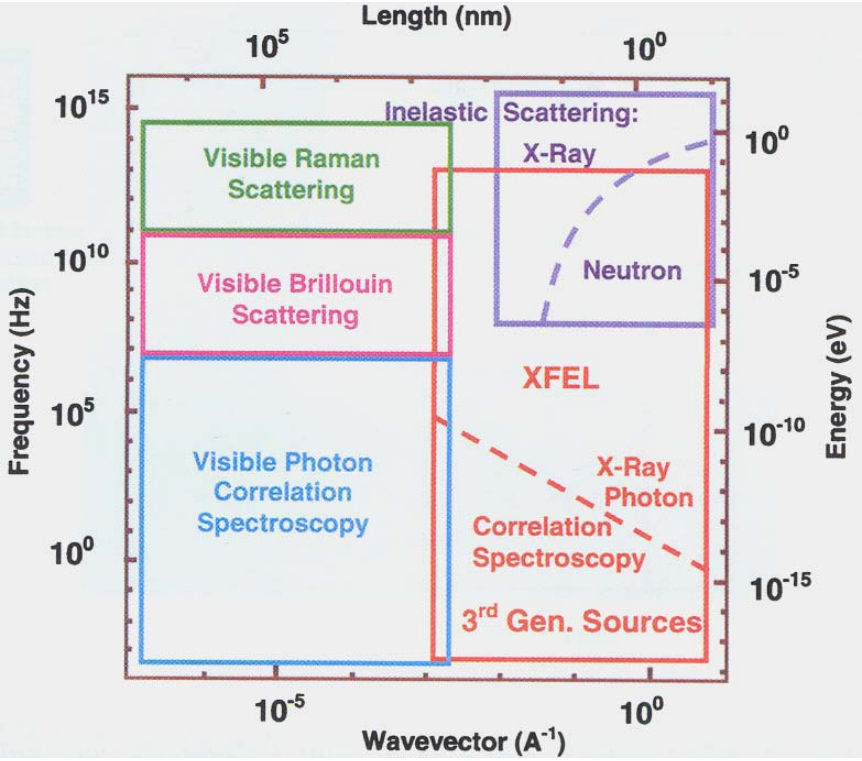

Figure 5-2. Frequency-Wavevector space covered by different experimental techniques for studying dynamics of condensed matter systems.

5.1. SCIENTIFIC PROGRAMS

Coherence properties of hard X-rays: Coherence is one of the most prominent features of the novel radiation produced by the LCLS. A comprehensive understanding of the X-ray laser coherence properties is not only of fundamental interest but a necessity for properly interpreting coherence-based experiments such as XPCS. The characterization of the coherence properties of a source in terms of correlation functions and photon statistics is theoretically well developed and experimentally established by the optical laser community [45] and was successfully used for characterizing 3rd generation sources XPCS instruments [46]. An experimental program is proposed with the goal of studying first- and higher-order correlation functions, which will allow one to not only determine the spatial and temporal coherence parameters (i.e., the longitudinal and transverse coherence lengths as well as the coherent flux) but also will provide insight into the mode structure, photon statistics (bunching/anti-bunching) and possible non-Gaussian properties of the source.

Phase Transition Dynamics: Atomic-scale fluctuations occur at equilibrium near many phase transitions. These fluctuations are the basis for the new phases that form when the phase transition point is crossed, e.g. by changing temperature or field. XPCS is an ideal tool for observing the equilibrium dynamics of these fluctuations, and understanding the mechanisms that control microstructure formation in materials. The diffusionless transitions in magnetic, ferroelectric, and ferroelastic materials exhibit time scales spanning from sub-picosecond to many seconds in the vicinity of the transition point. For example, in lead-niobate-based ferroelectrics the time scale of dielectric response has been found to change dramatically (from picoseconds to milliseconds) in a 65 K range near room temperature [47]. Nanoscale inhomogeneities in polarization, composition, and strain known as polar nanodomains have been observed

in these systems using diffuse X-ray scattering [48] and simulation [49], and are thought to be responsible for this glass-like "relaxor" behavior. XPCS studies of polar nanodomain dynamics will allow us to understand the nature of the interactions in this complex oxide system.

Dynamics of Glassy Materials: Many liquids, when rapidly cooled below their freezing points, form meta-stable glassy or amorphous phases. This applies for a wide variety of materials including metallic alloys, oxides such as silica, polymeric materials, and many others (e.g. colloidal dispersions for which the volume fraction is the analogous of the inverse temperature driving the phase transition). In general, glassy materials are among the least understood materials at a fundamental level. Conventional equilibrium statistical mechanics does not predict the existence of the amorphous state, whereas it can explain most other states of matter, even quite exotic ones like superconductivity and superfluidity. Understanding visco-elastic effects in glassy materials is thus an important topic of fundamental research.

Surface XPCS: Surface XPCS experiments at 3rd generation storage-ring sources have been performed successfully in the past, and surface dynamics have been investigated in a variety of systems, such as membranes, polymer films, and liquids [42]. Surface XPCS in combination with the X-ray standing wave technique allows the study of fluctuations of buried interfaces as well. However, surface dynamics at the nanometer length scale is not accessible today due to insufficient coherent photon flux. Here the LCLS will provide exciting new possibilities.

Non-Equilibrium Dynamics: When a disordered homogeneous material is rapidly brought to a new set of conditions, corresponding to the coexistence of equilibrium phases, a spatial pattern of domains of the phases develops. A change of conditions can be accomplished by a rapid quench from high to low temperature, below the miscibility gap. The result of such a quench is the creation of a microstructure of interconnecting domains. These domains grow in order to minimize the areas of the domain walls that separate the phases. Out-of-equilibrium behavior has been observed in soft condensed matter glassy systems as well (i.e. attractive and repulsive colloidal glasses), where the dynamics are slowed down as a function of time and are described as aging. XPCS is ideal for studying these non-equilibrium systems where the dynamic behavior needs to be probed on all length scales simultaneously.

5.2. INSTRUMENT DESCRIPTION

5.2.1. XPCS Technique

When coherent light is illuminating a disordered system the instantaneous far-field scattering produces a random diffraction or speckle pattern, as shown in Figure 5-1. These ‘‘speckle’’ patterns are related to the exact spatial arrangement of the scatterers. If the spatial arrangement of the scatterers changes with time, as is the case for colloidal particles dispersed in a fluid phase and undergoing Brownian motion, one will observe that the corresponding speckle patterns also changes and evolves in time (as can be seen online in [50]). A characterization of the temporal intensity fluctuations at a given wavevector within the speckle pattern can thus reveal information on the underlying dynamics of the system. In a XPCS experiment the time-resolved speckle pattern is measured with a 2-dimensional detector with pixel sizes roughly equal to the size of a single speckle in the far-field scattering region of the sample.

The shortest time scale probed by this technique is set by the time structure of the X-ray pulses, in this case, the width of the X-ray bunches, which is on the order of 230 fs with a repetition rate of 120 Hz. With the proposed XCS instrument, there will be three different types of measurement techniques (i.e. sequential, split and delay and pump-probe) designed to cover time scales from 10^{3} seconds down to 10^{-12} seconds.

Sequential technique (for time scales from 10^{-2} to 10^{3} seconds): The shortest time scale of this technique will be limited the LCLS repetition rate at 120 Hz. Important phenomena of microscopic system dynamics can occur on relatively long time scales, e.g. longer than 10^{-1} s. This means that it will be possible to employ the very high time-averaged coherent X-ray flux from the LCLS beam, averaged over the 120 Hz repetition rate, to investigate the dynamics using 2D-XPCS data collection and analysis techniques that are similar to those used now at 3rd generation sources. Such an experiment would consist of collecting a time-resolved sequence of speckle patterns on an area detector as shown in Figure 5-3. From an analysis of these sequences, correlation times from a few inter-pulse periods up to many minutes could be measured. The advantage of the LCLS pulses will be in higher signal rates than currently available, which will allow probing dynamics at much larger wavevectors than currently available.

Split-Delay (for time scales from 10^{-12} to 10^{-8} seconds): The short pulse duration of the LCLS FEL radiation (230 fs or less) will allow the extension of XPCS studies to much faster time scales than currently possible. For example, to understand the dynamics in glass-forming systems down to the nanoscale, it will be important to carry out studies spanning a very large range of time scales (10^{-12} to 10^{3} s) in order to observe the evolution of the dynamics from liquid to glassy state as the temperature is lowered. In order to probe time scales between 10^{-12} and 10^{-8} s, a split-delay technique shown schematically in Figure 5-4 will be used, taking advantage of the peak brilliance of the LCLS beam.

The concept is to split each X-ray pulse into two equal-intensity pulses separated in time, but propagating along the same path. The scattering from the two pulses will then be collected during the same exposure of an area detector. If the sample is static (i.e. does not present any dynamics on the time scale of the delay between pulses), the contrast in the summed speckle pattern will be the same as that from a single pulse. If the sample evolves on this time scale, then the summed speckle pattern will have lower contrast. By performing contrast analysis of a set of such patterns, each for a different time delay, the correlation time τ_C of the system can be measured on time scales down to the pulse duration. A pulse splitter with a path length difference variable from $3x10^{-6}$ to 3 m would give delay times from about 10^{-14} to 10^{-8} seconds.

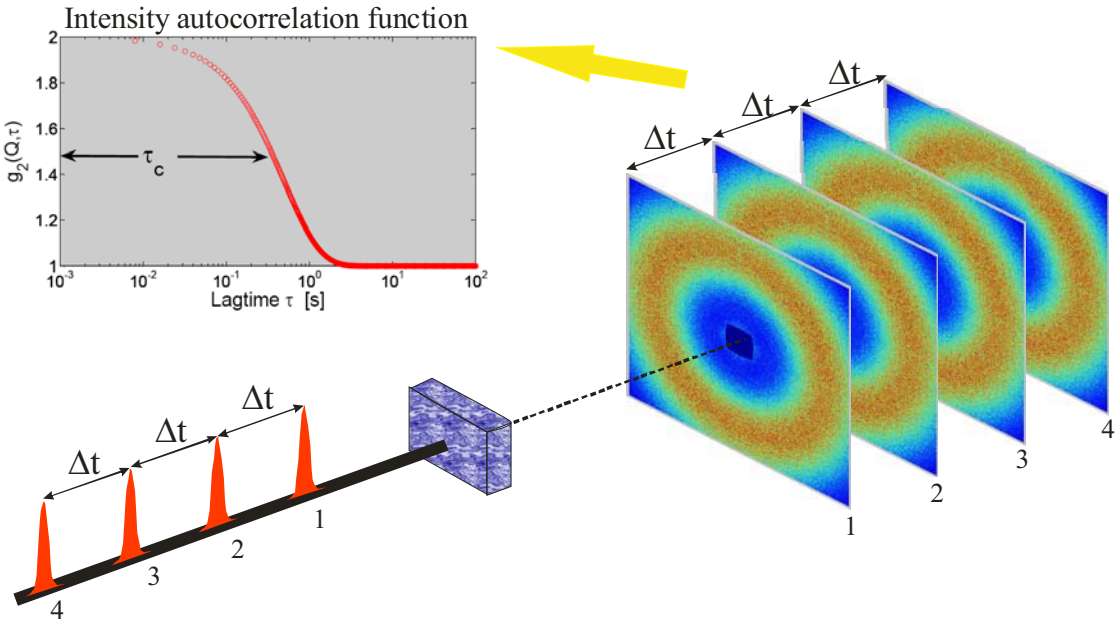

Figure 5-3. Illustration of the XPCS sequential technique. A speckle pattern is measured for each incoming pulse at a 120 Hz repetition rate. The intensity autocorrelation function for each Q is then calculated from which a characteristic time τ_C can be obtained.

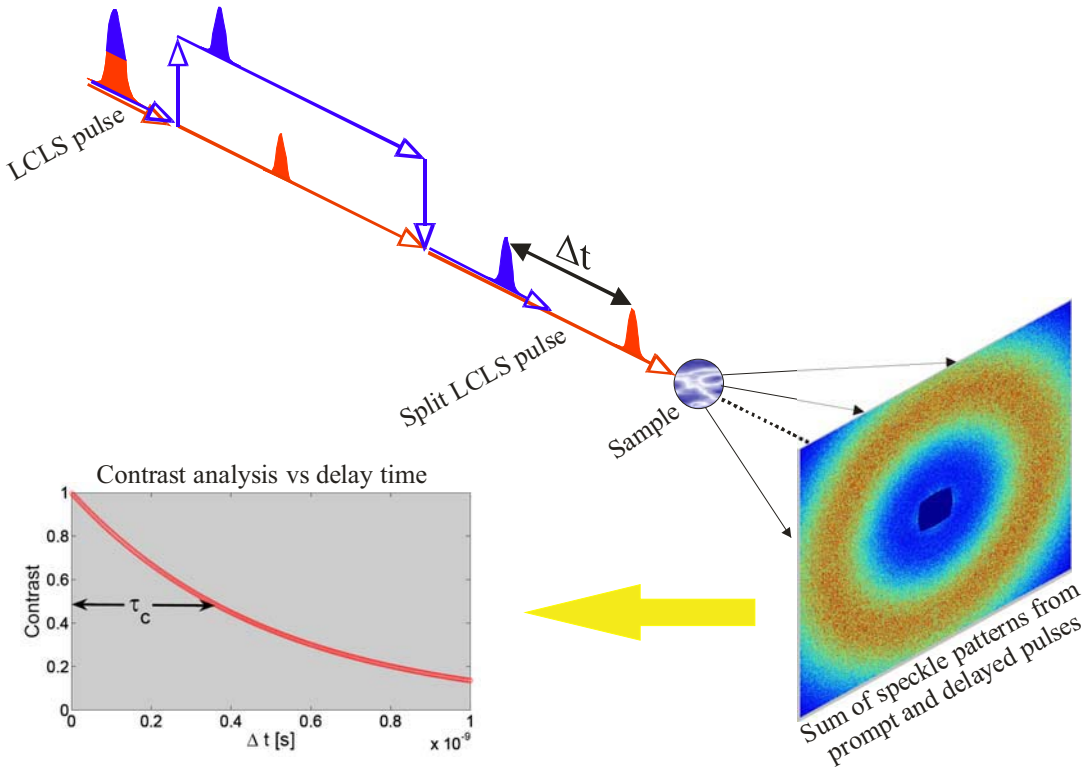

Figure 5-4. Illustration of XPCS split-delay technique.

Pump-probe technique: The XPCS pump-probe technique compares two speckle patterns: one taken before exposing the sample to a pump pulse, and a second pattern taken a time interval Δt after the pump pulse. The pump sources for reactions and transformations may involve optical lasers, the LCLS pulses themselves, a pulsed Terahertz source, pulsed electric and magnetic fields, shock waves, etc. Time scales between 100 fs and 200 ns or longer can be accessed with this technique, allowing the determination of the time scales for magnetization processes, phase transitions in ferroelectrics, surface dynamics, etc. In principle one could also combine the pump pulse with the split-pulse technique described above.

5.2.2. Overall Concept Layout

The XCS instrument will be designed to perform the XPCS measurements described above. It will have the necessary X-ray optics to deliver the LCLS X-ray beam to the experimental area in a manner that preserves the coherence of the beam by having as few optical elements as possible. It includes a large-offset monochromator, beam transport, electrical, and vacuum systems that will be installed in the 200 m transport tunnel connecting the NEH and the FEH. It will have a 2D detector compatible with the repetition rate of the LCLS beam at a maximum rate of 120 Hz. A diffractometer, local optics and a specific detector stages will be provided.

To enhance the instrument, additional equipment will be provided by the XCS collaborative team, including the split-delay optical elements (SLAC/DESY MoU).

System Specifications: The specifications for the major components of this instrument are based on the requirements pertinent to the XPCS experimental measurement technique developed and refined by the scientific team, as presented in Table 5-1.

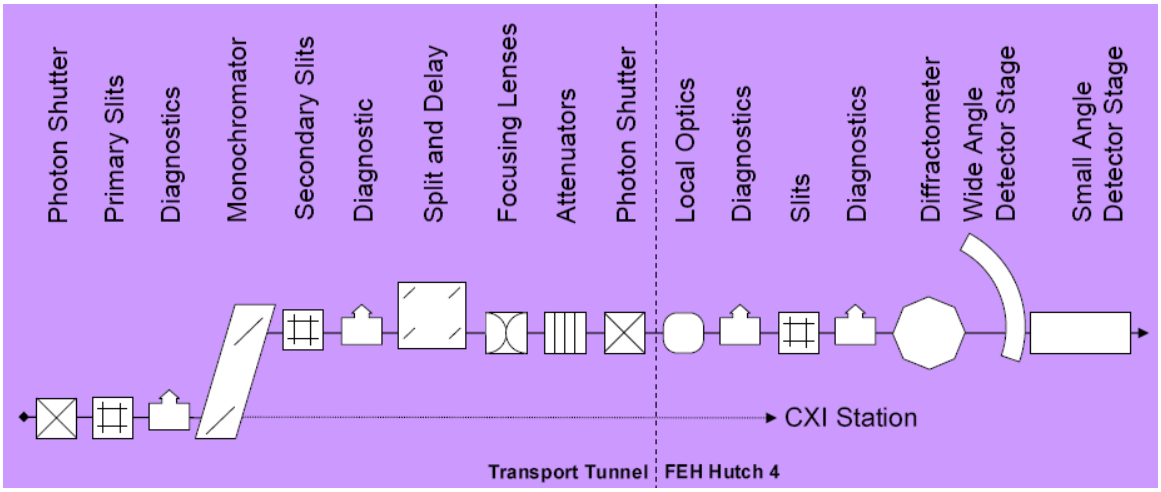

Figure 5-5. Block diagram of the XCS instrument.

Item	Purpose	Specification
Large Offset Monochromator	Deflecting beam to XCS endstations and provide monochromatic beam	Non-monolithic channel-cut crystals, 600 mm offset, 0.04 arcsec in θ, energy tunability (6 - 25 keV)
Be Focusing Lenses	Provide focusing at sample while preserving coherence	Small beam size at the focus (< 10 μm)
Slits/Apertures	Beam definition, Beam halo cleaning	0.25 μm accuracy, 1 μm repeatability
Attenuators	Provide variable attenuation for alignment	Variable, up to 10^6 reduction
X-ray Diffractometer	Orient the sample	
Wide Angle Detector Stage	Move the detector in reciprocal space	7 m sample detector distance up to 2θ = 60° in diffraction geometry
Small Angle Detector Stage	Move the detector in reciprocal space	Large sample detector distance (i.e. up to 20 m) enabling high resolution speckle observation in the forward direction
2D Detector from BNL by MOU	Provide 2D pixelated detection capability	1024 x1024 pixels, 120 Hz frame/s, dynamic range 1000, single-photon sensitivity, pixel size 35x35 μm^2

Table 5-1. Specifications of XCS Instrument Components.

5.2.3. X-ray Optics

Offset Double-crystal Monochromator (ODCM): The current XCS design for the large-offset monochromator is similar to that for the X-ray pump-probe instrument (XPP). It will be located at the beginning of the transport tunnel delivering the beam to the FEH. The concept is based on a horizontal scattering geometry using two Bragg thin crystals. The large 600 mm horizontal offset allows sufficient space to position the XCS endstation diffractometer without interfering with the vacuum beam transport systems delivering the beam to the CXI endstation as presented in Figure 5-6.

The first thin crystal transmits a large fraction of the LCLS beam to the next station while selecting a monochromatic fraction of the spectrum, thus permitting parallel experiments to be performed at different experimental stations. The transmitted part of the beam through the second thin crystal can be used for diagnostics, providing reference information at the origin of the path delivering X-ray photons to the XCS station. The energy tunability requirement (6 - 25 keV, allowing access to the entire LCLS spectrum up to the 3rd harmonic), fixed large exit, as well as the bandpass requirements for increasing the longitudinal coherence length (i.e. $\xi_L = \lambda(\lambda/\Delta\lambda)$ as indicated in Table 5-2, favor a monochromator design with multi-crystals capabilities. (The possibility of splitting spatially the beam by inserting a thick crystal half way in the beam will be as well investigated.) The details of the design proposed for the monochromator are presented in Section 6.1.

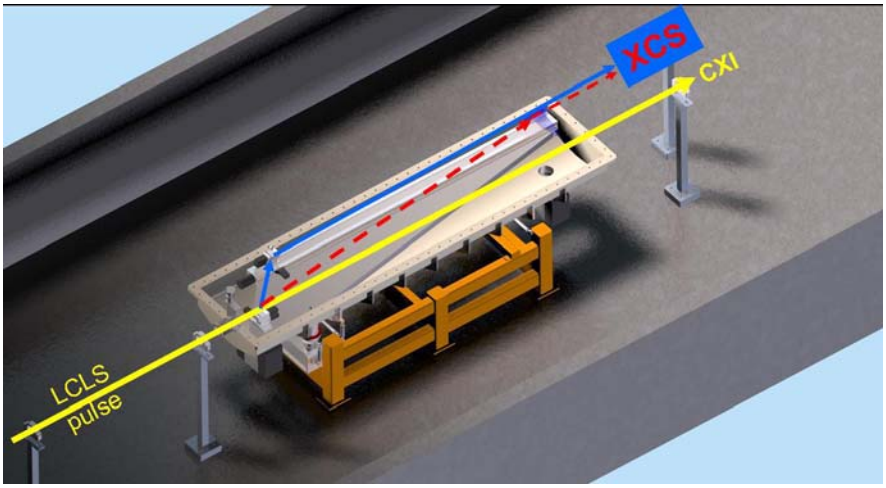

Figure 5-6. Large-offset fixed-exit monochromator, located at the beginning of the transport tunnel. The blue and red dashed lines show the monochromatic X-ray beam at 8 and 24 keV respectively.

Monochromator Crystal	$\Delta\lambda/\lambda$	Coherence Length ξ_L [μm]	
		λ = 1.5 Å	λ = 0.5 Å
Si(111)	1.4×10^{-4}	1	0.3
Si(220)	6.1×10^{-5}	2.45	0.8
C*(111)	5.9×10^{-5}	2.54	0.9
C*(220)	2.3×10^{-5}	6.5	2.2

Table 5-2. Longitudinal coherence length for two wavelengths of 0.5 and 1.5 Å for a selection of silicon and diamond monochromator crystals. These two cases correspond to the undulator 1st and 3rd harmonic of the LCLS x-ray spectrum.

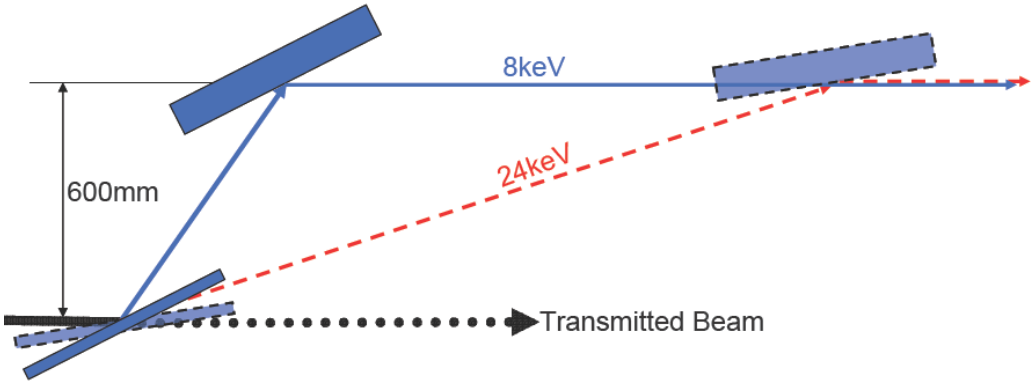

Figure 5-7. Large-offset and fixed-exit monochromator for Si(111) thin crystals performing at 8 or 24 keV. The offset is 600 mm, and the blue and red dashed ray tracing represent 8 keV and 24 keV respectively. The first thin crystal allows the selection of a specific energy while transmitting a portion of the beam to the next endstation (CXI). The second thin crystal allows the transmitted beam to be used as a diagnostic.

Split and Delay Line: Two pulses of approximately equal intensity and a defined time delay in between them are needed to probe fast dynamics (i.e., for characteristic times ranging from 10^{-12} up to 10^{-8} seconds). An incoming pulse of LCLS FEL radiation will be split into two pulses by a thin Bragg or Laue reflector. Additional Bragg reflectors will be used to construct independent optical paths for the two pulses. The path will be independently varied in a controlled way between typically 30 μm and 3 m, thus giving delays of 100 fs up to 3 ns. A simple geometry for the pulse splitter involves a fixed delay leg and a variable one (in order to allow the delay to be tuned through zero delay), with two pairs of crystals in symmetric Bragg geometry on each leg as shown schematically in Figure 5-8.

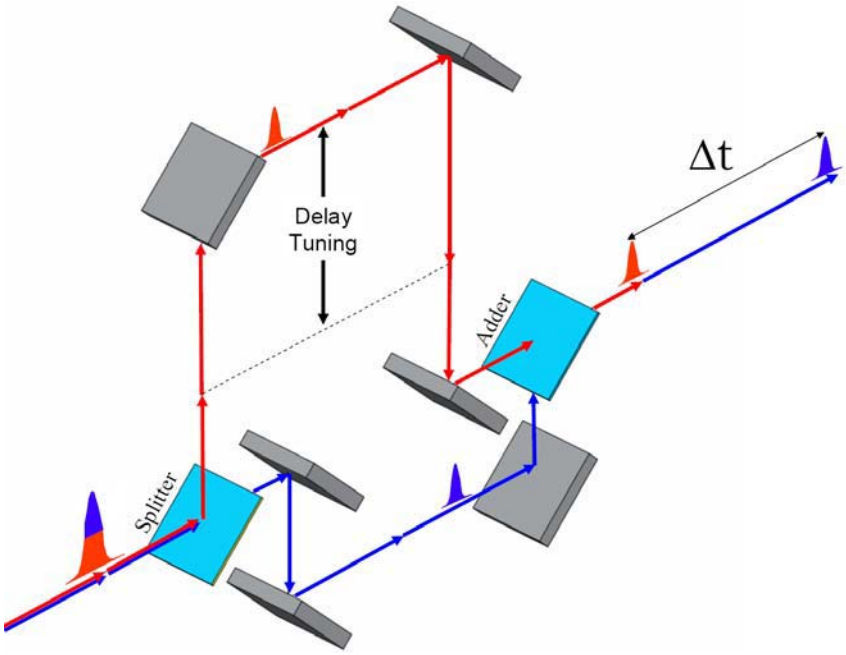

Figure 5-8. Schematic diagram of the Split-Delay unit. The incoming LCLS XFEL pulse is split in two pulses (red and blue), each following a path of different length before getting recombined by the "adder" thin crystal into a single beam with the requested time-structure.

The two "blue" crystals will be sufficiently thin to transmit the undiffracted beam and act as a "Splitter" and "Adder", respectively. The first one performs the splitting role and separates the incoming FEL pulse in two different pulses of equal intensity. The blue path would be the fixed path. The pulse traveling on the red path would have its path length tuned relative to the blue one by translating the two crystals located at the top of the unit. After the second thin crystal, the "Adder", the two delayed pulses are recombined in a single beam, having the appropriate time structure for performing the experiment.

An alternate scheme for the Split and Delay unit would be to spatially split the incoming FEL pulse in two parts and then recombine them by overlapping the two beams coming from each of the paths.

Beryllium Lens Focusing: XPCS experiments rely on the capability of resolving speckles. The speckle size (≈L(λ/D)) is directly related to the beam size D at the sample position and the sample-detector distance L. In the small angle regime for 1.5Å X-rays, a beam size of 50 μm at the sample gives a speckle size of typically 60μm at 20 meter from the sample. The finite dimension of the XCS experimental endstation limits the availability of using the complete LCLS beam size (typically of 350 μm at the hutch 4 FEH-location) and thus requires the use of beam-defining slits. If the speckle size does not match the 2-dimensional detector pixel size a degradation of contrast will be observed. Reducing the beam size by using defining slits dramatically reduces the available incident coherent flux at the sample. Thus, Beryllium focusing lenses will be used to produce a small beam size without significant flux reduction. A selection of lens configurations is foreseen in order to achieve small beam sizes (i.e. in steps down to 10 μm) at the sample both for 8.265 and 24.795 keV photons (corresponding to the 1st and 3rd harmonic of the undulator respectively).

Slit Systems: Precision slit systems are required to define the spatial region of the sample that is being probed by the X-ray beam and to define the speckle size. This device is of paramount importance due to the large spatial fluctuations of the LCLS, which can be very large for the measurements. The details of the design of the slits can be found in Section 6-3.

Attenuators: In some instances it may be required to attenuate the X-ray intensity to prevent either sample or detector damage due to the extremely high peak power of the LCLS. Variable attenuation can be achieved by inserting a combination of foils into the beam bath. However, the material must be able to withstand the LCLS beam without damage and low-z material such as beryllium must be used. Details can be found in Section 6.4.

Diffractometer: A standard 4-circle diffractometer is required to perform experiments using a detector located in the horizontal scattering plane. For small angle XPCS experiments, the diffractometer would hold a SAXS sample environment. For wide angle XPCS experiments, the sample will need to be aligned regarding its crystallographic orientation. Standard sample environment compatible with diffractometer motions will be used.

Local Optics: A selection of local optics will be used for some experiments. A standard double mirror system in vertical scattering geometry will be used for harmonic rejection purposes. The same system can be used to perform XPCS experiments in grazing incidence geometry, where the beam will impinge the sample with a specific incidence angle.

Small and wide angle detector stages: Two different detector stages will be constructed for the XCS instrument to position the 2D detector provided by BNL. Two distinct classes of XPCS experiments are considered: those using small angle scattering geometry, and those using diffraction geometry. Both types of experiment require a large sample-detector distance in order to match the speckle size (scaling as the inverse of the beam size at the sample). For diffraction experiments, in order to be accommodated within the lateral dimension of the XCS experimental hutch, a fixed distance of 6-7 m is proposed, thus permitting

2θ angle up to 60°. The detector would be placed in a long evacuated tube that rotates in the horizontal plane around the diffractometer axis. Inside the tube the detector would move both horizontally and vertically. This geometry would allow one to work either in diffraction geometry in the horizontal plane, or to investigate the sample in grazing incidence geometry (using the internal vertical translation).

For small angle scattering experiments, a variable sample to detector distance from 10m up to 20m is proposed in the forward direction. The end of the stage consists of a large evacuated chamber in the forward direction which could accommodate sample-detector distance from 10 to 20 m. The chamber can be connected to the diffractometer with a removable evacuated flight path. In the 20 meter configuration at 8.265 keV, the incident beam size can be 100 μm and still allow the 2D detector pixel size to match the speckle size, thus offering maximum contrast. In addition a standard 2θ arm with a short sample detector distance could be used for sample alignment purposes. Figure 5-9 presents a conceptual sketch of the proposed instrument.

Sample environment: Two sample environments will be constructed for the XCS instrument. A temperature regulated small angle scattering chamber will accommodate samples contained in capillaries or other cells, with a temperature stability of 0.1K. The ability to apply external excitation to the system (such as magnetic fields) will be considered. For diffraction experiment, a high-stability furnace (stability better than 1mK) as well as a cryostat will be used covering the complete range of temperature required to probe phase transitions in hard condensed matter dynamics.

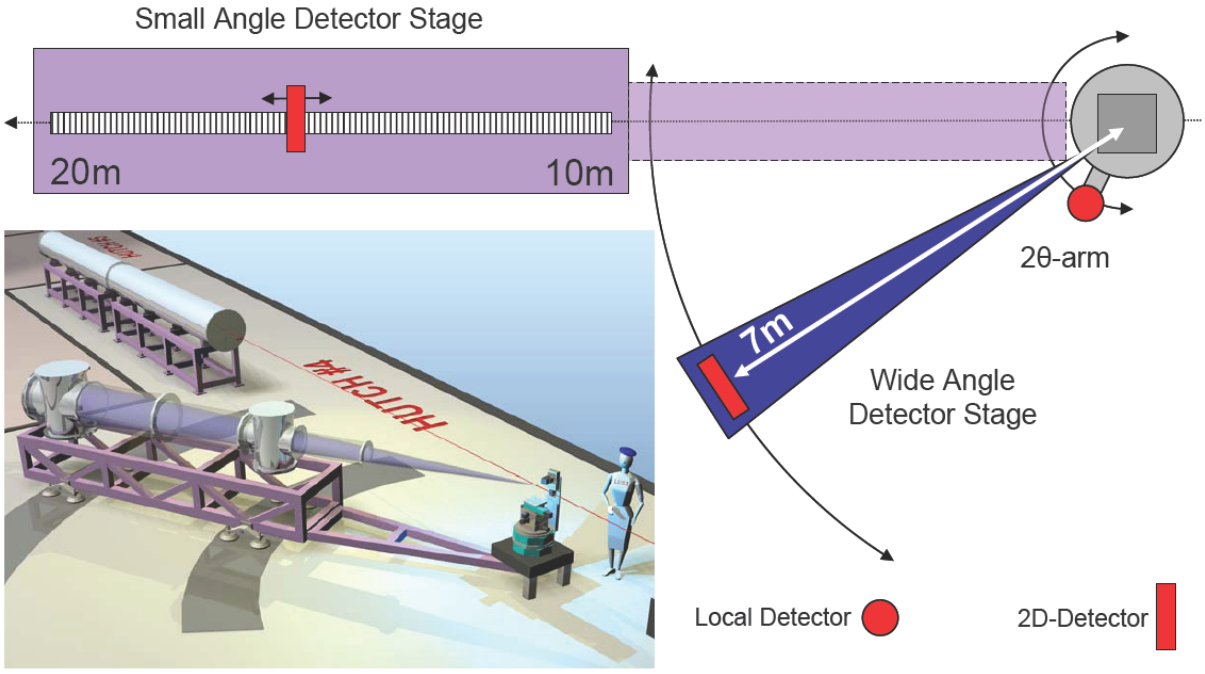

Figure 5-9. Conceptual layout of the XCS endstation with the two detector stages (wide and small angle) and the local detector for alignment purpose. The insert present a 3D artistic view of the hutch with its two detector stages. The small angle setup could provide a sample-detector distance of up to 20 meters in the forward direction. The wide angle detector stage would allow 2θ scattering angles up to 60° with a sample-detector distance of 7 meters.

5.2.4. XCS 2D Detector System

Technical Requirements: A very important component of this instrument will be the X-ray detector. XPCS requires a pixelated detector with relatively small pixel size. The pixel size must be smaller than the speckle size, preferably by a factor of two to three to allow for sufficient oversampling and provide maximum contrast. The speckle size is inversely dependent on the beam size at the sample, which is at most given by the transverse coherence length of the X-ray beam at the sample. If the pixel size becomes the limiting factor, the detector distance can be increased to satisfy the oversampling requirement, but at the expense of scattering intensity. Assuming a sample-detector distance of 7meters with coherent X-rays of 8.265keV and a beam size of 30×30μm^2, the pixel size is estimated to be 35x35 μm^2. The requirements for the detector are summarized in Table 5-3.

The BNL XAMPS detector system: The XPCS 2D-detector will be a custom system built by Brookhaven National Laboratory since no commercial detector is available that meets the XPCS specifications. The detector performance parameters will be optimized for scattering experiments to be performed at the LCLS. Like the Pump-Probe 2D-detector this design is based on an X-ray active matrix pixel sensor (XAMPS) technology. However, in this design the switch is replaced by a charge-pump device which allows for smaller pixel size and lower noise.

The XAMPS detector is a semi-monolithic device. A pixilated high resistivity silicon sensor serves as the detection volume where incoming X-rays are converted into electrons. This design ensures optimal quantum efficiency, since the entire wafer thickness is sensitive to X-rays. The number of diffracted X-rays is deduced from the integrated charge per pixel. In this detector integrated charge-pump devices control, for each pixel, the readout of the collected charges. The charges are stored in a potential well in each pixel and released by applying a controlled potential. A separate readout ASIC contains a charge-sensitive amplifier. The analog signals coming from the readout chip are multiplexed and then digitized in a 12 bit ADC. The XAMPS is read out one row at a time (1024 pixels) which results in a total readout time of about 1 ms per frame. A row-by-row readout requires only one amplifier channel per column which reduces the interconnect complexity.

Parameter	Specification
Energy Range	6 - 24 keV
Dynamic Range	100
Readout Frame Rate	> 120 Hz
Quantum Efficiency	> 90% at 8 keV
Noise	<< 1 photon
Pixel size	≤ 35x35 μm^2
Detector Area	1024x1024 pixels

Table 5-3. Detector specifications for the XCS instrument.

The following technical challenges will be addressed by the XPCS detector development team:

- Engineering the readout of the ASIC to have a very low noise figure while maintaining single photon sensitivity.
- Overcoming the fabrication of a sensor with a small pixel size of 35×35 μm^2 with an integrated charge-pump.
- Sustaining a 2 Gbit/s peak data rate throughout the readout and storage process.
- Engineering a data acquisition boards that will merge beam diagnostics data and perform real time data processing.

5.3. REFERENCES

[39] G. Grübel and G.B. Stephenson, in Proceedings of the 4th Generation Light Source Workshop, Advanced Photon Source, Argonne National Laboratory, 10/27-29/97, and references therein.
[40] A. Robert, Private Communication.
[41] S. Brauer et al., (1995) Phys. Rev. Lett. 74, 2010; S.B. Dierker et al. (1995) Phys. Rev. Lett. 75, 449; T. Thurn-Albrecht et al. (1996) Phys. Rev. Lett. 77, 5437; S.G.J. Mochrie et al. (1997) Phys. Rev. Lett. 78, 1275; A. Malik et al. (1998) Phys. Rev. Lett. 81, 5832; A.C. Price et al. (1999) Phys. Rev. Lett. 82, 755; L.B. Lurio et al. (2000) Phys. Rev. Lett. 84, 785; D.O. Riese et al. (2000) Phys. Rev. Lett. 85, 5460; D. Lumma et al. (2001) Phys. Rev. Lett. 86, 2042; D. Pontoni et al. (2003) Phys. Rev. Lett. 90, 188301; K. Ludwig et al (2005). Phys. Rev. B.72, 144201 A. Robert et al. (2005) J. Chem. Phys. 122, 084701, A. Robert (2005) J. Magn. Magn. Mat. 289, 47, A. Robert et al. (2006) Europhys. Lett. 75, 764.
[42] A. Fera et al. (2000) Phys. Rev. Lett. 85, 2316; I. Sikharulidze et al. (2002) Phys. Rev. Lett. 88, 115503; H.J. Kim et al. (2003) Phys. Rev. Lett. 90, 068302; A. Madsen et al. (2003) Phys. Rev. Lett. 90, 085701; C. Gutt et al. (2003) Phys. Rev. Lett. 91, 076104; 91, 179902(E) (2003); I. Sikharulidze et al. (2003) Phys. Rev. Lett. 91, 165504; A. Madsen et al. (2004) Phys. Rev. Lett. 92, 096104, S. Streit et al. (2007) Phys. Rev. Lett. 98, 047801.
[43] G. Grübel et al (2004) J. All. Comp. 362, 3.
[44] LCLS "the first experiment", September 2000 SLAC-R-611 -- LCLS The First Experiments; http://tesla.desy.de/new_pages/tdr_update/ supplement.html;
[45] J. W. Goodman, Statistical Optics (Wiley, New York, 1985).; B. Chu, Laser Light Scattering: Basic Principles and Practice (Academic Press, Boston, 1991).
[46] J. Mainville et al (1997) J. Appl. 30, 828, D. Abernathy et al. (1998), J. Synchrotron. Rad. 5, 37, A. Sandy et al (1999) J. Synchrotron. Rad. 6, 1174.Cryst.
[47] J. Macutkevic et al. (2006), Phys.Rev. B 74, 104106.
[48] G. Xu et al. (2006), Nature Materials 5, 134.
[49] S. Tinte et al. (2006), Phys. Rev. Lett. 97, 137601.
[50] A. Robert (2007) J. Appl. Cryst. 40, s34.

6 - X-RAY OPTICS

A common suite of X-ray optics will be constructed to prepare the LCLS beam for experimentation. The optics will be used to tailor the FEL wavelength, size and intensity for each individual endstation, as well as provide multiplexing capability. Although many of the optical components are similar to current instrumentation at 3rd generation X-ray light sources, the design of the optics must account for the unique challenges presented by the LCLS FEL radiation. In particular, the enormous peak power and the transverse coherence of the X-ray beam must be considered. This chapter describes the current concepts of the various X-ray optical components for the LUSI project.

6.1. OFFSET MONOCHROMATOR

The XPP and XCS instrument designs include a large offset double-crystal monochromator (ODCM) that operates in the horizontal scattering geometry. Thin Bragg crystals will be utilized to transmit a small monochromatic portion of the 0.3% natural bandwidth of the LCLS FEL radiation to the XPP or XCS experiment, while transmitting a large fraction of the FEL radiation downstream to another experiment. A 600 mm horizontal offset between the monochromatic beam and the direct LCLS beam will allow sufficient space to position and operate X-ray diffractometers without interfering with the vacuum beam transport of the transmitted direct beam. The monochromator is designed to permit all crystal scattering angles (2θ) between 9 and 50 degrees. The components of the ODCM will reside in a vacuum environment to avoid contamination of the Bragg reflectors and to avoid attenuation of X-ray flux due to air scattering. A conceptual image of the ODCM is displayed in Figure 6-1.

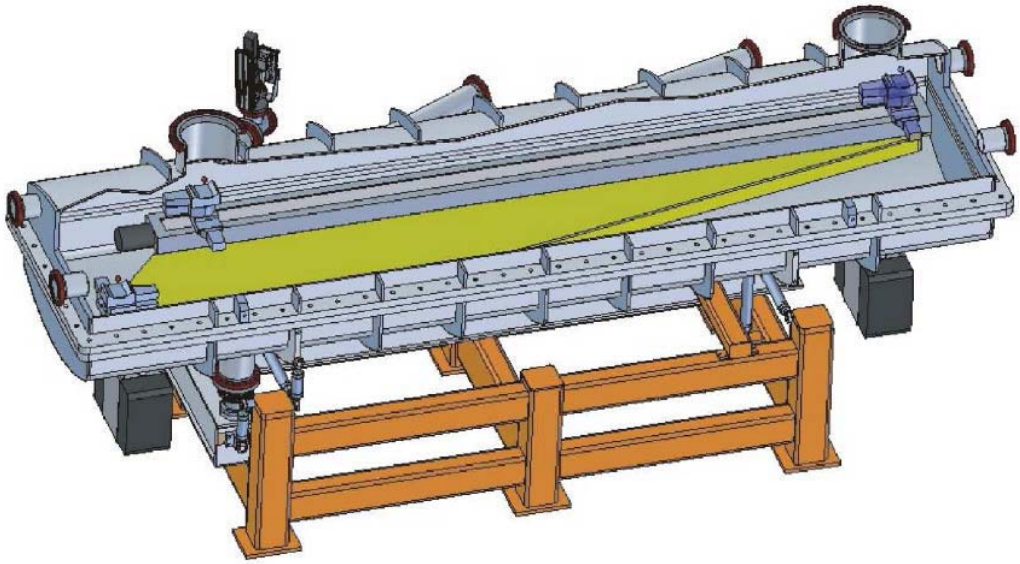

Figure 6-1. Schematic of the double-crystal offset monochromator. The second Bragg reflector is displayed at the extreme locations of the scattering range.

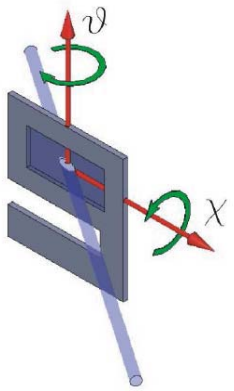

Figure 6-2. Schematic of a Bragg crystal showing the χ and θ rotation axes. The blue line represents the incident X-ray trajectory.

Two material choices are being considered for the monochromator crystals: silicon and diamond. Silicon crystals have the advantage that they can be manufactured with a very high crystalline quality, i.e. dislocation-free. However, due to the relatively large attenuation coefficient, the silicon crystal thickness must be limited to a few microns to have an appreciable transmission of the 1.5 Å FEL radiation. The attenuation coefficient of diamond is significantly smaller than silicon and thus much thicker crystals can be accommodated. Additionally, diamond has superior thermal properties [51] and damage resistance. However, the manufacturing of high quality single crystal diamond is difficult. Only small portions of currently available single crystal diamonds are dislocation-free [52]. Both materials are being considered for the ODCM design.

Precise control of the Bragg crystal orientation is required for operation of the monochromator, particularly for the horizontal scattering angle (see Figure 6-2). The resolution of this motion is determined by the rocking curve width of Si (2 2 0) computed for an X-ray wavelength of 0.5 Å (3rd harmonic at 24 keV). The required motion step resolution is calculated to be 0.15 arcsec, which is approximately 1/10th the FWHM value of the rocking curve. However, an angular precision of 0.04 arcsec is required to steer the X-ray beam to a precision of 40 μm at the FEH location, a distance of greater than 150 m from the XCS monochromator (see Section 5.2.2). Beam-based closed loop feedback systems likely cannot be implemented to control the angular orientation of the Bragg reflector due to inherent pulse-to-pulse instabilities of the LCLS beam in both intensity and position. Thus, it is a necessity that the repeatability of the motion system is at the same level as the angular precision. The various parameters of the ODCM are displayed in Table 6-1.

Parameter	Value
Horizontal Offset	600 mm
2θ Scattering Angle	9-50 degrees
θ Precision	0.04 arcsec
χ Precision	2 arcsec

Table 6-1. Specifications for offset double-crystal monochromator.

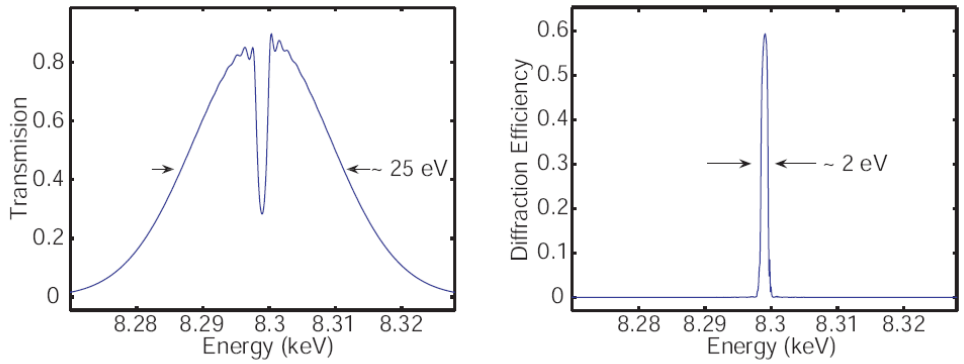

Figure 6-3. Transmission and efficiency of a 2 μm perfect Si (111) Bragg reflection. The transmission is shown on the left and the efficiency on the right.

The spectral bandwidth of the LCLS is expected to be 0.3% of the mean photon energy for operation at 1.5 Å. This photon energy spread exceeds the energy acceptance of a silicon Bragg reflector. Thus, a portion of the LCLS pulses can be spectrally selected with the use of a thin Bragg reflector to allow concurrent delivery of the X-ray beam to XPP experiments as well as to the FEH. Figure 6-3 displays the transmittance and diffraction efficiency of a 2 μm Si (111) Bragg reflector. The LCLS photon energy spectrum is approximated as a Gaussian distribution with a FWHM of 25 eV (0.3%). Calculations suggest that up to 2.5% of the 1.5 Å LCLS intensity will be accepted by the ODCM using a 2 μm and 4 μm Si (111) Bragg reflector for the 1st and 2nd crystal. With this arrangement as much as 85% of the incident intensity transmits through the 1st reflector into the X-ray transport tunnel and 1.3% transmits through the 2nd Bragg reflector into the diagnostics beamline.

6.2. X-RAY FOCUSING OPTICS

In certain experimental situations, it is necessary to focus the LCLS FEL radiation to a significantly smaller spot size than the nominal size at the sample position. Two focusing technologies will be used: refractive lenses and Kirkpatrick-Baez mirrors. Numerous advantages and disadvantages exist for both technologies. The trade-offs between the two focusing options will be considered and the focusing choice will be made based upon the experimental requirements of each LUSI instrument.

6.2.1. Refractive Lens Systems

The index of refraction of hard X-rays in materials differs from unity. Thus, it is possible to focus X-rays using an appropriately shaped lens in much the same way as a visible wavelength lens [53]. In general, a stack of lenses is required to focus the beam at manageable focal lengths since the index of refraction ($1-\delta$) only slightly differs from unity (δ typically on the order of 10^{-4}). The lenses will be manufactured from beryllium to minimize the X-ray attenuation through the lens as well as maximize the damage threshold of the lens. High purity beryllium with a very good surface finish must be used to minimize degradation the coherent phase front of the FEL beam.

The primary advantage of the refractive lens system is that the beam is not deviated from the unfocused trajectory when the optic is inserted, as well as the ease of alignment. The two major disadvantages of refractive lenses are the chromaticity of the optic and transmission loss. The index of refraction of hard X-rays varies with wavelength and thus for a single lens system different wavelengths

will have different focal properties (focal length, spot size). The transmission loss will generally be ~ 60% but this will depend upon the number of lenses required for each particular system.

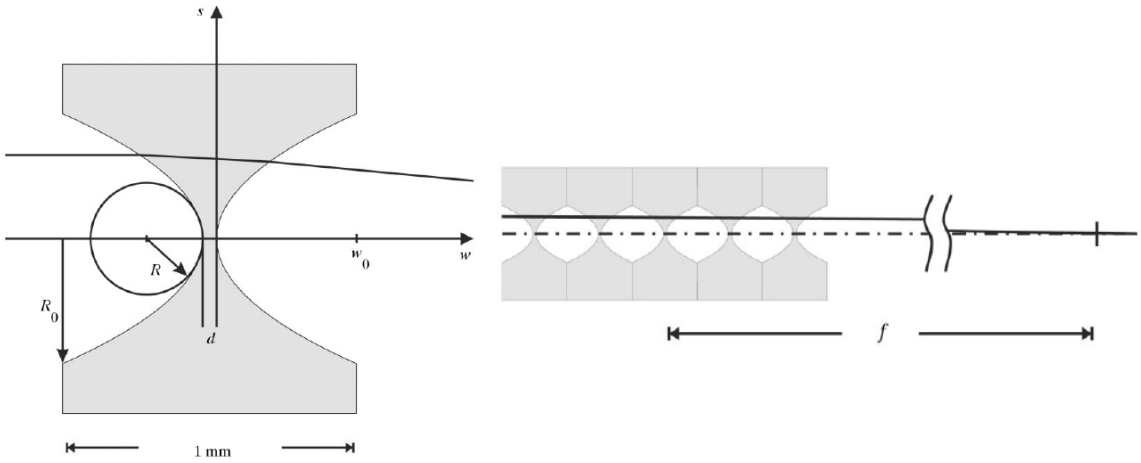

Figure 6-4. Schematic of a single parabolic refractive lens and a compound stack of lenses. The single lens is shown on the left and the compound on the right [53].

6.2.2. Kirkpatrick-Baez Mirror Systems

The extreme focusing required to image single bio-molecules will be achieved using Kirkpatrick-Baez (KB) mirrors. The KB concept was developed in the late 1940's as an X-ray microscope [55]. As early as 1953 Kirkpatrick and Pattee [56] proposed that the KB configuration could be used as to produce a small focus for a microprobe. The concept involves two mirrors and though it lacks the simplicity of a Be lens system it is achromatic and has already been demonstrated to be capable of achieving focal spot sizes of ~ 50 nm at synchrotron radiation sources [57]. In order to mitigate surface damage from the LCLS beam the mirrors will be coated with B_4C. Not only is B_4C damage resistant, but it introduces little effect on the reflectivity due to absorption.

6.3. X-RAY APERATURE SYSTEMS

A precision slit system is required to define the spatial region of the sample that is being probed by the X-ray beam and to remove parasitic scatter. This device is a critical beamline component due to the relatively large shot-to-shot spatial fluctuations of the LCLS FEL in comparison to storage ring based sources. Spatial fluctuations of the X-ray beam on the sample can be problematic since there may be spatial dependences of the sample being studied. This can lead to alterations of the measured X-ray scatter. For pump-probe experiments the signal being measured is, in general, a fractional change to the equilibrium X-ray scatter. When spatial fluctuations are present, the incident intensity probes different regions of the sample and this either skews the data or prevents the study from being successfully performed. These problems are mitigated when an aperture is used. The spatial fluctuation in the position of the X-ray beam is converted into an intensity fluctuation and can be monitored. This ensures that the measured intensity is the intensity that is incident upon the sample in the region of interest and can be properly normalized.

Precision slit systems are common at current X-ray light sources. These systems generally consist of a set of precision motors that are used to position polished blades. The blade material is designed to provide maximum X-ray attenuation and is thus made of a high Z material such as tungsten or tantalum. However, some customization is required for this system to ensure that the slit blades are not damaged by the high peak power of the LCLS FEL radiation. In particular, the front side of the blades must be bonded to a low Z material to provide sufficient attenuation so the high Z material is not damaged. The current slit design for the LCLS front end optics specifies a blade material composed of a Tungsten Heavy Alloy bonded with Boron Carbide (see Figure 6-5). A similar design will be implemented for the various endstation precision slit systems for the LUSI project. However, the blade thickness will be significantly reduced from the 50 mm required for the front end system since the blade will only interact with the FEL radiation (downstream of the front end offset mirrors).

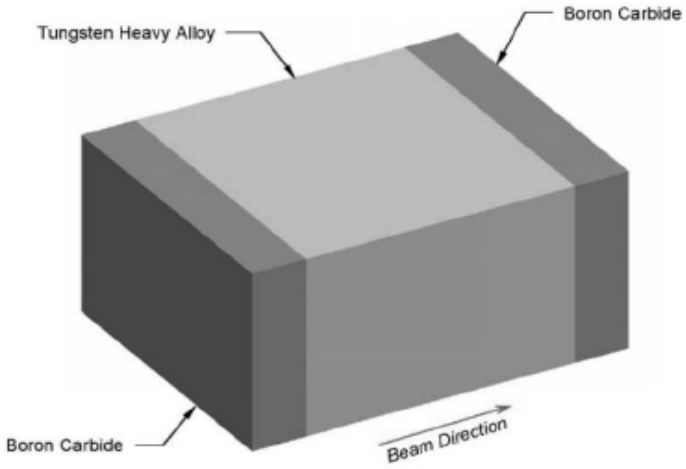

Figure 6-5. Composition of the slit blade used for the front end of the LCLS.

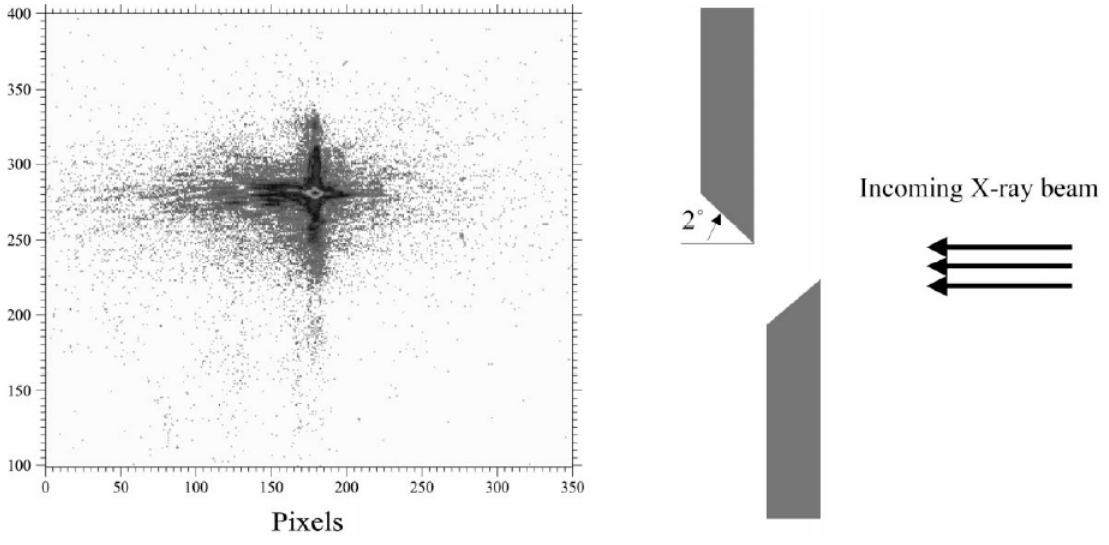

Figure 6-6. Parasitic scattering observed from a set of 2 mm-thick tungsten blades. The beam was apertured to a 2 μm x 2 μm spot size and the camera pixel size is 22 μm [54].

The transverse coherence of the FEL radiation must be considered in the design of the slit system. In particular, parasitic scattering from the slit blade itself can be significant when a coherent beam is apertured. Experiments were performed at the ESRF to characterize this effect [54]. Figure 6-6 displays the X-ray profile measured after a 2 μm square aperture was placed in the X-ray beam. A cylindrical slit blade design was implemented to reduce the background scatter from the slit blades. Similar solutions will be considered for the LUSI slit systems.

6.4. ATTENUATOR SYSTEMS

In some instances it may be required to attenuate the X-ray intensity to prevent either sample or detector damage due to the extremely high peak power of the FEL radiation. Variable attenuation can be achieved by inserting a combination of foils into the beam path. The foil material must be able to withstand the LCLS beam without damage and a low-Z material such as beryllium must be used. A high purity beryllium must be manufactured with a highly polished surface finish to preserve the X-ray beam coherence as much as possible. The LUSI attenuator system will provide a 10^6 factor in attenuation with an incremental attenuation of 4-steps-per decade at a photon wavelength of 1.5 Å.

6.5. REFERENCES

[51] L. Zhang, A.K. Freund, T. Tschentscher and H. Schulte-Schrepping, SRI 2003 Conference, San Francisco, *AIP Conf. Proc*. **705,** 639 (2004).
[52] A. K. Freund, J. Hoszowska, J. P. F. Sellschop, R. C. Burns and M. Rebak, *Nucl. Instrum. and Meth. A*, **467-468,** 384-387 (2001).
[53] B. Lengeler, C. Schroer, J. Tummler, B. Benner, M. Richwin, A. Snigirev, I. Snigireva and M. Drakopoulos, *J. Synchrotron Rad.*, **6,** 1153-1167 (1999).
[54] D. Le Bolloc'h, F. Livet, F. Bley, T. Schulli, M. Veron and T. Metzger, *J. Synchrotron Rad.*, **9**, 258-265 (2002).
[55] P. Kirkpatrick and A.V. Baez, *J. Opt. Soc. Am*., **38**, 766 (1948).
[56] P. Kirkpatrick and H. H. Pattee, *Adv. Bio. Med Phys*., **3**, 247 (1953).
[57] Yamauchi et al., *SRI 2006*.

7 - X-RAY DIAGNOSTICS

The development and engineering of the diagnostic devices for all three LUSI instruments described in Chapter 3 - 5 are grouped and described in this chapter, including the EOS used to determine the relative timing between the electron pulse and a reference laser pulse. All LUSI diagnostics are X-ray diagnostics, except for the EOS measurement, which uses the electron beam.

7.1. INTRODUCTION

Fluctuations in the X-ray pulse characteristics from the LCLS will be much larger than at storage ring based X-ray sources. This stems from the fact that each LCLS electron pulse is created and accelerated fresh, as well as the inherent noise in the Self Amplified Spontaneous Emission (SASE) process. Thus, the fluctuations in the pulse intensity, pointing stability, wavelength, pulse duration, and arrival time of the LCLS X-ray pulses will be significant even when LCLS is fully commissioned and the FEL lasing process running at saturation. Furthermore, depending on the exact location of the point at which the FEL beam saturates and reaches its minimum emittance, the source point viewed from any location downstream of the beam will exhibit longitudinal jitter. Thus the source at the exit of the last undulator will show apparent size variation. Table 7-1 shows the expected parameter fluctuations for the LCLS X-ray pulses.

Unless effectively mitigated or characterized, the level of pulse-to-pulse fluctuations expected from the LCLS X-ray pulses would limit the experiments that can be performed. For example, the experiments carried out at the XPP instrument will typically detect fractional changes in the X-ray scattering intensity induced by an excitation pulse. Only systems that exhibit changes on the order of the inherent X-ray pulse intensity fluctuations would be successfully probed unless a diagnostic is used to measure the incident intensity, thus allowing normalization of the detected X-ray scattering intensity to the incident intensity.

Parameter	Value
Pulse Intensity Fluctuation	≥ 30 %
Spatial Jitter	~ 25 % of the beam diameter
Center Wavelength Variation	~ 0.2 %
Pulse Duration Jitter	~ 15 %
X-ray to RF Timing Jitter	~ 1 ps FWHM
Source Point Jitter	~ 5 m

Table 7-1. Expected pulse-to-pulse fluctuations of the LCLS X-ray beam.

7.2. DIAGNOSTIC SUITE

To fully characterize the LCLS X-ray pulses in all physical aspects, a diagnostics suite will be developed and constructed to measure the X-ray pulse intensity, position, profile, and timing on a pulse-by-pulse basis. Five X-ray diagnostics will be designed to individually measure these characteristics, some being destructive to the X-ray pulse, and some that are capable of running concurrently with the experimental measurement. The specifications of the diagnostics are summarized in Table 7-2. The design and implementation of the diagnostics instrumentation will be modular and standardized whenever possible, allowing flexible placements. The performance goal, technology and concept of each diagnostic instrument are described in this chapter. The performance and flexibility of the diagnostics instrumentation will be critical to both the commissioning of X-ray optics and to the experimental success of the LUSI instruments.

Unlike the photon diagnostics used in the Front End Enclosure (FFE), the LUSI photon diagnostics will only be exposed to either un-attenuated or attenuated FEL radiation, not the full LCLS beam which includes the spontaneous and the FEL at the center. The full LCLS beam will be apertured, with a fixed mask, beam defining slits, and a collimator in the FFE, to spatially filter out the spontaneous radiation outside of the FEL angular and spatial distribution, and then reflected from a set of offset mirrors to spectrally filter out the higher energy FEL components [58]. As such, the maximum energy deposited will be that of a saturated FEL pulse, i.e. 2.4 mJ/pulse (at 0.79 nC charge per electron bunch) in integrated intensity for photon energies up to the 3rd harmonic at 25 keV. Further attenuation of the FEL beam may be necessary so that there will no permanent damage to the detecting elements to allow for prolonged usage.

Diagnostic Item	Purposes	Specifications
Pop-in intensity monitor	Coarse beam alignment/monitoring	Destructive; Retractable; Dynamic range 10^4; Per-pulse operation at 120 Hz; Relative accuracy < 10^{-2}
Hard X-ray in-situ intensity/position monitor	Per pulse normalization of experimental signals; High-resolution beam position monitoring	In-situ; Transmissive (< 5% loss); Dynamic range 10^6; Per-pulse operation; Relative accuracy < 10^{-3}
Pop-in position/profile monitor	Beam alignment/monitoring	Destructive; Retractable; At 50 μm resolution 25x25 mm^2 field of view; At 10 μm resolution 5x5 mm^2 field of view
Wavefront sensor/monitor	Characterization of wavefront; Locating foci of focused beam	Destructive; Retractable; Per-pulse operation at 120 Hz; 0.15 nm < λ < 1.5 nm
Electro-optic sampling timing measurement	Measure the relative timing between the LCLS electron beam and a pump laser pulse	In-situ; Non-destructive; Per-pulse operation at 120 Hz; 200 fs resolution

Table 7-2. Summary specifications of the LUSI diagnostics suite.

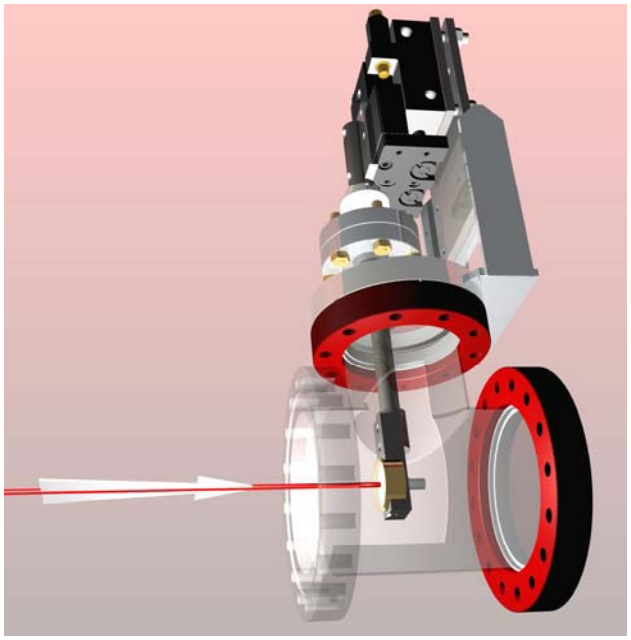

Figure 7-1. Conceptual design of the X-ray pop-in diode intensity monitor. The sensor assembly can be moved in and out of the beam path.

7.2.1. X-ray Pop-In Intensity Monitor

An X-ray diode assembly will be designed and implemented to measure the X-ray beam intensity. This device consists of an X-ray diode, a vacuum actuator for pop-in insertion and readout electronics (see Figure 7-1). Pop-in diode monitors will be strategically placed along the X-ray beamlines, usually in close proximity to a reflecting optic, to aid in alignment of various components.

The main purpose of these monitors is to detect when the reflection condition of a Bragg reflector or mirror is satisfied. It is necessary to have the ability to retract the diode from beam path since the diode is not transmissive. Thus a pneumatic actuator will be used to position the detector. Depending upon the spot size of the X-ray beam at the location of the monitor and the beam intensity, it may be required to either attenuate the X-ray beam or use a diamond X-ray diode to avoid damage.

The requirements for the X-ray diode are low noise, large dynamic range up to 10^4, and short-pulse operation (unlike in the photon counting mode, individual photons will not be time-resolved). The diode could be Si based. A similar device was used at the SPPS [59]. A charge-sensitive-amplifier will be needed for pulse operation to integrate the charge from the electron-hole pairs created by the X-ray pulse. At 8 keV, each absorbed photon produces around 2000 electron-hole pairs in silicon. If this charge is collected on a 1pF capacitor, it will produce a voltage step of 0.3 mV. A full-scale signal of 10^4 photons will generate a step of 3 V. The charge pulse will be shaped using a shaping amplifier for condition before the shaped signal is digitized by an ADC of 14 bit or more.

7.2.2. Hard X-ray In-Situ Intensity/Position Monitor

Pulse-to-pulse fluctuations of the X-ray pulse intensity are expected to be greater than 30% once the LCLS has been fully commissioned and running at saturation. Thus, a single-shot transmissive intensity monitor is required for signal normalization. This capability is important for the alignment of X-ray optics and is paramount for experiments that are detecting induced changes in the X-ray scattering due to external influences, particularly for the XPP instrument.

A non-destructive hard X-ray intensity monitor will be constructed based on the detection of inelastically scattered X-ray photons from a thin foil. Calculations suggest that 0.2% of incident photons are inelastically scattered by a 100 μm thick piece of beryllium [60]. As much as 30% of the scattered photons can be collected by an X-ray diode placed a few millimeters upstream of the foil. When used in the direct LCLS beam (10^{12} photons/per pulse), this equates to 10^{9} photons incident upon the X-ray diode. The shot noise for this amount of photons is $3x10^{-5}$. Thus, an intensity measurement with a precision of 10^{-3} should be achievable with appropriate designs for the X-ray diode and readout electronics.

The intensity monitor can also serve as a beam position monitor (BPM) with the use of a quadrant X-ray diode array. A similar concept, based on X-ray fluorescence, has been developed at the Advanced Photon Source and is currently being commercially manufactured by Oxford Danfysik [61]. Calibration of the BPM is performed by precisely translating the diode array by known distances while monitoring the signals in the diode array. A schematic of the hard X-ray intensity monitor is displayed in Figure 7-2, where a fraction of the X-ray beam, incident from right to left, is backscattered from a foil target onto a quadrant diode array.

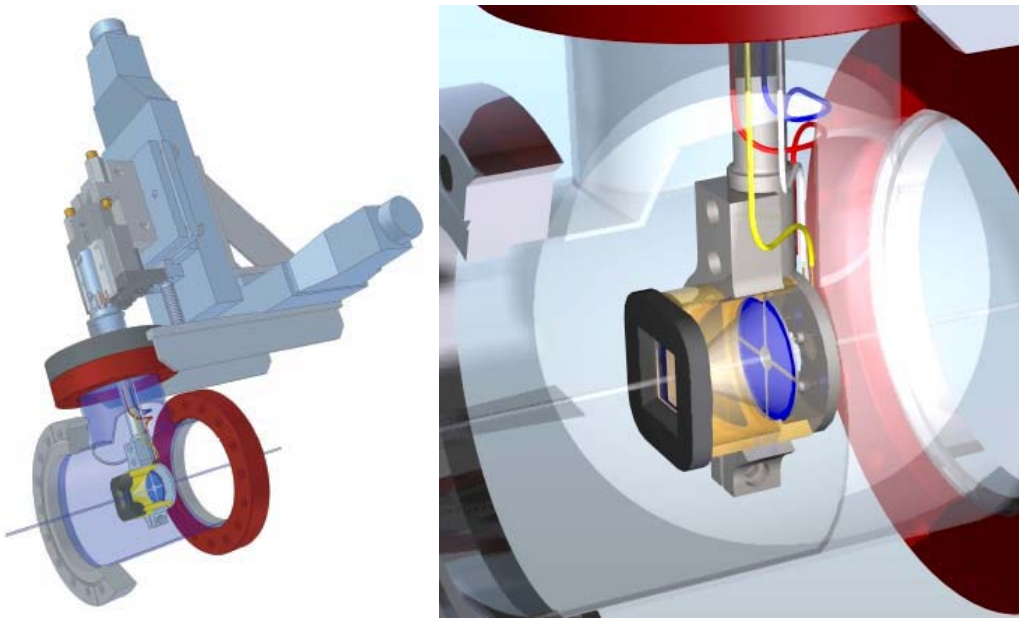

Figure 7-2. Conceptual design of the hard X-ray in-situ intensity/position monitor. On the left is the overall assembly with translational stages, and on the right is an expanded view of the scattering foil and the quadrature cell for position monitoring.

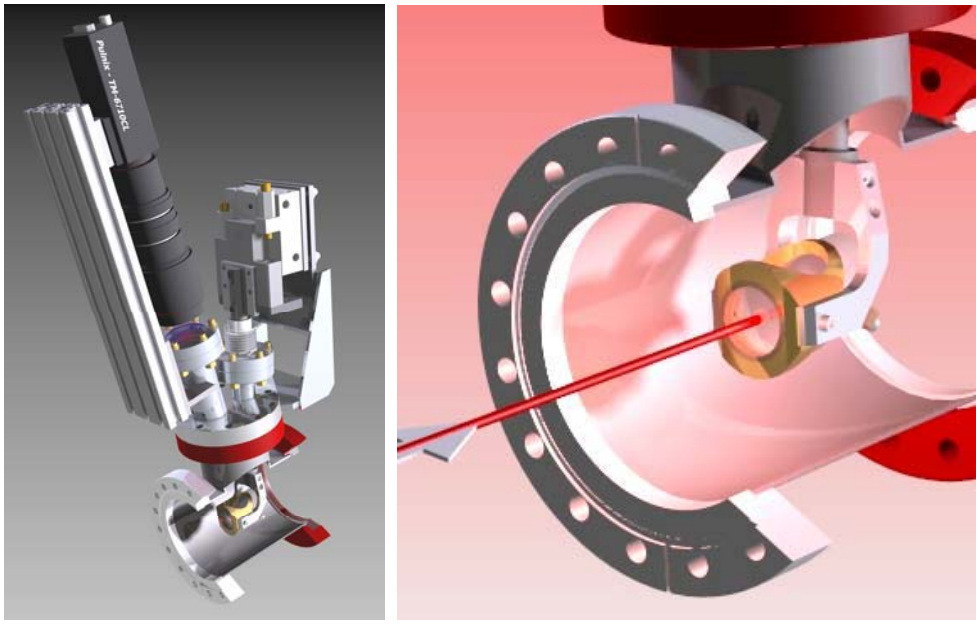

Figure 7-3. Conceptual design of the X-ray position/profile monitor. On the left is the full assembly with the imaging module with a CCD camera, and on the right is the scintillator screen. The sensor assembly can be moved in and out of the beam path.

7.2.3. Pop-In Position/Profile Monitor

A pop-in position diagnostic that can capture a direct image of the X-ray beam position and profile is required for assisting the alignment of optical components. A fluorescent screen assembly will be designed and implemented for accomplishing this. The assembly is composed of a fluorescent screen, a mirror for visible wavelength light, a vacuum actuator and an optical imaging system (see Figure 7-3). This position monitor absorbs the entire X-ray pulse.

A cerium-doped yttrium aluminum garnet (YAG:Ce) or cerium-doped lutetium oxyorthosilicate (LSO:Ce) crystal could be used as the scintillating element of the profile monitor. These materials have been chosen for their high damage threshold and high luminescence yield. The scintillating element converts X-rays into visible light, which in turn can be captured optically.

The X-ray position monitors will be designed to operate in two configurations. The first is a large field of view configuration (25.4 mm x 25.4 mm) with coarse spatial resolution (55 μm). This operating mode will be used for locating and steering the X-ray beam. The second configuration has a narrow field of view (5 mm x 5 mm) with a higher resolving power (10 μm). This operating mode will be implemented when precise positioning of an optic into the X-ray beam is required.

The optical imaging system for the X-ray profile monitor will have a CCD camera with moderate resolution and readout speed. The optical element consists of a zoom lens that is placed some distance (200 mm) away from the scintillating screen. If an image needs to be captured digitally, a frame grabber application will be used. If per pulse operation is required, the scintillating materials should have short enough decay time to allow images lit from a given pulse to be read out in time before the arrival of the very next pulse. Whether the readout electronics have the readout speed to do that depends on the

resolution required. Typical commercial CCD camera has a readout speed of 10 Hz at full frame, thus reading at 120 Hz would mean less number of pixels, i.e., lower resolution.

7.2.4. Wavefront Monitor

A diagnostic that has the ability to measure the spatial profile of a sub-micron X-ray beam is required for successful commissioning of the focusing optics implemented in the LUSI project. Techniques such as scanning a knife-edge across the focused beam or imaging the focus with a scintillating material cannot be used since no material can withstand the peak energy density of the focused LCLS beam. There are two possible options, one option being a Hartman wavefront analyzer that is used to measure the focal properties of the X-ray beam and another based on diffractive imaging of the focal field distribution.

7.2.4.1. Hartmann Wavefront Sensor

A Hartmann wavefront sensor works by subdividing an input wave into multiple elementary beams by a micro hole array. The multiple elementary beams are then imaged onto a X-ray CCD camera placed at a known distance from the hole array. A software algorithm analyzes the image and determines the local wavefront slope of each elementary beam. A reconstruction of the focal spot size is then determined by a second algorithm that back propagates the measured wavefront. This metrology technique circumvents the damage problem since it operates significantly downstream of the focus. It also has the ability to operate in single shot mode, which is important since jitter in the focal spot size and position is expected.

A diagram describing the operational principles of a Hartmann wavefront sensor is displayed in Figure 7-4. First, an image is of the X-ray transmission through a pinhole array is acquired with an X-ray CCD camera. The local phase front tilt of the X-ray beam profile is then computed with knowledge of the pinhole array orientation with respect to the X-ray detector. The focal properties of the X-ray beam are then computed by an algorithm that back-propagates the X-ray wavefront. Table 7-3 shows the specifications for an X-ray Hartman sensor at 8 keV based on a 4 keV model HASO^{TM} X-EUV wavefront sensor by Imagine Optics [62].

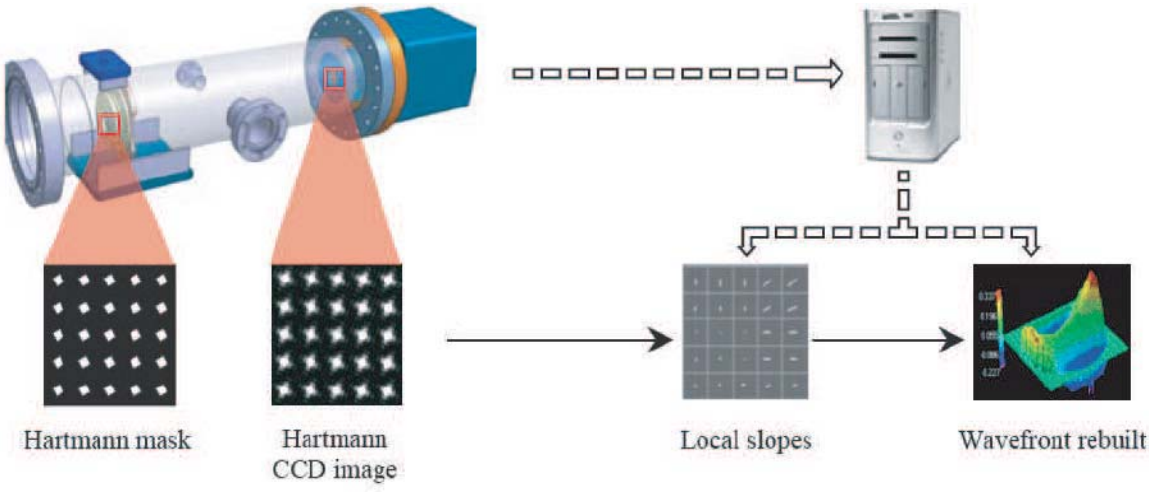

Figure 7-4. Operational schematic of a Hartmann wavefront sensor.

Parameter	Value
Aperture dimension	10 x 10 mm²
Number of sub-aperture dedicated for analysis	75 x 75
Curvature dynamic range ± 0.5 m to ± ∞	0.4 to 4 m - divergent beam
Repeatability (rms)	~ λ/10
measurement accuracy in absolute mode (rms)	~ λ/5
measurement accuracy in relative mode (rms)	~ λ/4
Tilt measurement sensitivity (rms)	0.05 µrad
Focus measurement sensitivity (rms)	< $1x10^{-4}$ m^{-1}
Spatial beam sampling step	~ 130 µm
Minimum readout time	~ 0.6 sec (@2 MHz digitization)
Working photon energy (wavelength)	8 keV (0.15 nm)
Storage temperature / Operating environment	< 55°C / 5°C - 30°C
Compliant vacuum	10^{-6} bar

Table 7-3. Specifications for a Hartmann Wavefront Sensor.

7.2.4.2. Diffractive Imager

It is also possible to reconstruct the wavefront based on a newly-developed technique called diffractive imaging whereby the intensity pattern of a focused beam is over-sampled and used for field reconstruction using iterative phase retrieval algorithm [63].

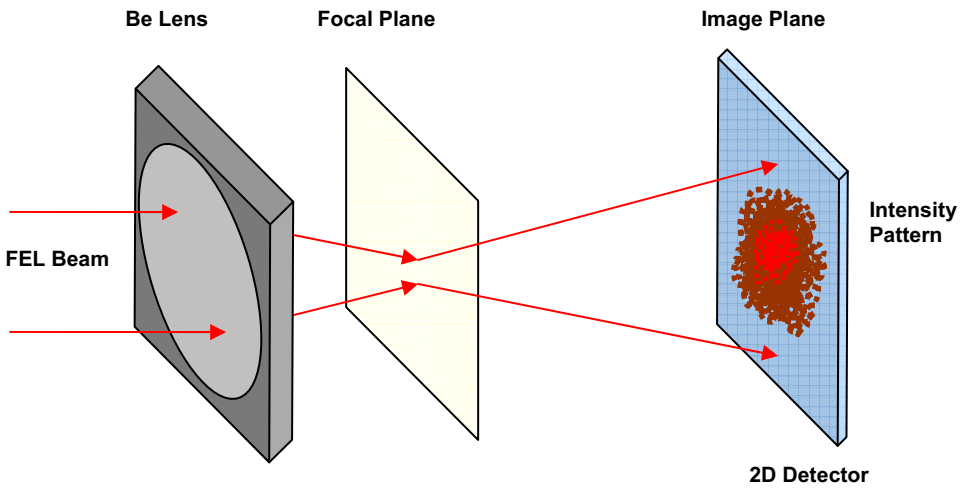

Figure 7-5. Schematic of diffractive imaging of a focused beam from a Be lens.

A conceptual experimental setup for the diffractive imaging is shown in Figure 7-5 for a focused beam using a Be lens. The far field intensity pattern is recorded using a CCD camera and used for reconstruction of the field anywhere between the zone plate and the image plane. The phase retrieval algorithm involves iteratively propagating fields between these two planes and imposing support at these two planes by confining the lateral extents of the zone plate and the image intensity until a stable solution is found. The advantage of the diffractive imaging is its simplicity in implementation and application. Its potential difficulty may lie in defining the support at the focusing optic in the case of Kirkpatrick-Baez mirror pairs.

7.2.5. Electro-Optic Timing Diagnostic

The temporal resolution of laser pump/X-ray probe experiments, in general, is limited by the convolution of the probe pulse duration with the synchronization precision of the pump and probe. The LCLS FEL pulses are expected to have duration of 230 fs FWHM, however, the pulse duration will decrease to 100 fs if lasing can be achieved with less charge in the electron bunch. Additionally, there are schemes to decrease the pulse duration to as short as a few femtoseconds with the use of a slotted foil at the center of the second electron bunch compressor [64]. Laser excitation pulses must be synchronized to within a fraction of the FEL pulse duration to realize the ultimate temporal limit of the LCLS and thus 10 fs X-ray/laser synchronism is desired.

The synchronization of optical laser pulses to accelerator generated X-ray pulses will be partly accomplished by frequency stabilizing the laser repetition rate to a subharmonic of the low-level radio frequency (LLRF) electrical signal used to time the components of the accelerator. Adjustment of the laser frequency is achieved with the use of feedback electronics and a piezoelectric actuator to adjust the laser cavity. Sub-100 fs short term laser/LLRF phase jitter can be realized. However, the X-ray pulse arrival time will jitter with respect to the LLRF at a level of ~ 1 ps primarily due to shot-to-shot energy fluctuations of the electron bunch. Therefore, to perform pump-probe experiments with sub-ps resolution, an additional diagnostic will be required.

7.2.5.1. Electro-Optic Sampling

The temporal resolution of pump-probe experiments can be reduced by measuring the arrival time of each individual LCLS electron bunch with respect to the pump laser using electro-optic sampling (EOS) [66]. In this technique, the electric field of the electron bunch that generates X-rays is used to alter the optical properties of an electro-optic crystal. This alteration is probed with an optical laser that is precisely synchronized to the accelerator LLRF. Only the portion of the laser that is propagating within the electro-optic crystal when the electric filed is present will be altered. In this manner, the arrival time of the electron bunch is encoded onto spatial profile of the optical laser.

Figure 7-6 displays EOS data collected at the SPPS. The centroid of the electro-optic feature is analyzed and used to time stamp each X-ray pulse and the data is compiled accordingly. The position (timing) of the centroid is determined to be better than a fraction of the FWHM to less than 100fs. Recent experiments at the SPPS clearly demonstrated the feasibility of the EOS timing method [67].

The EOS apparatus will be installed in the Linac-to-Undulator (LTU) section of the LCLS. At SPPS a common laser system was used to make the EOS measurement as well as photo-excite samples for pump-probe experiments. Due to the large distances separating the NEH and LTU, duplication of this setup at LCLS is not readily feasible and a separate laser system will be used to perform EOS. Thus, the two laser systems must be precisely synchronized to each other. Another distinction that must be considered is that

the LCLS is a self-amplified source and SPPS was a spontaneous source. EOS measures the arrival time of the electron bunch and at a spontaneous source this timing information will faithfully map onto the timing of the X-ray pulse. This conclusion cannot be drawn for a SASE-based source since there may be intra-bunch timing jitter of the FEL radiation within the electron bunch profile. Therefore, the temporal resolution provided by EOS in this context will be limited by the convolution of the intra-bunch timing jitter and the synchronization precision of the EOS laser and pump/probe laser. A 200 fs temporal resolution is expected.

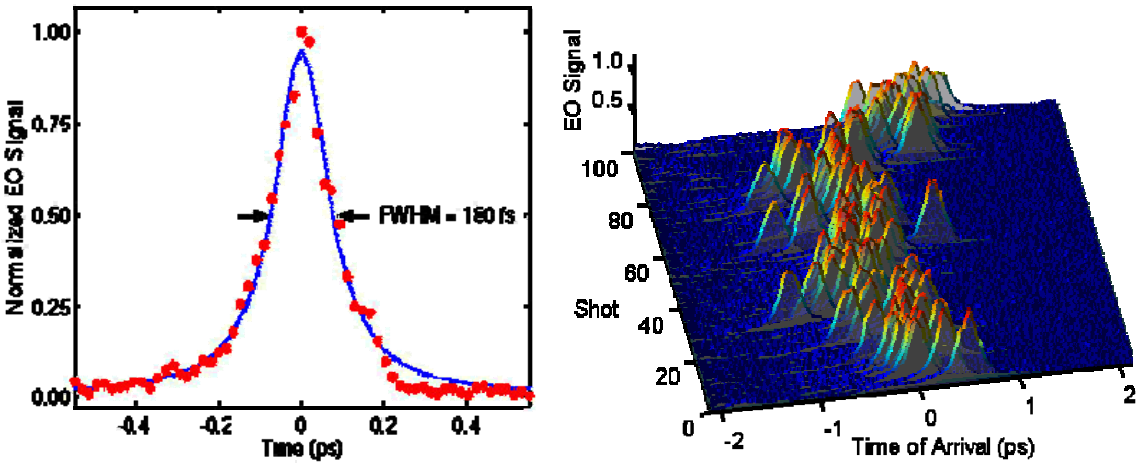

Figure 7-6. EOS data acquired and analyzed at the SPPS. A single electro-optic signal is displayed on the left with a Lorentzian fit. One hundred consecutive EO samples is displayed on the right.

Figure 7-7. Conceptual design of the electro-optic diagnostic vacuum chamber.

Figure 7-7 displays a conceptual design of the EOS vacuum chamber. The EO crystal will be in close proximity from the trajectory of the electron beam. The electric field lines will be almost perpendicular to the beam direction (opening angle = $1/\gamma \sim 1/30000$ at 15 GeV for LCLS electron energy) and thus the exact location of the EO crystal will not impact the temporal resolution but only the signal strength. The EOS laser will be introduced into the chamber via visible ports, and the angle of incidence onto the EO crystal will define the dynamic range of the measurement. The chamber design will permit some adjustment of the incident angle.

7.2.5.2. Stabilized Fiber Optic LLRF Network

The synchronization of all LCLS timing critical system will be achieved with the help of the stabilized fiber optic LLRF network being developed by a team at LBNL in collaboration with the LCLS project. This network will distribute LLRF signals on a length-stabilized fiber network with jitters less than a few fs to distribution points in a start-configuration, with each branch individually stabilized.

The long geographical separation of the distribution points necessitates that the length of the fiber distribution network be stabilized to counter thermal drifts, ground motions, or seismic activities. The LBNL team uses an interferometric technique, whereby the timing delay jitter through the fibers will be stabilized by comparing a retro-reflected pulse from the distribution point end with a reference pulse from the sending end, and actively controlling the fiber length. The most current version of the LBNL fiber stabilization network has a dynamic range of 1 ns and a timing stability of a few fs.

The distribution points include the gun laser system for the photo-injector in Sector 20 (controlling electron beam pulse), the individual RF cavities along the linac cavities (also controlling electron-beam pulse timing), the EOS apparatus, and the each experimental endstation where there is a pump laser (controlling pump laser pulse timing) shown schematically in Figure 7-8. The RF cavities are actively locked to the optical clock phase. Most of the RF timing error is contained within a 10 kHz bandwidth, so these errors and any others affecting X-ray pulse timing (such as RF gun phase) can be detected and transmitted to correct laser timing at the endstations.

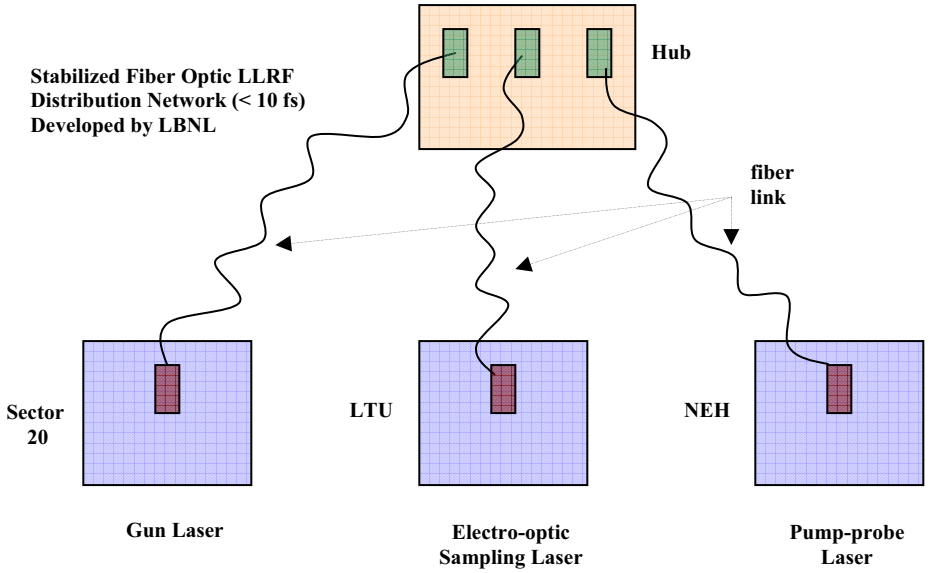

Figure 7-8. Stabilized fiber optic LLRF network for fs timing.

7.2.6. Interconnection with Control/Data Systems

The diagnostic signals are ultimately measured and used for analyzing the experimental measurement. The mechanism for distributing theses measured parameters is discussed in the diagnostics section of the Control/Data System (Chapter 8) in this document. In particular, we discuss the following important cases.

Beam Characteristics Monitoring for Data Acquisition: X-ray beam intensity, position, direction, energy, and profile will be measured, some at the 120 Hz rep rate. The parameters will be distributed to the experimental stations on the 120 Hz real-time network. The motion of all movable parts in the diagnostic apparatus will be controlled via the Control Subsystem, and the detectors sampled by the Data Subsystem.

Feedback to Electron Beam: The X-ray beam characteristics are fed back to electron beam diagnostic system for optimizing beam steering, etc. The feedback could be at 120 Hz or lower frequency for slower drift problem corrections. The network again should provide real-time performance at 120 Hz rep rate of the LCLS beam.

EOS to Controls/Data System: The X-ray beam/electron beam relative timing measurement will be measured at 120 Hz rate. The timing signal will be distributed to pump-probe type of experiments on the 120 Hz real-time network. The slow controls in the EOS chamber will be controlled by the Controls Subsystem. The detectors including the CCD camera will be sampled using the Data Subsystem.

7.3. REFERENCES

[58] J. Krzywinski, et al. “Physics Requirements for the XTOD Direct Imager”, LCLS-1.5-010.

[59] D. P. Siddons, et al., Detectors for Ultrafast X-ray experiments at SPPS, *9th Intl. Conf. on Synch. Rad. Instru.. AIP Conf. Proc.*, **879** (2007), 1176-1179.

[60] Private communication with Prof. Keijo Hamalainen, University of Helsinki, Finland.

[61] R. W. Alkire, G. Rosenbaum, and G. Evans. Design of a vacuum-compatible high-precision monochromatic beam-position monitor for use with synchrotron radiation from 5 to 25 keV. *Journal of Synchrotron Radiation*, **7(2)**:61_68, Mar 2000.

[62] http://www.imagine-optic.com/iop_en_products_hasoxeuv_main.php.

[63] H. M. Quiney et al., Diffractive Imaging of Highly Focused X-ray Fields, *Nature Physics*, **2** (2006) 102.

[64] P. Emma, K. Bane, M. Cornacchia, Z. Huang, H. Schlarb, G. Stupakov and D. Walz, Femtosecond and Subfemtosecond X-ray Pulses from a Self-Amplified Spontaneous-Emission-based Free-Electron Laser. *Phys. Rev. Lett.,* **92** (2004) 074801.

[65] F. B. Kiewiet, A. H. Kemper, O. J. Luiten, G. J. H. Brussaard and M. J. van der Wiel, Femtosecond synchronization of a 3 GHz RF oscillator to a mode-locked Ti:sapphire laser. *Nucl. Instrum. Meth. A* **484** (2002) 619-624.

[66] A. L. Cavlieri et al., Clocking Femtosecond X Rays. *Phys. Rev. Lett.,* **94** (2005) 114801.

[67] D. M. Fritz et al., Ultrafast Bond Softening in Bismuth: Mapping a Solid’s Interatomic Potential with X-rays. *Science* **315** (2007) 633-636.

[68] A. Fohlisch et al., Workshop Presentation, "Challenges and Opportunities in the Study of Materials with Soft X-rays at FLASH and LCLS", May 24-25, 2007, Hamburg, Germany

8 - CONTROLS AND DATA SYSTEMS

The 120 Hz per pulse data collection, high data rate, large data volume, and precise timing control of the LCLS experiments go much beyond those at 3rd generation or older synchrotron sources and require considerable complexity and sophistication in the control and data system in design, implementation, and integration, making them unfeasible for any individual experimental team. As such, the LUSI controls and data infrastructure will provide standard controls, timing measurement, data acquisition capabilities, data storage and management capabilities, and certain common data analysis capabilities to all instruments.

8.1. SYSTEM SCOPE

Included in the scope of the LUSI controls and data system are the Coherent X-ray Imaging (CXI) instrument, the X-ray Pump-Probe (XPP) Instrument, and the X-ray Correlation Spectroscopy (XCS) Instrument including the long in-tunnel beam transport. The XPP instrument will be located in the Near Experimental Hall (NEH), and the CXI and XCS instruments will be located in the Far Experimental Hall (FEH) (see Figure 2-2 and Figure 2-3). The scientific programs that will be conducted in all three instruments are described in Chapters 3, 4, and 5, and present similar generic needs in conventional vacuum and motion control, as well as the ability to use fast 2-D pixelated detectors being developed by the detector groups at Cornell University and BNL. The scope will also include the controls and data acquisition of the common diagnostic components being developed for the three instruments as described in Chapter 7. An important objective is to identify and take advantage of the requirements commonality of all LUSI instruments, as well as the AMO instrument being developed by the LCLS, to arrive at a single standardized architectural framework for controls, data acquisition, and data management systems. The specific needs of individual instruments will be addressed on this common framework.

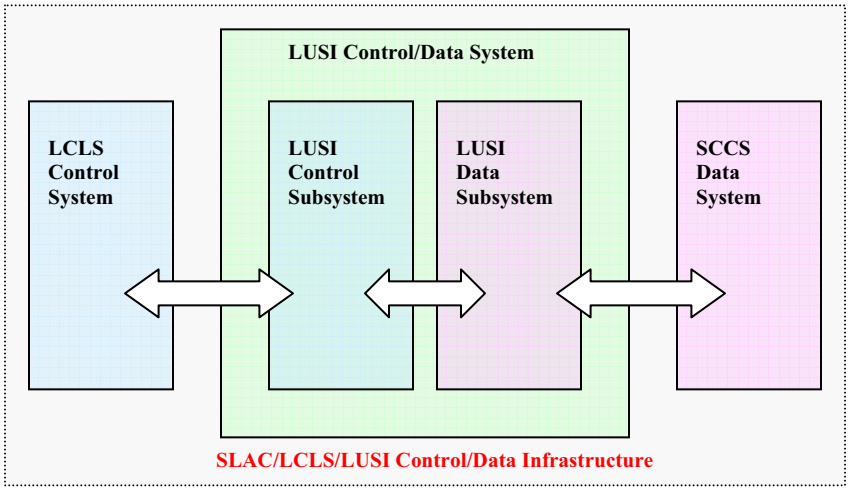

Figure 8-1. Schematic Diagram of LUSI Controls/Data Acquisition System.

8.2. SYSTEM OVERVIEW

The LUSI controls/data system will have two major subsystems, the control subsystem and the data subsystem, that interact with the LCLS and SLAC control/data systems as illustrated in Figure 8-1. It will be designed to interoperate with all relevant existing hardware and software infrastructure at SLAC, especially the LCLS and SLAC's Scientific Computing and Computing Services (SCCS). Object-oriented design, upgradeable to take advantage of the fast moving technological advances in data acquisition and management, will be implemented to provide plug-and-plays capability for certain equipment. In application development, popular software techniques such as multiple-threading, message based inter-process communication will be used to avoid implementations that are monolithic and thus have poor maintainability.

8.2.1. System Functionalities

Controls Subsystem: The LUSI control subsystem will consist of three major components: the slow control component, the 120 Hz real-time operation component, and the fast timing component as shown in Figure 8-2. The slow control component will perform vacuum and motion control. Substantial commonality exists between the LUSI and LCLS slow control system requirements. Wherever applicable, the LCLS control system hardware and software architecture will be adopted. As such, it will be implemented on the EPICS platform [69] used by the LCLS control system [70]. But unlike the LCLS control system, there will be very minimal direct communication between the LUSI control subsystem and the existing SLAC accelerator control system. Instead, the accelerator-experiment interaction, if any, will be facilitated via the LCLS controls.

The 120 Hz real-time operation component will be designed to embed pulse characterization information with experimental data acquired with the 2D pixelated detectors on a per pulse basis. This requirement stems from the intrinsic wavelength, intensity, timing, positional, and directional jitters in the FEL pulses generated via the SASE process. As a result, each pulse must be fully characterized. In addition to providing information for experimental analysis, the 120 Hz operation will provide electron beam feedback to the accelerator system. To implement 120 Hz operation, the non-deterministic nature of the EPICS platform will necessitate a separate network infrastructure such as a reflective memory system [71] such as SCRAMNet to achieve latency of < 8.3 ms required by the 120 Hz operation frequency.

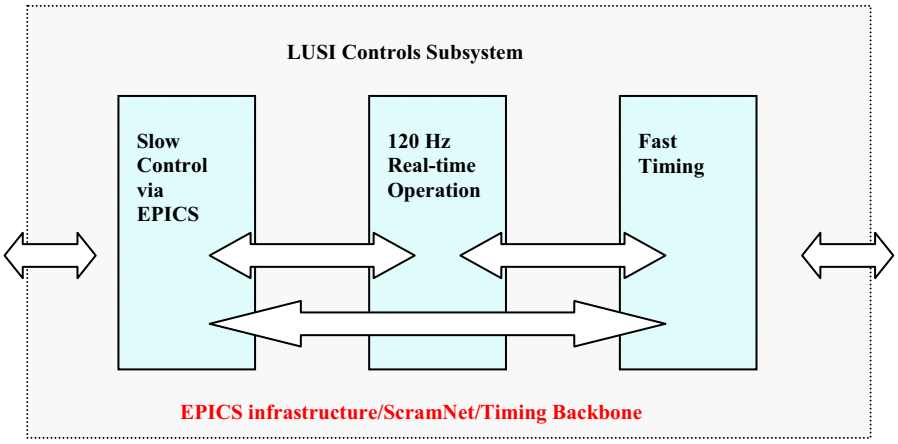

Figure 8-2. Component Level Block Diagram of LUSI Control Subsystem.

The XPP instrument requires additional controls functionality in timing synchronization between the pump laser pulse and the probe X-ray pulse, with an ultimate timing resolution of order 100 fs. This resolution will be achieved by the EOS measurements (see Section 7.2.5). The EOS timing component must be able to, on per pulse basis, receive the pulse information and encode it with the timing delay parameter, and distribute the encoded pulse information to the data subsystem. The receiving/dispatching task will be implemented on the 120 Hz framework. In addition, the EOS measurement will rely on a timing distribution network, which is being developed by a team from LBNL and distributes timing signals to the photo-injector, the low-level RF system, and other distribution points with less than 10 fs jitter.

The Control Subsystem described above will provide the following functionalities:
(1) Beamline Operation;
(2) Optics Controls;
(3) Timing and Triggering;
(4) Fast Feedback to the Photon/Electron Beam;
(5) Diagnostics of the Photon Beam;
(6) Laser Control and Safety System;
(7) Machine Protection Systems;
(8) Vacuum System Controls;
(9) Interface to the Data Subsystem and LCLS Control System.

Data Subsystem: The LUSI Data Subsystem will consist of three major components: the Data Acquisition Component, the Data Management Component, and the Data Analysis Component as shown in Figure 8-3. All LUSI instruments will be equipped with 2D multi-megapixel detectors that generate raw data flow at a peak rate of greater than a few Gbit/s or even tens of Gbit/s in the not so distant future, thus requiring a data acquisition system with architecture, implementation, and technology comparable to those having traditionally been used for high energy physics experiments such as BaBar at SLAC. In addition, single molecular imaging experiments will often require up to 10 million frames of good images to achieve desired statistics, totaling 20 TB of data volume assuming 2 MB per frame. Assuming a 50% successful frame rate, a 50% duty cycle, and a 120 Hz operation, the total measurement time needed to acquire all 10 million frames will last up a little over 4 days. As such, a data storage system and network infrastructure compatible with the high peak rate and long experimental duration will be needed. Furthermore, the intrinsic FEL fluctuations make it imperative to implement capabilities for doing on-the-fly data analysis to provide real-time feedback to users.

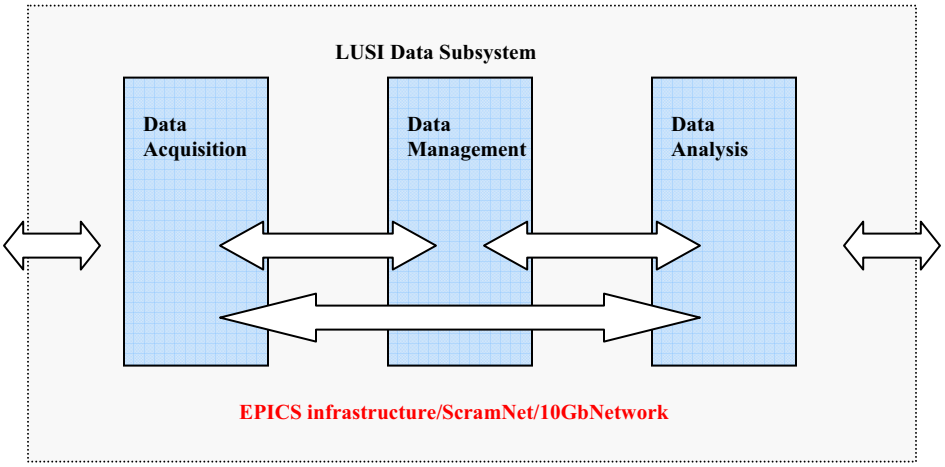

Figure 8-3. Component Level Block Diagram of LUSI Data Subsystem.

The Data Subsystem will use functionalities provided by the Control Subsystem to achieve its own as in the case of a specific type of measurement whereby certain optic element may be moved while various detector signals are being acquired. It will also use the EPICS framework for controls/communications tasks that do not require low latency. On the other hand, the low latency network will be used for the 120 Hz data acquisition. For on-line data storage, a network with an aggregated bandwidth of multi Gbit/s will be used. For longer term data archival, data in the on-line storage will be transferred to the data farm in SCCS, in a way similar to what the BaBar project had implemented for managing its massive data volume. In addition to hosting the LUSI data archiving, SCCS with its computer clusters will need to provide computational resources for certain offline analysis and data visualization for LUSI experiments as well.

The Data Subsystem described above will provide the following functionalities:
(1) Experimental Measurements;
(2) Detector Controls ;
(3) Interface to Canned Software for Experimental Controls;
(4) Real-Time Data Processing;
(5) Quick View Rendering and Visualization;
(6) On-line Storage;
(7) Interface to Long Term Storage for Data Archiving/Retrieval;
(8) Offline Data Analysis;
(9) Volume Rendering and Visualization;
(10) Interface to High-Level Applications;
(11) Interface to Control Subsystem;

8.3. CONTROLS SUBSYSTEM

8.3.1. Controls Architecture

The architecture of the Control Subsystem is schematically shown in Figure 8-4. It will be primarily built on the EPICS framework, with additional real-time applications deriving services from the EVG/EVR network, the low-latency network, and the fast timing network. The EPICS network will have aggregated bandwidth exceeding 10Gbit/s and will be a part of the LCLS EPICS network, or a separate subnet supporting only LUSI clients and servers. The servers are the device controller for pumps, diffractometers, etc; the clients are the experimental control stations.

The LUSI Control Subsystem will control the basic operations of all experimental endstations in the two experimental halls, the NEH and FEH, perform experiments by controlling beamline optical elements and scattering/diffraction instruments, provide fast feedback to the electron beam via LCLC control system for optimizing LCLS operation, perform X-ray beam diagnostics by monitoring various beam positioning and intensity sensors, obtain the timing of electron beam to facilitate synchronization between the X-ray pulses and those of the pump laser. It will provide all the safety and interlock systems for the X-ray and laser beams for personnel and machine protections, and control vacuum gauges and controllers in endstations and along the long transport tunnel connecting the NEH and FEH.

The Control Subsystem will be based on a network architecture as shown in Figure 8-5 with high level applications and functionalities being the top most layer, the communication networks being the bottom layer for executing network primitives, and in between the middle layer of functional blocks for performing specific tasks such as controlling a laser, etc. Below each of the three layers will be described below in more details.

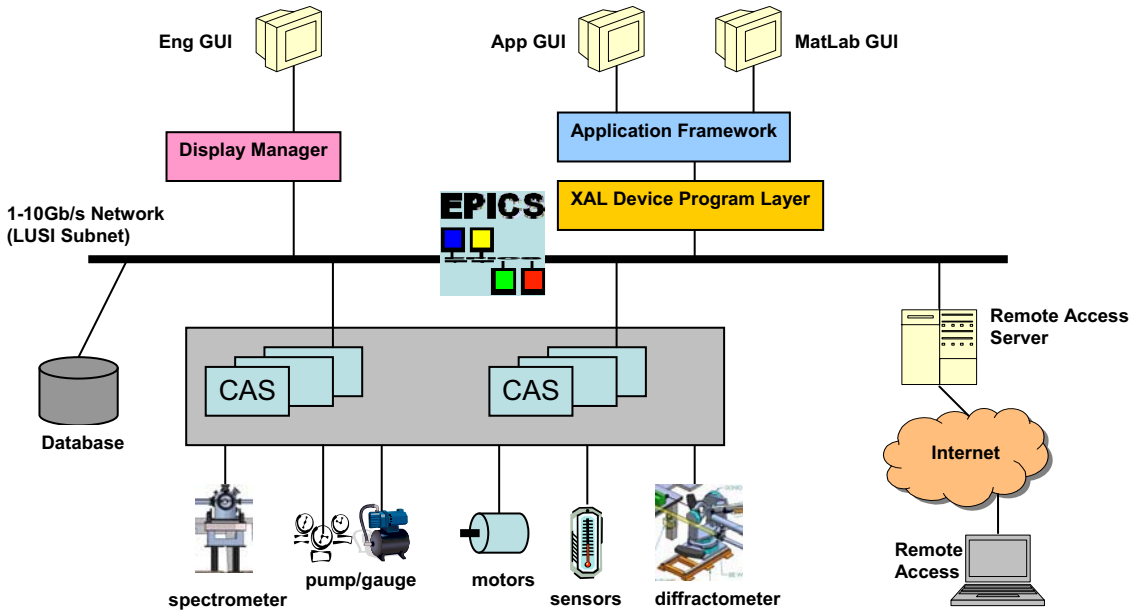

Figure 8-4. Architecture of the Control Subsystem.

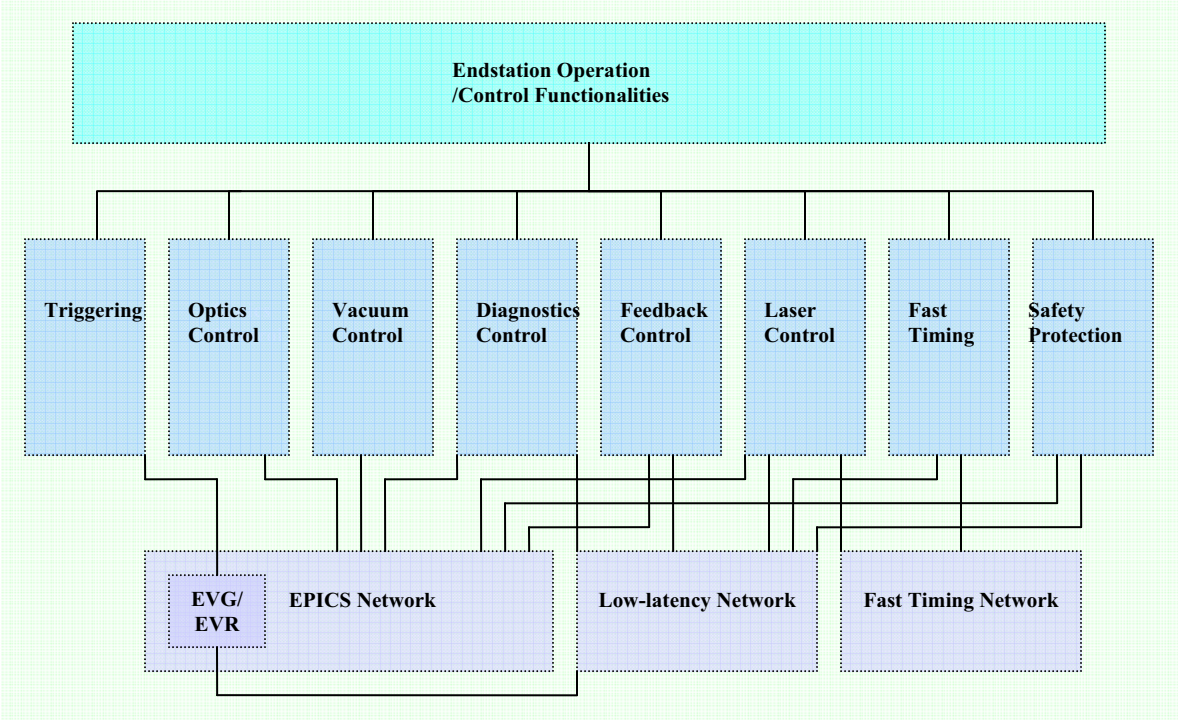

Figure 8-5. Layered Model for Controls Subsystem.

8.3.2. Control Networks

EPICS Network: The LUSI Control/Data System like the LCLS Control System will be based on the EPICS platform [70], which is widely used by the scientific community for controlling experimental systems. The EPICS platform uses Client/Server techniques to provide communication among various control entities. Most servers, called Input/Output Controllers (IOCs), perform real-world I/O and local control tasks, and make information about their states available to their clients via the Channel Access (CA) network protocol, which is designed for high bandwidth, quasi real-time network applications. The hardware architecture of EPICS is distributed such that each IOC or OPI (OPerator Interface) can communicate with all the others, providing flexibility and scalability to system implementation [69]. However, the CA protocol, in its most native implementation using UDP protocol, is not deterministic in timing and delivery, making its real-time applications questionable at best. Therefore, in timing critical applications, either performance enhancement implementation on top of the Channel Access protocol or other alternative network architecture must be used.

Event Generator/Receiver: Separated from the EPICS network infrastructure, there is another dedicated private network used for the timing and triggering for the LCLS accelerator system, whose role is to provide synchronization among a number of processes:

- The injection of the electron bunch into the accelerator.
- Energizing pulsed devices like klystrons and pulsed magnets.
- Data acquisition from accelerator diagnostic devices such as BPMs to coincide with the passage of the beam pulse.

This timing/triggering system is the so-called Event Generator/Receiver system and has been used by the existing SLC control system for all beam programs at SLAC [72]. The timing is to be synchronized with the SLAC 476 MHz reference RF signal and the 360 Hz power line frequency by generation of 360 Hz timing fiducials on a 476 MHz carrier frequency broadcast on the Main Drive Line (MDL) running the entire length of the accelerator including the undulator, beam transport, and the front end enclosure.

For the LUSI Control Subsystem EVR's should be placed in experimental stations in both NEH and FEH for per pulse triggering. The EVR's can receive beam code information distributed by SLC via a Master Pattern Generator (MPG) which broadcasts a 128-bit word at a rate of 360 Hz over a dedicated network, PNET. This enables EPICS to deliver timing distribution for synchronized operations between different IOC's and controlling the sequencing of various processes. This EVG/EVR network, however, is point to multiple-point and one directional, and lacks bandwidth for other type of real-time applications where large amount of data needed to be moved around from anywhere on the network as in the case of the low-latency network to be described below.

Low-Latency Network: The 120 Hz real-time operation requires a network implementation that provides guaranteed delivery and a latency of at most 8.3 ms. The applications include embedding diagnostic signals into experimental measurement data on a pulse by pulse basis or feedback to the electron beam based on endstation photon beam measurements for orbital correction before the very next pulse is directed down the accelerator path. A similar requirement comes from the Machine Protection System where the only way to prevent equipment damage in case of faults is to dump the next electron beam before the next pulse due to the slowness of the very heavy photon beam shutter.

One possible implementation to achieve this network performance is to add retransmission mechanisms on top of the UDP protocol, such as that used by the RUDP or TCP, but at the expense of increasing network traffic, which could be alleviated by using a separate network, or allocating more

bandwidth to avoid collisions. However, this approach still lacks the deterministic nature due to the fact that it is really a software implementation for real-time performance.

A more straightforward approach that derives real-time performance in hardware implementation is to use a network infrastructure such as a SCRAMNet system, which delivers ultra-low network latency of less than 1ms and a few hundreds of MB/s throughput using the replicated shared-memory network technique. A special feature of SCRAMNet is the network interrupts which are generated on SCRAMNet when a certain event happens and then translated into a local interrupt on computers in the network that are interested in that specific interrupt. The SCRAMNet is typically in a ring topology but other topology is also possible by using passive switches or other calling options.

Fast Timing Network: The sub-picosecond pulse nature of the LCLS beam represents a unique opportunity for experimental measurements that aim to study ultra-fast dynamics in physical systems, and at the same time creates a formidable challenge for timing and synchronization at the sub-picosecond level. For example, in the X-ray pump-probe experiment, the pump laser pulses needs to be synchronized with the probe X-ray pulses to less than 10 fs at point of interaction. However, the timing of the X-ray pulses is rather difficult to measure. Instead, the timing of the electron beam bunch that generates the X-ray pulse is used.

To achieve required fs timing synchronization, a collaboration between the LCLS project and team at LBNL is developing a fiber distributed optical timing network that distributes timing signals with jitters less than a few fs to the photo-injector for the, the low-level RF system of the linac, the Electro-Optic timing measurement apparatus for the electron beam to X-ray beam synchronization, and the each experimental endstation where there is a pump laser. A high frequency clock signal is distributed via fiber to the gun laser for the photo-injector (controlling electron beam pulse), to RF cavities (also controlling X-ray probe pulse timing), and to mode-locked lasers at endstations (controlling pump laser pulse timing). The RF cavities are actively locked to the optical clock phase. Most of the RF timing error is contained within a 10 kHz bandwidth, so these errors and any others affecting X-ray pulse timing (such as RF gun phase) can be detected and transmitted to correct laser timing at the endstations.

The long geographical separation of the distribution points necessitates that the length of the fiber distribution network be stabilized to counter thermal drifts, ground motions, or seismic activities. The LBNL team uses an interferometric technique, whereby the timing delay jitter through the fibers will be stabilized by comparing a retro-reflected pulse from the distribution point end with a reference pulse from the sending end, and actively controlling the fiber length. The most current version of the LBNL fiber stabilization network has a dynamic range of 1 ns and a timing stability of a few fs.

8.3.3. Slow EPICS Controls

All controls that are slow, supervisory, and not timing critical are handled by the EPICS Control Component, including motion controls for optical elements along the transport and in the endstation, vacuum system controls, and in general the communication among entities that are not timing sensitive and not required of being deterministic. The controls of all diagnostic equipment will be made via the EPICS control network, although the distribution of the diagnostic data will be coordinated by the Diagnostics Component. Other functional task such as triggering is also handled by the EPICS control such as the simple signaling applications with a small or minimal network bandwidth requirement in case of starting the detector integration cycle shortly before the arrival of the X-ray pulse, EVR's can be used.

Optics Controls: The X-ray optical elements associated with all three endstations will be controlled by the Optics Control Component and include:

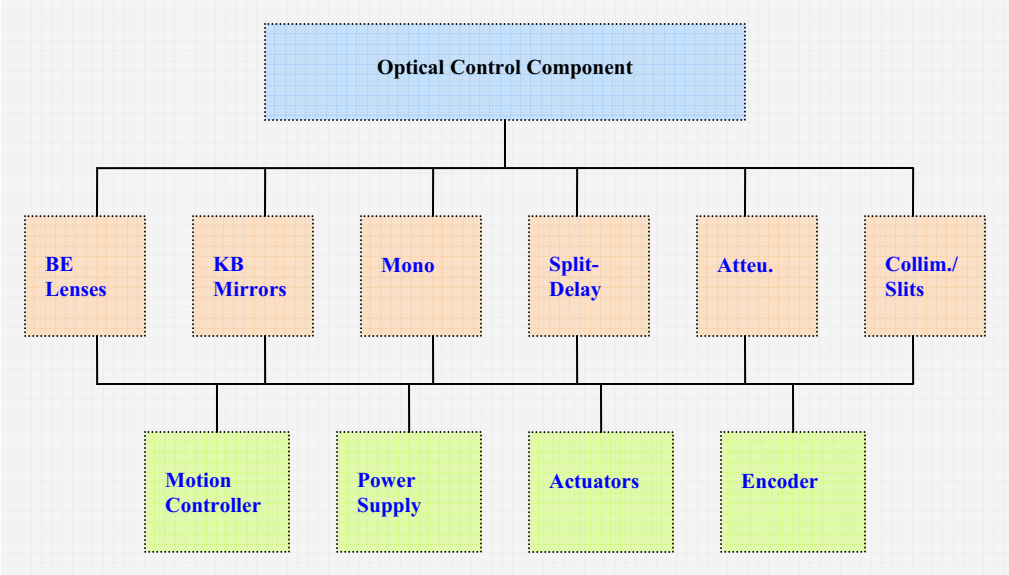

Figure 8-6. Block Diagram of the Optics Control Component.

(1) CXI and XPP Be lens focusing elements;
(2) CXI hard X-ray KB focusing mirrors;
(3) XPP and XCS hard X-ray monochromators;
(4) XCS hard X-ray split-delay element;
(5) Attenuators;
(6) Collimators;
(7) Adjustable precision slits;
(8) Fond End Enclosure (FEE) elements that may need to be controlled for beam steering;

Motion Controls: Optics Control Component will execute translations and rotations of the optical elements in terms of specified range, accuracy, and stability. The extremely collimated LSLC X-ray beam coupled with the large distance between the source and the final measurement spot, which can reach 500m from the end of the undulator to the experimental endstations in the FEH, will demand very tight tolerances on all linear and angular controls. In addition, the intrinsic beam jitters in transverse positions, beam pointing, and X-ray energies will put additional limits on the control stabilities. In cases where fine angular motion and stability, a level arm will be used in place of a rotational stage. Almost all motions will always run in open loop and will need to have encoders for position read-back to correct for beam jitters on per pulse basis.

Position Read-Back: The linear position will be measured directly with linear variable differential transformers (LVDTs) in some cases or capacitance gauges in others where nm or even sub-nm resolutions will be required. LVDTs can provide moderate resolution (essentially determined by the number of bits in the read-out ADC and the LVDT range of travel), and good linearity (< 0.15%), and are very ease to use. Other applications may need to use optical interferometric encoders for sub-nm precision.

Vacuum System: The vacuum associated with all three endstations will be controlled by the Vacuum Control Component and include:

(1) CXI sample chamber;
(2) CXI KB focusing mirrors chambers;
(3) XPP sample chamber;
(4) XPP and XCS hard X-ray monochromators chambers;

(5) XCS hard X-ray split-delay element chamber;
(6) Beam transport within endstations;
(7) Long beam transport in tunnel connecting FEH and FEH;

Vacuum Controls: Vacuum control will consist of controlling of the pump power supply, reading and controlling of the gauges and actions of the gate valves to either open or close. The values of gauge readings and status of the valves are made available to the control system both for long-term archiving and for alarm monitoring. A vacuum valve logic controller determines whether a valve can be opened or closed according to the state of the machine, other valves and measured vacuum pressure. The controllers can be stand alone units which can be operated independently of the rest of the control system, but always report their status to the control system. They also allow for remote operation.

Triggering: The LUSI Instruments will use the LCLS timing triggering system to provide hardware triggers and the data required at the beam rate for control and data acquisition purposes. The LCLS timing trigger system will provide operations with the ability to select beam rates of up to 120 Hz, deliver independent subsystem triggers over a 1 second super cycle, support synchronized data acquisition for applications, provide triggers up to 120 Hz with long term jitter of less than 20 picoseconds, and provide gates with a resolution of 8 ns [74]. The LCLS timing system consists of the LCLS Master Pattern Generator (MPG) and the Event Receivers. The Main Drive Line (MDL) supplies the RF phase locked fiducial and 360 Hz timing triggers to the LCLS MPG; the SLC MPG supplies timing information via PNET to the LCLS MPG. The LCLS MPG integrates the SLC timing information with the LCLS timing information, writes it to a buffer in the Event Generator (EVG) which then sends it out over fiber optic cable to the EVRs distributed throughout the control system to provide synchronized timing triggers and timing information.

Detector Triggering: The 2D pixelated detector often times needs to start and stop integration cycle shortly before the arrival of the X-ray pulse and for a preset integration time to minimize the effect of charge leakage. The triggering functionality is thus very crucial for this application no other timing signal can be used for this purpose with the required resolution and deterministic behavior. The important feature of the triggering system is that the triggering can happen before the arrival of the pulse, whereas other timing measurements provide the timing information only after the fact. The triggering can also support fan-out to allow multiple triggers with adjustable time delays.

8.3.4. Pulse-by-Pulse Measurement

For the LCLS X-ray pulses, there will be expected intensity fluctuations exceeding 30%, and spatial jitter of order 25% of beam diameter, wavelength fluctuations of order 0.2% of center wavelength equivalent to the LCLS intrinsic bandwidth, pulse duration variation of order 15%, and X-ray pulse/LCLS RF timing fluctuations of order 1 ps. To take measurements at the maximum possible rate, each measurement for a given pulse must be properly analyzed, thus requiring diagnostic measurements of the electron beam as well as the photon beam on per pulse basis. The diagnostic information must be available to both the accelerator operations and the experiment itself. Therefore, the LUSI instruments must support this pulse-by-pulse operation not previously required of those at conventional synchrotron sources.

X-ray Beam Diagnostics: The diagnostics hardware associated with all three endstations will be controlled by the Diagnostic Control Component and include:
(1) Beam Profiler/Imager;
(2) Beam Intensity Monitor;
(3) Compton Beam Position Monitor/Intensity Monitor;
(4) Wavefront Sensor;

(5) Spatial Correlation Apparatus (to be implemented in the future);
(6) Temporal Correlation Measurement Apparatus (to be implemented in the future);

The hardware required to operate the X-ray beam diagnostics are described in the Chapter 7. In general, the diagnostics will generate diagnostic signals that must be processed to provide information to the user. The type of signals can be separated into two categories: point detectors (intensity monitors, position monitors) and 2D images (beam profiler and wavefront sensor). There will also be motion controls to move diagnostic elements about their central positions or to perform scans. The signal acquisition and processing are handled by the Data Acquisition Component of the Data Subsystem.

Point Detector Processing: The LCLS X-ray beam will initiate either a voltage pulse or current spike in the various intensity monitors. These electrical signals must then be processed using various electronic devices such as shaping amplifiers, current preamplifiers, pulse height analyzers, and pulse integrators. Once processed the signal must be digitized, stored, and distributed.

Beam Profiler Acquisition: The beam profiler utilizes a high-resolution monochrome camera to capture an analog image of the X-ray induced fluorescence from a scintillating material. An image capture card is required to interface to this device and integrate the captured images into the endstation Data Acquisition Component. This measurement is destructive and thus not necessarily required to be running at the beam rate.

Wavefront Sensor: The wavefront sensor is traditionally used to diagnose the phase distortion of the beam wavefront (see Section 7.2.4.1). In the current application, it will be used to determine the location of the focus after beam demagnification. The sensor's own control unit will need to be integrated into the Diagnostic Component. The operation of the wavefront sensor is mainly an image recording and subsequent image processing, and thus making the sensor primarily a component in the Data Acquisition Component and its primary functionality a part of the Diagnostics Component.

Fast Feedback: The feedback system for stabilizing the electron beam or the photon beam within the confines of the front end enclosure falls under the LCLS control and is described in LCLS CDR [75] There will be, however, a need to stabilize the photon beam at the point of the experiment downstream of the undulator in the NEH or the FEH. In the latter case the need is even more pronounced given the large distance from the source to approach 500 m, which by its own virtue will provide far better positional and angular sensitivity. For example, experiments that require irradiation of a fixed sample point (e.g., diffraction from an individual microstructure) require the stable positioning of the beam to within 10% of its diameter, making beam stability an important consideration in instrument design.

Factors contributing to positional beam jitter or drift at the sample plane might include the following: (1) power supply and other component fluctuations in the gun-to-undulator system, (2) phase shifts in linac klystron low-level rf, (3) vibration or positional drift in the linac and undulator structures, (4) vibration or positional drift of the X-ray optics system components. For factors contributing to beam motion that have sufficiently long time constants, detection of jitter or drift and their stabilization may be accomplished with suitable detectors providing feedback to any of the upstream LCLS system elements that govern beam position and direction. Detection of positional and directional jitter or drift will be accomplished with non-destructive photon beam position monitors. The output signal of the monitor will be fed back to positional/angular controllers of upstream optical components or the electron beam components.

The beam is sampled up to the maximum rate of 120 Hz and a processor uses an algorithm to calculate the new settings of a group of actuators. For transverse feedback the measurement is made with beam position monitors (BPMs) and corrected with magnetic steering coils driven from small power suppliers. Longitudinal feedback uses beam energy determination from BPMs and bunch length from fast monitors to

control the amplitude and phase of the RF. A tentative timing budget consists of 1ms to read and convert the beam parameters, 1ms to send the information to the fast feedback controllers, 1ms to compute and set the new settings, and 5 ms for the new values to settle. This is all driven from the estimate that the actuators take 5 ms to settle. These response times imply the use of dedicated networks such as the SCRAMNet, or networks known to have limited traffic, in order to guarantee a deterministic response.

Safety and Protection Systems: The safety and protection systems for LUSI will be an integral part of those for LCLS. LUSI instruments will only use the Personal Protection System of the LCLS and will have no implementation responsibilities. The Machine Protection System for LUSI instrument will be identical in system design and implementation to that of the LCLS [76].

8.3.5. Fast Timing and Synchronization

Various LCLS timing signals are required to trigger LUSI equipments. The readout of detectors, firing of laser systems, and the initiation of pulsed power supplies are examples of events that require an instigating electrical signal that is synchronized to the LCLS X-ray beam. The triggering provide by LCLS timing triggering system [74] will deliver timing signals that are synchronized to the LCLS Low Level Radio Frequency (LLRF) with an rms timing jitter of 2 ps and long term stability of 20 ps. The system is specified to have a delay range of 1 sec with a fine step size of 20 ps. This triggering signal should suffice for application such as the synchronization of the 2D detector integration to the arrival of the X-ray pulses.

For applications such the pump-probe experiments, additional and more sophisticated fiber and microwave timing instrumentation is necessary for synchronization, as well as test and measurement of the level of synchronization. These instruments require synchronization of the X-ray pulse with that of a pump stimulus, such as an ultra short laser pulse. Precise synchronization of the laser system with the LCLS is achieved by phase locking the laser pulse train to the LLRF clock signal.

EO Sampling Measurement Apparatus: The timing synchronization applications involve using the EO Sampling Apparatus and the Fiber Distribution Network which distributes a RF signal that is phase stabilized to 10 fs (see Section 7.2.5). The EO Sampling Apparatus includes an EO sampling laser, CCD camera, a fiber receiver interfacing to the fiber network, and EO sample translator, etc. For synchronization, the EO sampling laser, and the pump laser for the pump-probe experiments will all be phase locked to this RF signal, thus achieving temporal resolution limited only by how well the phase lock and the intra-bunch timing jitter in the SASE process.

Laser Control and Safety System: The XPP Instrument will definitely use a pump laser for the pump-probe experiments. The pump laser system consists of a Ti:Sapphire oscillator, regenerative amplifier, optical parametric amplifier (OPA) and a multi-pass power amplifier (see Section 3.2.4).

Laser Control: Motion controls are required to control the various motorized optical components for the XPP laser system. The three categories of components are linear stages, rotational stages, and motorized mirror systems. Image capture electronics are required to interface to analog CCD cameras that will be used to image a small fraction of the laser beam obtained from a beam splitter. The positional information obtained from the cameras will be used to drive the motorized mirror systems to create a positional feedback loop.

Laser Safety System: The XPP laser system will be categorized as a class IV laser system. Accordingly, a safety interlock system will be implemented in the XPP end station and the laser laboratory. The interlock system will control various laser shutters and will integrate with the internal safety controls of the commercial laser systems that comprise the XPP system.

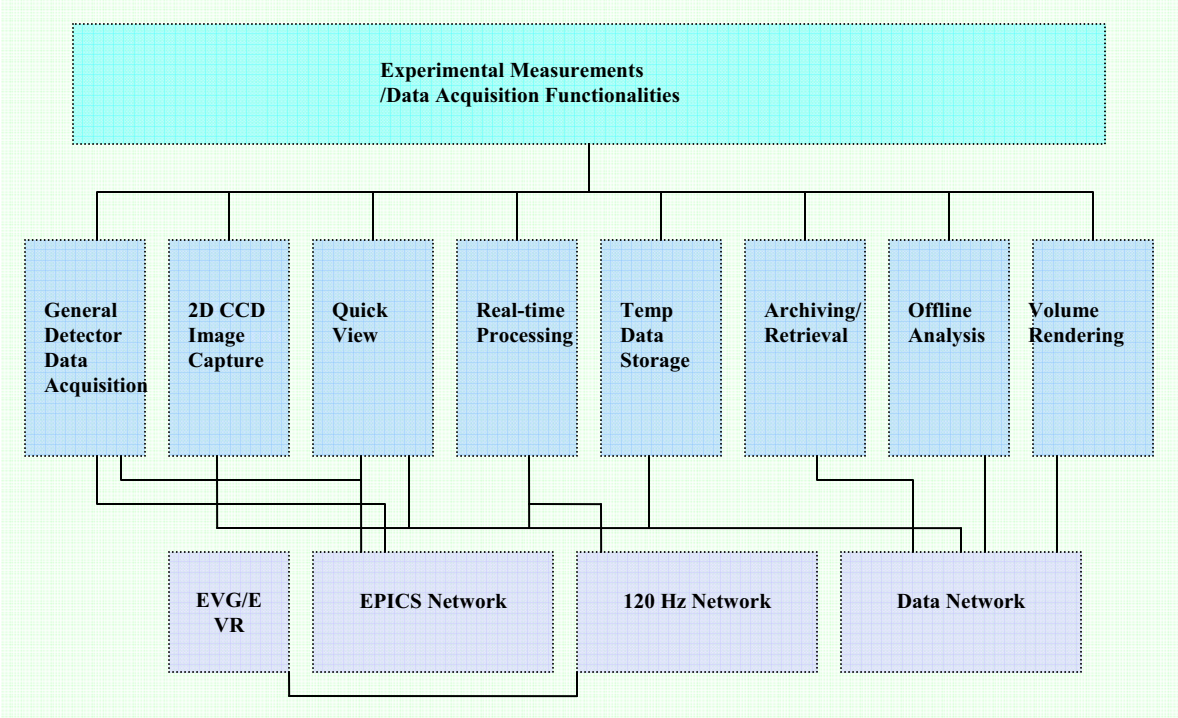

Figure 8-7. Layered Model for Data Subsystem.

8.4. DATA SUBSYSTEM

Unlike experiments performed at 3rd generation or older X-ray sources, those that have been envisioned and planned at LCLS will put the data acquisition and management in a quite different perspective due to the high raw data rate and potentially large volume of accumulated data. As such, a separate Data Subsystem based on EPICS as well as a data acquisition and management platform must be designed and implemented to meet the challenges to seamlessly integrate it into the Control Subsystem described in Section 8.3, and the existing SLAC data farm system and computer clusters housed at SCCS.

The Data Subsystem will be based on a layered architecture as shown in Figure 8-7 with high level applications and functionalities being the top most layer, the communication networks being the bottom layer for executing network primitives, and in between the middle layer of functional blocks for performing specific tasks such as acquiring data from a PIN diode, or grabbing an image from a CCD camera. It is responsible for the acquisition, storage, analysis, rendering, archiving, and retrieving of all experimental data. It will be responsible for all controls in so far as experimental measurements are concerned by calling services from the Control Subsystem.

8.4.1. General Requirements

There will be different kinds of detectors used for the three instruments, with the 2D pixelated X-ray detectors being the most significant in terms of generating experimental data. The general requirements for the Data Subsystem will be largely based on the 2D detectors. Other signals such as those from Si diodes, for example, will not be discussed in any details.

Year	Average (in 2009)	Lower Limit	Upper Limit
Rep Rate (Hz)	120	120	120
Detector Size (Megapixel)	1.16	1.16	1.16
Intensity Depth (bit)	14	14	14
Peak Rate (Gigabit/s)	1.95	1.95	1.95
Success Rate (%)	10%	5%	100%
Ave. Rate (Gigabit/s)	0.20	.097	1.95
Daily Duty Cycle (%)	25%	10%	100%
Accu. for 1 station (Terabyte/day)	0.53	0.11	21
Yearly Uptime (%)	25%	10%	100%
Accu. (Petabyte/year)	0.048	0.0038	7.7
3 yrs lifetime (Petabyte)	0.14	0.012	23

Table 8-1. Projected data rates and accumulation for CXI instrument.

Front End Data Flow: *Peak Raw Data Rate and Volume* - All first experiments for CXI, XPP, and XCS instruments will produce 2D scattering/diffraction images using megapixel pixelated detectors currently under development, which permit the detector readout rate to be synchronous with the X-ray pulse repetition rate, which is slated to run at 120 Hz. Table 8-1 shows the projected data rate and accumulation for the CXI experiment described in Chapter 4 in 2009 when LCLS will start operation, including the lower and upper limits. For the XPP and XCS experiments the rates and volumes are very similar with higher average data rates due to lower frame rejection rates.

The peak rate at 2 Gigabit/s is quite high even comparing with that of the BaBar experiment after the triggering electronics layer. If only minimal real-time processing, such as data reduction or compression, is performed, the average data generation rate for the entire duration of the measurement, which may be minutes, hours, or days, is determined by the success rate of the images. For the CXI, the success rate is the percentage of good images from only one single molecule scattered by the X-ray pulse that actually lased; whereas for the XPP or XCS, the percentage is simply the percentage of the lased pulses, thus higher. The high average rate combined with the potential long duration can generate upwards of a few Terabytes of raw data per day.

The high peak rates and large total accumulation are the driving parameters for the design of the LUSI Data Subsystem. The high rate at prolonged duration will require an acquisition system that can handle this rate in terms of getting data off the detector and getting them onto a storage device, with a multi-Gigabit/s transmission rate that is sustainable and reliable and a large on-line data storage system with comparable write speed and a capacity of tens of Terabytes. Such a system will need computing resources comparable to those for the high energy physics experiments such as BaBar. Specific requirements for the data subsystems are as follows.

Real-Time Processing - Given the potential large data volume, it is important to perform real-time screening and processing to the extent possible. Real-time screening/rejection is often times very straightforward such is the case when the FEL beam did not lase and the resultant image is essentially unusable. The feasibility of real-time processing depends largely on the type of processing that needs to be done and done within the intra-pulse duration of 8.3 ms. Due to the intrinsic fluctuations in the FEL SASE process, each X-ray pulse is an different measurement, averaging different measurements needs the help of diagnostic signals such as intensity, beam positions, etc. In case of XPP, simple binning based on time delay between the pump laser pulse and the probe X-ray pulse should be possible; whereas for the CXI experiments, the classification and averaging of diffraction images of different orientation may present significant challenges. The simple screening will be done by Field Programmable Gate Arrays (FPGA) collocated with the detector control electronics, whereas more complicated real-time processing will be done by processing farm nodes which have much higher computing power and are more flexible in terms of algorithm implementations.

Quick-View Rendering - When real-time rendering and visualization is needed, the corresponding computer node must be capable of processing and displaying tens or even hundreds of data frames as they are being collected for on-the-fly data exploration or assisting alignment at a display speed of 5 frames/s. If averaging is necessary, the diagnostic signals must be used to properly process the frames; whereas for simple viewing of the beam position on the detector, only certain frames can be displayed by skipping other ones.

On-Line Storage - Depending on the degree of buffering in the front end of the acquisition system, the processed data will be streamed into the on-line data storage system either synchronously or asynchronously, but the average throughput must meet the requirement set by the readout rate of the detector and the data reduction ratio. The architecture and implementation must be flexible, scalable, and upgradeable, and minimal data loss of less than 0.1%. It must have enough capacity for data collection of an extended period of one week to reduce its dependency on the availability of the permanent data farm in SCCS. Data in the on-line storage should be mirrored in real-time to a mirrored system in a load-sharing configuration.

Data Archiving and Retrieval: Once generated, the potentially large volume of data will be transmitted from the on-line temporary storage system to a permanent data farm system based on the tape or other cost effective technologies for storage, archiving, and subsequent retrieval. Coexisting with the long-term storage is a server system comparable to the front end temporary system for loading the data from the tape system, and for keeping the data sets available to analysis clusters during the offline processing. There are a few requirements on the content and format of the stored data.

Pulse Tagging: The image data for the experimental measurement will be uniquely tagged on a pulse by pulse basis, and this tag will be used as the key for retrieving meta-data associated with a particular image frame. The tag could simply contain the time stamp at the required 120 Hz repetition rate. Likewise, for the accelerator system logging, the same tag can be used for pulse identification, along with e-beam characteristics.

Meta-Data Storage: There will be two different approaches to deal with the pulse-wise meta-data associated with the electron and photon beam. The first approach stores the accelerator data, such as the e-beam positions, bunch characteristics, etc, in a separate file system keyed by a tag or pulse identification number; while the experimental image data is stored in a different file system. The image frame and its associated meta-data are only linked logically by the tag and only the tag. This approach is especially useful when the set of meta-data is very large in size, and can reduce the overall image size. A second approach has a self-contained data format that includes a pre-determined set of meta-data in each frame of experimental data.

Data Format: At the experimental run level, parameters such as date and time and station ID can be combined for use as file identification. Within each run file, the frame images will either have a pulse tag or a full set of pulse meta-data. If only a tag is included, meta-data will be queried using the pulse tag log file archive. The experimental data file content can be either the raw pixilated data, or processed information in preferably self-describing file format. The system that was developed by the BaBar project for organizing its event data could be ported over to the LUSI data system, although there is the clear distinction between HEP and BES experiments that there are many more separate experiments for BES rather than one single giant experiment with world-wide collaboration of thousands of scientists.

Backend Data Flow: At the backend and offline, large data sets of potentially 10^5 to 10^7 frames for the CXI experiments will be retrieved from either the on-line storage system or the permanent storage farm and processed to produce much reduced Gigavoxels volume sets for image reconstruction. Other experiments will retrieve much smaller data sets in the order of thousands of frames. The requirements on the backend are as follows:

Offline Data Storage - The data farm system in SCCS is shared by the high energy physics community, as well as the astronomy physics organizations. To facilitate the offline analysis of the LUSI experimental data, a separate offline storage system will be beneficial especially when large volume sets are needed. The on-line storage system can not be used for this purpose as new data are being collected and stored on it. In the early years of the LCLS when yearly uptime is quite low, the on-line system will be sufficient and the offline system will not be put in place immediately. When the yearly uptime begin to turn up, a separate offline system will become necessary.

Offline Processing - The most computational intensive experiment is the CXI, where the processing includes identifying and averaging diffraction patterns of like orientations, alignment of the averaged patterns with respect to each other to form a 3D volume set, which is ultimately converted to a 3D real-space structure. Each of the steps may require a large number of FLOPS on the order 10^{17}. It has been shown that the completion of the reconstruction alone will take several hours on a 32 single-core processor cluster. To reduce the computation time to less than a few minutes for a quicker turn-around will require a cluster with thousands of processors.

Volume Rendering - At the backend, volume rendering and visualization of large volume data sets is also needed; the corresponding computer node must be capable of processing Gigavoxels volume sets and displaying at speed of 5 frames/s. This requires a computer node with a large RAM space of tens of Gigabyte and the processing power of roughly a single workstation. The visualization node needs to have power graphics card and large enough memory.

8.4.2. Data Acquisition Architecture

The overall architecture of the Data Subsystem is schematically shown in Figure 8-8. It is divided in the on-line system and the offline system. The on-line system operates on the EPICS platform for slow controls of the optical and experimental elements such as the diffractometer, and uses the data acquisition system for generating experimental data and storing them on a pulse by pulse basis. The per pulse operation uses separate network infrastructure in the form of SCRAMNet and EVG/EVR in conjunction with the EPICS network. The data links to and from the detector and the storage are separate dedicated connections of high bandwidth. The major hardware components are:

(1) Detector control node
(2) Quick rendering node
(3) Detector interface board
(4) On-line cluster for real-time analysis within 8 ms

(5) On-line data sever and storage
(6) Network gears including networks, routers/switches

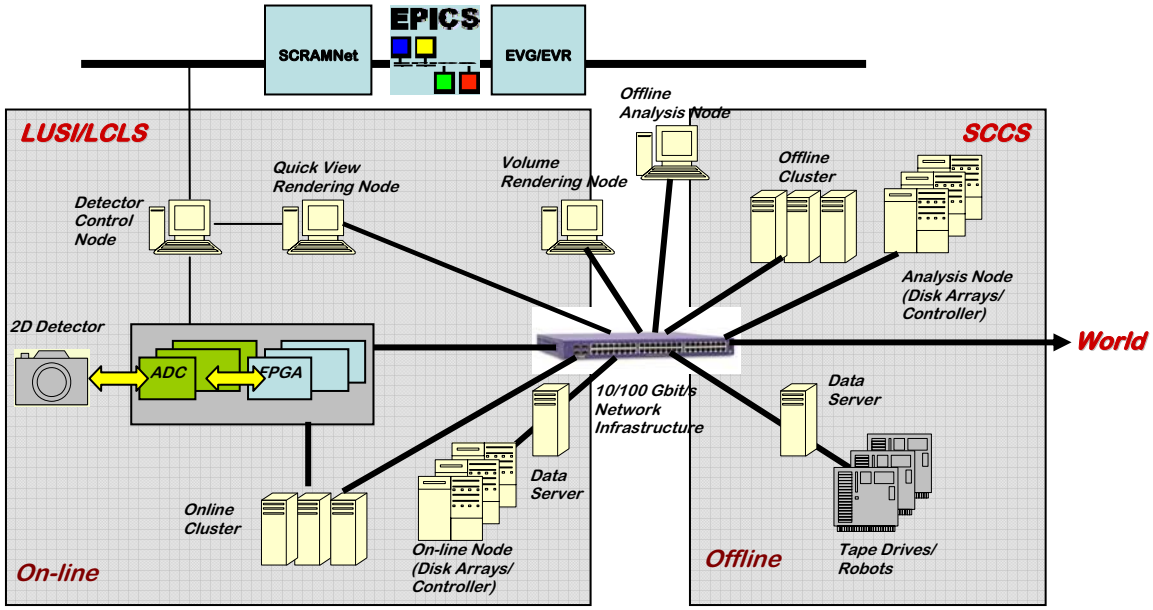

Figure 8-8. Data Subsystem Architecture.

The offline system is responsible for backend data management and data analysis. It serves as the gateway to other laboratory data resources such as the SCCS such as the large computing clusters, the tape archiving systems, and the managerial expertise that are associated with the data management. From a logistical point of view, LUSI will not take on the management of the computing hardware that require large amount of power or air conditioning, or replacement, etc, nor will it try to manage the data in terms of replication and persistency, which should be completely transparent to the experimental users. The major hardware components include:

(1) Tape drive/data server for long term achieving
(2) Offline cluster for offline analysis
(3) Offline staging storage
(4) Volume rendering node
(5) User portal for graphics display for large data sets.

8.4.3. Experimental Measurement Application

The topmost layer of the Data Subsystem is the application layer shown in Figure 8-9, which facilitates the experimental controls for taking measurements by running detectors, measurement instruments, and other controlling devices such as temperature controllers. The experimental controls will perform measurements using software specially written for the LUSI instruments in case of the CXI experiments or by porting diffraction software such as SPEC in case of the XPP instrument [77]. The porting of the SPEC or other exiting programs will be implemented on a high-level application frames with well defined API's that call functionalities from both the Control Subsystem and the Data Subsystem. The specific software development includes:

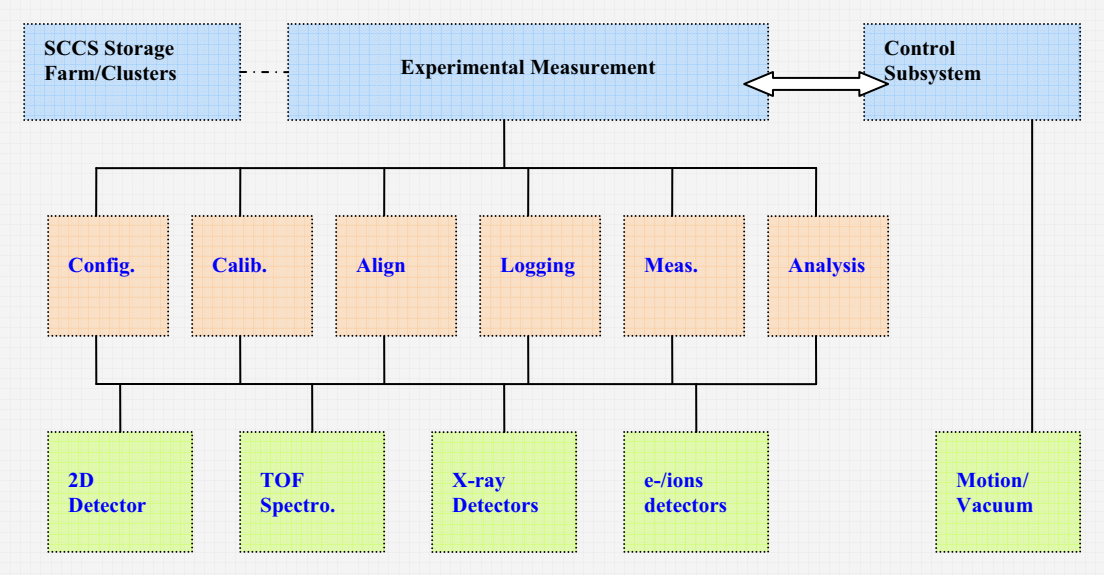

Figure 8-9. Block Diagram of the Experimental Control.

In-House Application Development: Use EPICS standard sequencer for developing measurement sequences to provide users with:

(1) Configuration routine for configuring the system, detectors, etc.
(2) Calibration routine for calibrating detectors
(3) Alignment routine for aligning optics such as mirrors, monochromators, etc.
(4) Data measurement routine for taking experimental data
(5) Logging routines for logging instrument operation such as temperature monitoring, etc.

Porting of Existing Applications: Use in-house developed Application Programming Interface (API's) to interface with legacy software such as SPEC to run diffraction measurements or MatLab analysis packages for routine data analysis or graphics:

(1) Diffraction experiments in various q scans, truncation rods in two-dimensional diffraction measurements.
(2) Non-linear least square fitting
(3) FFT calculations
(4) Graphical display of results
(5) Correlation calculations.

Interface to EPICS Controls: The motion controls that are needed in the experimental control functionalities described above will be carried out by the corresponding components in the Control Subsystem. The measurement applications can execute motions of certain elements but should be transparent to the details of the control architecture and implementation such the types of motors or stages that are used.

On the other hand, the controls and operation of the detectors including the 2D pixelated detectors, mass spectrometers, e- and ion TOF analyzers will be done by the Data Acquisition and Management Components. Depending on the mode of operation as to whether or not measurements are made on a pulse by pulse basis, and the data rates of the detectors, the data acquisition and management will follow different data flows to achieve optimal performance. Simple alignment procedure may involve data being taken and saved onto local hard disk on the controlling console rather than being streamed onto the on-line storage and subsequently onto the data farm.

8.4.4. On-Line Data Acquisition

There are two options in selecting the data acquisition, management, and analysis equipment and technology. There is the approach of using as much commercially available products as possible to leverage industries needs for continuing development and improvement, and their readily availableness, and the option to use equipment and components that are developed in-house or other scientific institutions in the case of the 2D detectors, where none of the available commercial devices will meet the requirements put forth by the proposed LUSI experiments, or the molecular injector for the CXI Instrument being developed by Lawrence Livermore National Laboratory under a MOU.

2D Pixelated Detectors: There will be three separate 2D detectors supplied by two vendors through MOU's, as listed in Table 3-3 and Table 5-3 with their key attributes. The detectors were designed to optimize their performance for the intended experiments, and their details are described in their relevant experimental sections.

The high repetition rate represents a significant challenge to the 2D detector technology available today. Most commercial X-ray 2D detectors are limited in the readout speed to about a few Hz for magepixels CCD or CMOS based devices, which is about two orders of magnitude too slow for the proposed LUSI experiments. The key matrices for the required detectors are sizes in total number of pixels and individual sensing element, dynamic range, signal-to-noise ratio, quantum efficiency as a function of X-ray energy, and finally dispersion if possible. Other fast detectors are being developed at DESY for the European XFEL where even faster data rates are possible.

Detector Controls: The detectors will be controlled from the experimental console by invoking the functionalities of the Detector Control Component, which perform tasks such as Configuration, Calibration, and Operation (start, stop, abort, etc.), etc. for more sophisticated detectors such as the 2D pixelated detectors, the CCD's. etc. For all other simpler detecting element, the controls are very straightforward and most consisting of digitizing the analog signals coming off them.

Common Front-End Interface to 2D Detectors: The fast data rates and high accumulation volume make it imperative that the design and implementation of the data infrastructure down stream of the detectors be relatively stationary and independent of the detector's design, and thus capable of the so-called plug-n-play interconnectivity. This requirement lends credence to the architectural abstraction of a front-end interface board that works as an adaptor to the detector, making the detector behave exactly the same to the rest of the system.

Backend Interfaces: The front-end board will interface with the quick-view rendering node for real-time display of the measurement data, stream data to the on-line storage, and receive diagnostic measurement signals form the Diagnostic Component for meta-data. This front-end interface board can either be a commercial product or an in-house development such as the CEM module being developed by the Electronics Group at SLAC for the LSST project [78]. The CEM board will have large on-board processing power for real-time data reduction, as well as fast to memory access which may be crucial in certain types of real-time processing such as classification in the CXI experiment.

Quick View Rendering: To help commission and perform experiments, real-time feedback on the beam itself provide invaluable information on the photon beam characteristics especially for X-ray FEL beams where intrinsic jitter occurs in the SASE process that will result in positional and angular shifts from pulse to pulse. To facilitate the visualization of that shifting beam, a quick rendering node will be built. Moderate graphics capability and RAM space will be required to store and process tens or hundreds frames and have them rendered and displayed at 5 frame/s rate. This dedicated workstation can be a standalone

unit to reduce its interference with the data acquisition station where processing power may be of great importance for handling real-time data management.

Real-Time Processing: The real-time processing will be based on the requirement that the system should be ready to deal with the data on per pulse basis, i.e. the latency of the processing should be less than 8.3 ms at most. For all likelihood, 5 ms or shorter should be used for calculating the latency budget. There are several types of real-time processing:

(1) Rejection/vetoing: Of measurement data that are the result of non-lasing FEL beam, or X-ray pulse missing the sample, etc.
(2) Frame Correction: Based on detector characteristics, dark-current, non-uniformity in amplifier gains are corrected once the frame is deemed good.
(3) Normalization: Based on diagnostic signals to remove effects from fluctuations in incident beam intensity, variations in wavelength due to that in e beam bunch, positional and angular jitter.
(4) Transformation: Transform data into its counterpart in the Fourier Space using FFT.
(5) Running Averaging: Average frames based on a set of parameters such as timing delays in XPP or XCS experiments.
(6) Calculation of Experimental Result: To extract experimental results by calculating the final physical parameters such as that is done in an auto-correlator for the XCS experiments.
(7) Classification of Like Frames: Specific to the CXI experiments whereby frames of diffraction patterns from molecules of similar orientations are identified and averaged.

The possibility of carrying out these real-time processing largely depend on the type of algorithms, which in turn impacts the architectural design requirement on the real-time processing node in terms of optimizing memory capacity and access bandwidth, CPU power, and I/O bandwidth. It is possible to build the real-time processing farm or cluster using the CEM modules as the nodes. Other approach will be using cluster technology with off-the-shelve components in processors, networking gears, and firmware for inter-processor communications.

Data Streaming and Content: The format of the data depends on whether real-time processing is performed or not, and on what kind of processing. If no processing is performed, a serial bit stream will be the most efficient transfer mode, whereas if sparsification is rendered on the raw data, coordinates of the pixels with intensities must be included as well. Additional meta-data describing the e-beam and photon beam characteristics will be embedded in the data stream as well on a pulse-by-pulse basis. The peak rate for a 1 megapixel/14 bit 2D detector will approach 2 Gbit/s. This rate must be sustained for the entire duration of the measurement. More than one measurement may be needed to complete a run, in which case, the date, time, measurement sequence, run ID will also be stored in some preconceived data format. The design of the file header is extremely important for data management in terms of archiving and retrieving efficiency.

Fast On-Line Storage: The fast on-line but temporary data storage is needed to off load the data stream coming off the detector at a very high peak rate of > 1 Gbit/s for even a 1 megapixel 14 bit 2D detector. The technology will necessarily have the write speed that is comparable to that of the detector and sustainable, which can be realized by using disk arrays running on Fibre Channel protocol [79]. The complete storage system will have two subsystems residing in the NEH and the FEH, each having its own drives and Gbit/s switch to support the entire experimental hall. The two subsystems are connected to act as the backup for its counterpart in the event of system failure. To reduce the risk of data loss due to single disk failures, a RAID-5 [80] configuration will be used.

Commercial Solution: The data storage network for the on-line data management will be based on the Storage Area Network (SAN) technology with Fibre Channel connectivity [81]. The major components of the SAN configuration will include:

(1) Multiple Storage Servers,
(2) Disk Arrays with RAID 5 configuration,
(3) Fibre Channel Host Bus Adaptors (HBAs),
(4) 4Gbit Fibre Channel switches.

The BaBar On-line System: An alternative approach has to do with the very successful high energy physics programs at SLAC, for which data acquisition and management systems have been also successfully developed in house by SLAC technical staff to address the very challenge that LUSI is facing in the case of the 2D detectors, that an proprietary system developed outside of industry is the only one that meets the technical requirement of the scientific programs. This approach will entail porting and tailoring existing high energy physics systems for LUSI implementation. This approach also has offer the advantage of having available to the LUSI project the data acquisition and management system expertise existed in house at SLAC.

8.4.5. Offline Data Management and Analysis

The total capacity of the temporary storage provided will be sufficient for storing data for a few days at most, thus requiring a semi real-time transfer to a data farm for longer term storage, archiving, and subsequent retrieval.

Long Term Archiving and Retrieval: Long term mass storage for data archiving and retrieval must provides data persistency and fast access. Such a storage facility will be equipped with a large number of fast disk arrays as well as high density tape drives, and will have capacity in excess of a few Petabyte and provide high throughput access compatible with the data generation rate at LCLS, which will approach 100 terabyte per day when multiple endstations are running concurrently. This mass storage should be completely transparent to the end users as to how and where his/her data is stored, and the only thing that the user must provide in order to access his/her data is an unique file identifier which is defined in a global naming space to which the mass storage serves. The file identifier is a key attribute of a data file system used by the mass storage for high-availability, fast access speed, and efficient data management. This mass storage system will be an extension to the existing SCCS of SLAC, whereas the data file system may be a newly designed one to meet the LCLS specific needs or a modified implementation based on an existing system such as the Object Database [82]. The mass storage system used by LUSI will have the following hardware and software components:

(1) Access Disk Servers for receiving data stream from the on-line storage and loading them onto the tape drives. Dedicated servers maybe needed to minimize conflicts with HEP experiments and other data intensive experiments.
(2) Permanent Tape Drives for long term safekeeping of the data. If persistency and redundancy are required, data mirroring, verification, and recovery will be implemented.
(3) Data File System for effectively organize LUSI experimental data. XrootD [83]may be used since it was proven to be very successful for BaBar data system. New data schema will be designed to meet LUSI specific needs.
(4) Data Access for users to perform analysis or simply retrieve the data. A staging storage farm will be needed for hosting analysis, especially for the CXI data sets, which may exceed 20 TB per set of 10 million frames of 1 megapixels. Policy and security are two important attributes for the LUSI data, because of the relatively smaller size of the collaboration in the X-ray community.

Off-line Analysis and Visualization: The LUSI Data Subsystem in conjunction with the SCCS computing infrastructure will enable additional capabilities other than data storage, namely data analysis. The analysis system will include the following hardware and software components:

(1) Multi-Processor Cluster for computational intensive analysis such as the phase-retrieval of the CXI experimental measurements of single molecules. This offline cluster should have enough computing power to render any given phase-retrieval algorithm within 1 hour. Simple extrapolation of exiting cluster at LLNL for similar purpose would suggest the size of the cluster to be on the order of 500 processors.
(2) Volume Rendering Node for rendering 1000^3 voxels data sets in a few minutes.
(3) Visualization Node for displaying the rendered results in preferably 3D manner. It will require powerful graphics capability.

8.5. REFERENCES

[69] See, for example, http://www.aps.anl.gov/epics/.
[70] "LCLS Conceptual design report-1", Chapter 11 (2003).
[71] Reflective memory, or replicated shared memory, systems are designed for ultra-low latency real-time applications with critical performance requirements. A specific example is the SCRAMNet network products.
[72] "LCLS Timing System Requirements", LCLS Physics Requirement Document.
[73] See, for example, R. B. Wilcox, J. W. Staples, L. R. Doolittle, "A fiber optic synchronization system for LUX", in http://repositories.cdlib.org/lbnl/LBNL-55661.
[74] "LCLS Timing Triggering System", LCLS Engineering Specification Document.
[75] See, http://www.slac.stanford.edu/grp/lcls/controls/global/architecture/presentations/LCLS%20PPS%20Intro_20050103.ppt.
[76] See, http://www.slac.stanford.edu/grp/lcls/controls/global/subsystems/mps/.
[77] See, http://www.certif.com/spec.html.
[78] Gunther Haller, private communications.
[79] See, for example, http://www.fibrechannel.org/technology/overview.html
[80] See, for example, http://en.wikipedia.org/wiki/Redundant_array_of_independent_disks.
[81] See, for example, http://en.wikipedia.org/wiki/Storage_area_network.
[82] Steffen Luitz, Private communications.
[83] See for example, http://xrootd.slac.stanford.edu/papers/Scalla-Intro.pdf.

9 - ENVIRONMENT, SAFETY & HEALTH

9.1. INTRODUCTION

It is SLAC's policy and objective to integrate safety and environmental protection into its management and work practices at all levels, so that its mission is accomplished while protecting the worker, the public, and the environment. To achieve this objective, SLAC has developed and implemented an Integrated Safety Management System plan (ISMS), required by DOE P450.4, Safety Management System Policy, which encourages and supports the use of: the Work Smart Standards process, development of measurable goals in the form of performance metrics, and uses existing programs and activities that have been deemed successful and which already incorporate the ISMS elements. (ISMS as a required element is implemented through the incorporation of a contract clause from the DOE Acquisition Regulations (DEAR), specifically DEAR 970.5204.-2, "Integration of Environment Safety and Health Into Planning and Execution". This clause was incorporated into the contract between DOE and Stanford University for operation of SLAC in February 1998).

Fundamental to the ISMS process is the application of Guiding Principals (GPs) and Core Functions (CFs). GPs are a series of best management practices or "basic philosophy" that ensure start-to-finish management of ES&H issues. CFs provide the necessary structure that describes the scope of work, identifies and analyzes the hazard, develops and implements hazard controls, allows work to be performed within the controls, and uses feedback from the work performed to improve the safety system. Responsibility for achieving and maintaining excellence in this system rests with line management, who implement the SLAC ES&H policy with the personnel under their supervision.

Existing and mature programs at SLAC will be used to ensure that all aspects of the design, installation, and testing phases of the project are properly managed. The LUSI project will be presented to the SLAC Safety Overview Committee, which coordinates and assigns safety reviews for new projects or facility modifications to other citizen committees, which have knowledge or skills in a specific area. The hazards for the LUSI may require reviews from such committees as: Radiation Safety Committee, Electrical Safety Committee, Earthquake Safety Committee and the Fire Protection Safety Committee.

At SLAC, the LUSI project will not generate any hazards that have not already been defined and addressed within the Work Smart Standards and will not present any significant challenges from the ES&H perspective. All aspects of the project will conform to the applicable Work Smart Standards SLAC has adopted and written into its contract with the DOE. Appendix A identifies the potential hazards, causes, and mitigating controls that the LUSI project may encounter. A complete list of SLAC's Work Smart Standards that have been included in its contract with DOE may be found at www.slac.stanford.edu/esh/reference/worksmart.htm.

9.2. IONIZING RADIATION

The design and operation of all radiation-producing facilities at SLAC are governed by the ALARA (as low as reasonably achievable) policy. SLAC has always maintained radiation dose limits below the maximum allowed by regulation.

9.2.1. Radiation Shielding

Shielding for the LUSI will conform to the Radiation Safety Systems Technical Basis Document, Chapter 1 Radiological Guidelines for Shielding and Barriers (SLAC-I-720-0A05Z-002). Under normal operation the design criterion will be (i) 1 rem/yr at 30 cm from the shield surface, assuming a 2000 hr working year and an occupancy factor of 1. In addition the LUSI will have non-radiological workers (Users); additional shielding may be required to maintain their annual effective dose equivalent below 0.1 rem/yr taking exposure duration and occupancy factors into account. SLAC internal design criteria also requires that under a system failure (ii) the total effective dose equivalent shall not exceed 3 rem for a broad beam and 12 rem for a narrow beam, and that under an accident scenario that requires human intervention to turn off the beam (iii) the maximum dose equivalent shall not exceed 25 rem averaged over a 1 hour period for broad beam exposure or 100 rem averaged over 1 hour for narrow beam exposure.

An analysis of the present shielding indicates that potential beam losses from the LCLS during operation could produce high radiation doses. Local shielding, in some cases movable, will be used to mitigate these hazards to acceptable values. Defining the type and amount of local shielding is dependent on the final configuration of the LCLS for the experimental halls and experimenter hutches. Installation of radiation loss monitors at the hutches for diagnostic capabilities may be used to determine where beam losses are taking place. Adding this monitoring package in addition to the Beam Containment System (BCS) will further help maintain dose levels below those limits allowed at SLAC.

9.2.2. Personnel Protection System

The personnel protection system (PPS) consists of electrical interlocks and mechanical barriers whose primary functions are to prevent entry of personnel into a beamline enclosure when prompt radiation and electrical hazards are operating, and to turn off the beam, RF, and electrical hazards when a security violation is detected. Other functions that it must also accomplish are: (i) provide interlocks for the orderly searching of an area before beam is turned on, (ii) allow for various access states, such as No Access, Controlled Access or Permitted Access, (iii) have emergency shut-off capabilities, and (iv) control the electrical hazards in beam housing areas. As installation of the LUSI instruments will not require a significant change to the present shielding footprint, the PPS will undergo only necessary upgrades and enhancements to address the instruments. These upgrades include: additional status and control interfaces to accommodate new power supplies, access control modules for the injector and experimental areas, logic upgrades, and interlocks with beam stoppers, Beam Shut Off Ion Chambers (BSOICs), and those burn-through monitors that are controlled through the PPS. The PPS will remain largely the same in terms of its design, function, and configuration as other PPS to installations used at SLAC and LCLS, and all additions will conform to the Radiation Safety Systems Technical Basis Document, Chapter 2 Personnel Protection Systems (SLAC-I-720-0A05Z-002).

9.2.3. Beam Containment System

The Beam Containment System (BCS) prevents accelerated beams from diverging from the desired channel, and detects excessive beam energy or intensity that could cause unacceptable radiation levels. Beam containment is usually accomplished by a combination of passive devices such as collimators, which are designed to absorb errant beams, and active devices such as electronic monitors that shut off the beam when out of tolerance conditions are detected. The present BCS in the Linac consists of passive mechanical devices (such as slits, collimators, magnets, electron beam stoppers, and dumps) and active electronic devices such as average current monitors, burn through monitors, and beam shut off ion chambers. Additionally the LCLS will install photon stoppers, ion chambers, and burn-through monitors for the proposed beamlines. Gas absorption cells are planned to be installed in critical places, for attenuating the beam as needed.

9.2.4. Radiation Safety Training

In accordance with SLAC's Site Access and Identification Badges Policies and Procedures (SLAC-I-720-0A0Z-002-R001), all individuals at SLAC who enter the Radiologically Controlled Area (RCA) or the Accelerator Area must be either properly trained or escorted by a properly trained individual. Levels of training depend on the area to be accessed and in some cases the duration of the individual's stay (see Table 9-1).

Access Required	Duration of Access	Potential Dose (mrem/yr)	Required Training Level					Dosimeter		
			Safety Orientation	EOESH	GERT	RWT I	RWT II	None	Annual	Quart
Industrial Areas, Accelerator Area - No RCA	< 60 days (within a yr)	0	x					x		
Industrial Areas, Accelerator Area - No RCA	< 60 days (within a yr)	0		x				x		
Accelerator Area RCA's	Any	< 100		x	x				x	
Accelerator Area RCA's, High Rad. Area	Any	Any		x	x	x				x
Accelerator Area RCA's, Cont. Area	Any	Any		x	x	x	x			x

Table 9-1. Minimum Training Requirements for Unescorted Access.

9.3. ELECTRICAL SAFETY

An accelerator facility by nature has subsystems that either produce or use high voltage or high current, either of which can present an electrical hazard to personnel if not managed properly. The LUSI project will operate in a similar mode to other research facilities at SLAC, control and work procedures for electrical subsystems, as well as entry into the accelerator housing are well understood. Primary mitigation of the hazard will be through de-energization of equipment, placement of barriers and the effective use of Lock Out and Tag Out (LOTO) procedures.

In as much as the design, upgrade, installation and operation of electrical equipment will be in compliance with the National Electrical Code, Title 29 Code of federal Regulations, Parts 1910 and 1926 (as applicable) and SLAC's policy on Electrical Safety, SLAC ES&H Manual, Chapter 8 (SLAC-I-720-0A29Z-001-R007); entry into the accelerator housing requires the mitigation of electrical hazards through either the lockout of power supplies or selective use of mechanical barriers, interlocked to further reduce the risk of exposure to electrical shock. Various levels of electrical safety training and LOTO training are provided by SLAC for those personnel who may work on or near potential electrical hazards.

Infrequently it may be necessary to complete work on energized equipment. This is conducted under very limited and controlled conditions, using qualified employees and where appropriate, under the full approval of the SLAC Director.

Special procedures will be developed to permit authorized personnel to occupy areas adjacent to energized magnets. These are called Electrical Hazard Test Procedures and allow local control of the electrical power supply feeding a single magnet, or unique string of magnets, that are to be tested.

9.4. EMERGENCY PREPAREDNESS

It has been estimated by the U. S. Geological Survey that the chance of one or more large earthquakes (magnitude 7 or greater) in the San Francisco Bay area in the coming 30 years is about 67 percent. All SLAC personnel are trained in the immediate response to earthquakes and other emergencies via their supervisors and employee orientation.

9.5. SEISMIC SAFETY

SLAC structures are designed and constructed to minimize the effects of a major earthquake to acceptable levels. The LUSI components will be installed in the new LCLS facility, whose seismic stability will be well documented and deemed acceptable by the time installation begins.

9.6. EMERGENCY PLANNING

The design, review, installation and operation of all experimental equipment at SLAC is done in a manner that minimizes the risk of accident or injury to personnel and property in the event of either a natural disaster or emergency situation. SLAC's formal emergency planning system as described in the SLAC Emergency Preparedness Plan (SLAC-I-730-0A14A-001) will help ensure a logical, organized, and efficient site wide response to any emergency. Facility specific procedures, which supplement the SLAC emergency plan, support a timely initial response, further decreasing the probability of personal injury and limiting potential loss or damage to both property and the environment.

9.7. HAZARDOUS MATERIALS

During the installation and operation phases of the LUSI it is anticipated that a minimum amount of hazardous materials will be used, examples would be paints, epoxies, solvents, oils and lead in the form of shielding, etc. There are no current or anticipated activities at the LUSI project that would expose workers to levels of contaminants (dust, odors, and fumes) above acceptable levels.

The SLAC Industrial Hygiene Program detailed in the SLAC ES&H Manual addresses potential hazards to workers from the use of hazardous materials. The program identifies how to evaluate workplace hazards at the earliest stages of the project and implement controls to eliminate or mitigate these hazards to an acceptable level.

Site and facility specific procedures are also in place for the safe handling, storing, transporting, inspecting and disposing of hazardous materials. These are contained in the SLAC Introduction to Pollution Prevention, Hazardous Material and Waste Management “A Hazardous Materials Management Handbook” (SLAC-I-750-0A06G-001), and the ES&H Manual Chapter 4, “Hazard Communication” (SLAC-I-720-0A29Z-011-R012) which describes minimum standards to maintain for compliance with Title 29, Code of Federal Regulations, Part 1910.1200.

The UTR or Project Engineer has added responsibilities with respect to the management of hazardous materials. They ensure subcontractor personnel are aware of, and remain in compliance with SLAC's written Hazard Communication Plan, also keeping affected SLAC personnel informed of hazardous material usage and the associated hazards and risks.

9.8. FIRE SAFETY

The probability of a fire during the assembly and installation of the LUSI instruments is expected to be comparable to other research facilities at SLAC since components are primarily fabricated out of similar, non-flammable materials and combustible materials in general are kept to a minimum. The most "reasonably foreseeable" incident or event with any substantial consequences would be a fire in the insulating material of the electrical cable plant caused by an overload condition. This differs from the maximum credible fire loss, which assumes proper functioning of the smoke detector system and a normal response from the on-site fire department. In this case, losses would be confined to isolated components, and associated cabling. The ES&H Manual Chapter 12, “Fire Safety” (SLAC-I-720-0A29Z-001-R007) address all fire safety issues.

Installation of new cables for the LUSI project will meet the current SLAC standards for cable insulation and comply with National Electric Code (NEC) standards concerning cable fire resistance. While this reduces the probability of a fire starting, an aspiration type smoke detection system (VESDA) in the accelerator housing and fire breaks in the cable trays will mitigate fire travel. Support buildings for power supplies, electronic equipment or experimental areas are protected by automatic heat activated wet sprinkler systems and smoke detectors. Fire extinguishers are located in the Experimental Halls for use by trained personnel. The combination of smoke detection systems, sprinklers and on-site fire department (response time ~3 minutes) affords an early warning and timely response to fire or smoke related incidents.

Burn injuries caused by a fire are not expected because nowhere in the Experimental Halls are personnel further than 150 ft from an exit and there is no location where two directions of egress are not available. Multiple entry/exit points also helps in keeping property damage to a minimum.

9.9. ENVIRONMENTAL PROTECTION

It is likely that the assembly and installation of the LUSI instruments may produce hazardous wastes, such as used solvent from degreasing baths or spent cutting fluids. These are ongoing operations at SLAC, disposal of wastes is routine, and in full compliance with SLAC's policies on the management of hazardous materials and waste minimization. Any hazardous waste would be disposed of in accordance with SLAC procedures and ultimately to a permitted Treatment, Storage and Disposal Facility, under regulations set forth in the Resource, Conservation and Recovery Act (RCRA).

9.10. QUALITY ASSURANCE

A Quality Assurance Program Plan (SLAC-I-770-0A17M-001-R001) conforming with DOE Order 414.1A, “Quality Assurance”, was established at SLAC to provide laboratory management with guidance and requirements toward achieving quality in pursuit of the laboratory mission. Overall responsibility for the implementation of this program lies with the SLAC Director, while accountability for managing the program at the divisional level rests with the respective Associate Director (AD). For the LUSI project, the "Project Leader" has been assigned by the Photon Sciences Division Director and given responsibility for staffing, documenting, generating Quality Implementing Procedures and implementing the QA program. At the project level this includes developing and maintaining required management systems, or using management systems that are already available.

The QA plan describes SLAC's approach to implementing the ten criteria of DOE Order 414.1A:

- Criterion 1 - requires specific Quality Implementing Procedures for all SLAC projects where total project costs exceed $5,000,000.
- Criterion 2 - as appropriate defines specific requirements and assures adequate qualification and training for individuals connected with the project, including retention of training records.
- Criterion 3 - defines requirements for management's responsibility with respect to identification, analysis, resolution and follow up of ES&H, technical and compliance issues.
- Criterion 4 - provides policy for identification of documents (policy, procedures, drawings etc.), records and other specific elements that will have a significant impact on the project and need to be entered into a document control system.
- Criterion 5 - requires project leaders to define and maintain work processes for R&D efforts that have a significant programmatic impact Criterion 6 - establishes a responsibility for line management to conduct design reviews and to promote the use of design standards.
- Criterion 7 - discusses a graded approach to the development of specifications for procurement of items and services based on cost and failure impact.
- Criterion 8 - established responsibility for the staffing, documenting, and performing of inspection and testing activities related to the project.
- Criterion 9 - requires participation in the SLAC Institutional Self-Assessment Program.
- Criterion 10 - provides the authority for the Quality Assurance and Compliance Department to conduct independent assessments of all SLAC facilities and projects as warranted verifying the degree of conformance to QA and ES&H requirements.

Effective use of these criteria will enable the LUSI project to:

- Design in quality and reliability.
- Promote early detection of problems to minimize failure costs and impact on schedule.
- Develop appropriate documentation to support upgrade and operational requirements.

- Establish methods to identify critical systems and to release these systems based on demonstrated performance.
- Define the general requirements for design and readiness reviews for all aspects of the project.
- Assuring personnel are trained before performing critical activities, especially those that have ES&H consequences.

9.11. PROCEDURES AND POLICIES REFERENCES

SLAC Work Smart Standards:
http://www.slac.stanford.edu/esh/reference/worksmart.htm;

SLAC Safety Management System:
http://www.slac.stanford.edu/esh/isms/sms.pdf;

SLAC Environment, Safety & Health Manual:
http://www.slac.stanford.edu/esh/manuals/eshmanual.html;

SLAC Radiation Safety Systems Technical Basis Document (SLAC-I-720-0A05Z-002):
http://www.slac.stanford.edu/esh/techbas/rss/rss.pdf;

Specification for Seismic Design of Buildings, Structures, Equipment, and Systems at the Stanford Linear Accelerator Center (SLAC-I-720-0A05Z-002):
http://www.slac.stanford.edu/esh/techbas/seismic.pdf;

Lock and Tag Program for the Control of Hazardous Energy (SLAC-I-730-0A10Z-001):
http://www.slac.stanford.edu/esh/manuals/locktag.pdf;

Electrical Hazard Test Procedures (SLAC-I-040-30460-002);

Introduction to Pollution Prevention, Hazardous Material and Waste Management (SLAC-I-750-0A06G-001-R001)
http://www.slac.stanford.edu/esh/training/study_guides/hmh.pdf;

SLAC Emergency Preparedness Plan (SLAC-I-730-0A14A-001):
http://www.slac.stanford.edu/esh/manuals/epp2000.pdf;

SLAC Institutional Quality Assurance Program Plan (SLAC-I-770-0A17M-R002):
http://www.slac.stanford.edu/esh/manuals/QAplan.pdf;

10 - WBS DICTIONARY

10.1. INTRODUCTION

The Work Breakdown Structure (WBS) is used for defining work packages and tracking the cost and schedule for the project. The work is broken down into tasks, each of which has a manager, costs and schedule, technical scope, and, to the extent possible, a specific geographic location in the LCLS.

Each level 3 element has a Task Manager who is responsible for the execution of the project plans for that element. The Task Manager is responsible for translating system performance requirements into design choices for the LUSI instruments. He/she is also responsible for control of cost and schedule, quality and safety, and documentation. Performance requirements for systems at level 3 and below will be established and advocated by a System Manager. The System Manager advises the Task Manager and LUSI Project Management as to whether the LUSI systems will meet specifications necessary for the success of the Project. The Systems Manager is primarily an advocate of the performance of each system, with no responsibility for cost and schedule. Line responsibility for design choices and execution flows through LUSI Management and the Task Managers.

The WBS is used to specify change control. The Project Management Plan specifies the levels of approval required for changes in cost and/or schedule at each level of the WBS.

In addition, the WBS is used for cost reporting. The project will report costs and progress to the DOE monthly at level 2 of the WBS. The project management will review costs and progress monthly at level 3. The System Managers will review costs and progress monthly at the lower levels of the WBS.

10.2. LEVEL 3 WORK BREAKDOWN STRUCTURE

The following describes the scope of work for each of the level 3 elements of the WBS. Each element includes design, simulations, documentation, fabrication, testing, and installation of the equipment. Commissioning of each instrument will be carried out by LCLS Operations.

1 LUSI Project

1.1 Project Management. This section of the WBS identifies the technical and administration management of the project, establishment and operation of the Project Management Control System (PMCS), generation of financial and technical reports, and organization of technical support and reviews. Costs related to management of project-wide ES&H issues are included.

1.1.1 ES&H. This element captures efforts and other costs associated with management of safety related issues in the design and construction phases of the Project.

1.1.2 Project Management. This element comprises the management and administrative activities of the project. It also takes account of the Project Management Control System operation and the cost of contracted management support.

1.1.3 Technical Support. This element captures all technical support, review activities, and general collaboration not identified with a specific instrument.

1.2 X-ray Pump-Probe Diffraction. This section of the WBS identifies all required the design, procurement, and fabrication efforts associated with this instrument, which utilize the ultra-bright, ultra-short X-ray pulses from LCLS, permitting a large class of dynamical processes in molecules and condensed matter systems to be studied directly, with atomic spatial resolution and sub-picosecond time resolution.

1.2.1 Physics Support & Engineering Integration. This element states all the Physics and Engineering support associated with the execution of the design, procurement and fabrication efforts for this instrument. Costs related to design reviews and vendor visits will be captured in this WBS element

1.2.2 X-ray Optics. This element captures the design, procurement, and fabrication of all components such as the Monochromator, the Beryllium Lenses, the Slits & Collimators, and the Attenuators.

1.2.3 Laser System. This element consists of all efforts to design, procure, and fabricate the laser system. Major components listed under this element are the Ti: Sapphire Oscillator & Amplifiers Systems & pumps, Temporal Pulse Shaper, Optics & Optomechanics, Laser Diagnostic, the Hutch Optical Table System, Laser Timing System, Optical Experiments, Laser Containment System, and Optical Parametric Amplifier.

1.2.4 Detector System. This element covers all efforts to develop, build, and test the 2D Pixel X-ray Detector System as stated in the MOU between SLAC and Brookhaven National Laboratory. This system will be used for the X-ray pump-probe diffraction (XRPP) experiments, which require a moderate resolution, full-well capability of at least 104 8keV photons, and moderate overall detector size. It also covers all major reviews by the LCLS/LUSI Detector Advisory Committee.

1.2.5 Sample Environment. This element consists of all efforts to design, procure, and fabricate the sample environment, including the Diffractometer.

1.2.6 Lab Facilities. This element captures the design, procurement, and installation of the Electrical Outlets.

1.2.7 Vacuum. This element sums up all efforts associated with designing, procuring, and fabrication of this system, including all hardware, bellows, and spools.

1.2.8 Installation. This element includes all labor and material required for the assembly and installation of this instrument.

1.3 Coherent X-ray Imaging. This section of the WBS identifies all required design, procurement, and fabrication efforts associated with this instrument, which take advantage of

the extremely bright, ultra-short LCLS pulses of hard X-rays to allow imaging of non-periodic nano-scale objects, including single biomolecules or small clusters, at or near atomic resolution.

1.3.1 Physics Support & Engineering Integration. This element covers all Physics and Engineering support associated with the execution of design, procurement and fabrication efforts for this instrument. Costs related to the coordination of design reviews and vendor visits are also included.

1.3.2 X-ray Optics. This element captures the design, procurement, and fabrication of the required components, including the Kirkpatrick-Baez (KB) mirrors, the Beryllium Lenses, the Slits, the Attenuators, and the Compressor.

1.3.3 Sample Environment. This section includes all efforts to design, procure, and fabricate all required parts to complete the sample chamber, the Ion ToF, the Electron ToF, and the Precision Instrument Stand.

1.3.4 Lab Facilities. This element captures the design, procurement, and installation of the Electrical Outlets.

1.3.5 Vacuum. This element sums up all efforts associated with designing, procuring, and fabrication of this system, including all hardware, bellows, and spools.

1.3.6 Injector. This element reflects the development effort for the particle injector by a MOU with LLNL.

1.3.7 Installation. This element includes all labor and material required for the assembly and installation of this instrument.

1.4 X-ray Photon Correlation Spectroscopy. This section of the WBS identifies all required design, procurement, and fabrication efforts associated with this instrument, which takes advantage of the brightness and short pulse properties of LCLS to give this instrument the ability to study atomic-scale dynamics over a range of time scales – picoseconds to microseconds – that is inaccessible by any other generally-applicable technique.

1.4.1 Physics Support & Engineering Integration. This element covers all the Physics and Engineering support associated with the execution of the design, procurement and fabrication efforts for this instrument. Costs related to the coordination of design reviews and vendor visits are also included.

1.4.2 X-ray Optics. This element captures the efforts to design, procure, and fabricate all required components, including the Monochromator, the Beryllium Lenses, the Slit System, the Split and Delay System, the Collimators, and the Attenuators.

1.4.3 Detector System. This element covers all efforts to develop, build, and test the 2D Pixel X-ray Detector System as stated in the MOU between SLAC and Brookhaven National Laboratory. This system will be used for the X-ray Photon Correlation Spectroscopy (XPCS) experiments, which require a resolution of <50um, a full-well of <100 8keV photons and very low noise. The detector's fame rate will match the 120

Hz pulse rate of the LCLS. It also covers all major reviews by the LCLS/LUSI Detector Advisory Committee.

1.4.4 Lab Facilities. This element captures the design, procurement, and installation of the Electrical Outlets and the Hutch.

1.4.5 Vacuum. This element includes all efforts associated with designing, procuring, and fabrication of this system, which include vacuum components, supports, bellows, and spools.

1.4.6 Sample Environment. This section includes all efforts to design, procure, and fabricate all required parts to complete the sample chamber.

1.4.7 Installation. This element includes all labor and material required for the assembly and installation of this instrument.

1.5 Diagnostics. This section of the WBS identifies all required design, procurement, and fabrication efforts associated with the LUSI diagnostics suite. Five X-ray diagnostics will be designed and constructed to individually measure the X-ray pulse intensity, position, and profile on a pulse-by-pulse basis.

1.5.1 Physics Development. This element covers the Physics and Engineering support associated with the execution of the design, procurement, and fabrication efforts for the diagnostic systems. Costs related to the coordination of design reviews and vendor visits are also included.

1.5.2 Position Monitor. This element describes the efforts associated with the design, procurement, and assembly of the X-ray position monitor for the instruments. This assembly consists of a fluorescent screen, visible wavelength mirror, vacuum actuator, and optical imaging system. It will be operated in 2 configurations: 1) Large field of view with coarse spatial resolution, which will be used to locate and steer the X-ray beam; 2) narrow field of view with high resolving power, which will be used when precise positioning of an optic into the X-ray beam is required.

1.5.3 IO Pop-In Monitor. This element covers all efforts and costs associated with the design, procurement, and assembly of the X-ray intensity monitor for the instruments. The assembly consists of a X-ray diode, vacuum actuator, and readout electronics. The main purpose of the monitor is to detect when the reflection condition of a Bragg reflector or mirror is satisfied.

1.5.4 Hard X-ray Intensity Leave-In Monitor. This element includes the required efforts to design, procure, and assemble the hard X-ray intensity monitor for the instruments.

1.5.5 Wavefront Sensor. This element includes the efforts associated with the design, procurement, and assembly of the Hartmann wavefront sensor for the instruments. An image is first acquired from a X-ray transmission through a pinhole array. The local phase front tilt of the X-ray bean profile is then computed with knowledge of the pinhole array orientation with respect to the X-ray detector. The focal X-ray beam is then computed by an algorithm that back-propagates the X-ray wavefront.

1.5.6 EO Monitor. This element includes the required efforts to design, procure, and assemble the EO sampling apparatus.

1.5.4 XCS Planning Package. This element includes the required efforts to design, procure, and assemble the diagnostic package for the XCS instrument.

1.6 Controls. This section of the WBS identifies all required design, procurement, and fabrication efforts associated with the control systems for the three instruments. It consists of 2 major areas, the control subsystems and the data subsystems. The control subsystem will control the basic operations of all experimental endstations in the two experimental halls, the Near Hall and the Far Hall. The data subsystems will acquire, store, analyze, and archive all experimental data.

1.6.1 Physics Development. This element covers all the Physics and Engineering support associated with the execution of the design, procurement, and fabrication efforts for the control systems. Costs related to the coordination of design reviews and vendor visits are also included.

1.6.2 In-Station Cabling. This element includes all efforts associated with designing, procuring, assembling, final installation, and testing of all cables for the instruments.

1.6.3 Computer Hardware/Administration. This element captures all efforts associated with designing, procuring, and installation of the computer workstations, network, and storages for the instruments.

1.6.4 Experimental Control (EPICS). This element describes the efforts associated with specifying and developing a distributed soft real-time control systems utilizing EPICS for the instruments.

1.6.5 Data Acquisition Hardware/Firmware. This element captures the costs and efforts to procure all required hardware and firmware for the instruments.

1.6.6 Timing and Triggering. This element covers the costs and efforts to design, procure, and integrate all required components to synchronize with the LCLS X-ray beam, to receive and read the various timing signals, and to trigger the firing of laser for the XRPP instrument.

1.6.7 Laser Control and Laser PPS. This element describes the efforts related to the design, procurement, and review of the XRPP laser control and safety system. The control system includes motion control drivers to control the various motorized optical components.

1.6.8 Vacuum Controls. This element captures all costs and efforts to design, procure, and integrate all components to build the Transport and Endstation Vacuum Controls for the instruments.

1.6.9 Diagnostics & Optics, and Sample Environment. This element sums up all costs and efforts related to design, procurement, and assembly of all required components for the instruments. The optical elements associated with each Endstations will be controlled by the Optics Control subcomponent.

1.6.10 MPS/PLC. This element covers the costs and efforts associated with the design, procurement, and integration of the Programmable Logic Controller & Interface HW for the Machine Protection Systems.

1.6.11 XCS Planning Package. This element includes the required efforts to design, procure, and assemble the controls package for the XCS instrument.